BCS-TO-BEC QUANTUM PHASE TRANSITION IN HIGH-T_c SUPERCONDUCTORS AND FERMIONIC ATOMIC GASES: A FUNCTIONAL INTEGRAL APPROACH

A Thesis
Presented to
The Academic Faculty

by

Sergio S. Botelho

In Partial Fulfillment
of the Requirements for the Degree
Doctor of Philosophy in Physics

School of Physics
Georgia Institute of Technology
December 2005

BCS-TO-BEC QUANTUM PHASE TRANSITION IN HIGH-T_c SUPERCONDUCTORS AND FERMIONIC ATOMIC GASES: A FUNCTIONAL INTEGRAL APPROACH

Approved by:

Dr. Carlos Sá de Melo, Advisor
School of Physics
Georgia Institute of Technology

Dr. Phillip First
School of Physics
Georgia Institute of Technology

Dr. Andrew Zangwill
School of Physics
Georgia Institute of Technology

Dr. Prasad Tetali
School of Mathematics
Georgia Institute of Technology

Dr. Brian Kennedy
School of Physics
Georgia Institute of Technology

Date Approved: September 9$^{\text{th}}$, 2005

ACKNOWLEDGEMENTS

There are definitely more people that I am indebted to for the completion of this work than I could possibly list in a few pages. Therefore, I will adopt the convenient strategy of limiting myself to those who, one way or another, have had some direct influence on my life for the past few years.

I start thanking my advisor, Carlos Sá de Melo, without whose insightful suggestions and knowledgeable guidance this work would not have been possible. His deep understanding of Physics has helped me several times during moments of uncertainty. I am also grateful to many professors in the School of Physics at Georgia Tech, including Ron Fox, Andrew Zangwill, Ray Flannery, Chandra Raman, Phil First, Roman Grigoriev and Alexei Marchenkov. My knowledge of Physics was immensely benefitted from classes taken with these fine instructors. I also thank Eric Murray for being such a supportive "boss", and the members of my thesis committee - Andrew Zangwill, Brian Kennedy, Phil First and Prasad Tetali - not only for their valuable feedback, but also for their willingness to undertake such an arid assignment. Special thanks to Menderes Iskin and Wei Zhang, two very talented physicists I had the privilege to work with, and without whose friendship my years of graduate school would not have been as enjoyable. I also owe special gratitude to Fábio Reis for his constant encouragement and help during decisive moments of my life.

Many thanks will always be due to my parents for their unconditional love and support, and for being responsible for much of what I am today. And, finally, I thank my wife Luciana Diniz for all that she is. Without her presence in my life, none of this would have made sense.

TABLE OF CONTENTS

LIST OF FIGURES

SUMMARY

The problem of the evolution from BCS theory with cooperative Cooper pairing to the formation and condensation of composite bosons has attracted considerable attention for the past several decades. It has gained renewed impetus in the mid-eighties with the discovery of the high-T_c superconductors, which have a coherence length comparable to the interparticle spacing. More recently, this subject has spurred a great deal of research activity in connection with experiments involving dilute atomic gases of fermionic atoms. The initial objective of this work will be to use functional integral techniques to analyze the low-temperature BCS-to-BEC evolution of d-wave superconductors within the saddle point (mean field) approximation for a continuum model. Then, the same mathematical formalism will be applied to the problem of the BCS-to-BEC evolution of fully spin-polarized p-wave Fermi gases in two dimensions. We find that a quantum phase transition occurs for both systems as they are driven from the BCS-like regime of weakly interacting fermionic pairs to the opposite BEC-like regime of strongly interacting bosonic molecules. This is in contrast to the smooth crossover predicted and observed in systems that exhibit s-wave pairing symmetry. We calculate several spectroscopic and thermodynamic properties that signal the occurrence of this phase transition, and suggest some possible experimental realizations. Finally, fluctuations about the saddle point solution are included in the calculations, and the effects of such correction are analyzed in the low ($T \approx 0$) and high ($T \approx T_c$) temperature limits. We conclude that, at high temperatures, the bosonic degrees of freedom that arise from two-particle bound states become essential to describe the strong coupling limit, as the saddle point approximation alone becomes unreliable.

CHAPTER I

INTRODUCTION

1.1 Overview and Survey

Nature has a very peculiar and unexpected behavior at extreme conditions. The general perception that we have of the world around us, which is the ultimate responsible for defining what we understand by common sense, is usually based upon the information that our human senses allow us to extract from nature. However, as it turns out, these senses have a quite limited range of validity, and only work in a rather special limit that we now call the "classical" regime. In fact, what modern physics teaches us is that the description of the world as we learned from Newton and Galileo constitutes a mere approximation to the actual laws of nature, which is valid only under certain conditions. This description quickly breaks down as one tries to explain phenomena that fall outside the realm of classical physics, as for instance when dealing with microscopic length scales or velocities comparable to the speed of light.

One could say, in quite general terms, that human beings are rather "big" and "slow" creatures, and that the physical laws that we built from our direct observation of the world are, consequently, applicable only in the limit of large typical sizes and small velocities. In fact, classical mechanics becomes inadequate to describe phenomena that occur at very small length scales, and the more comprehensive formulation provided by quantum mechanics has to be used instead. As a practical rule, classical laws start to break down when the deBroglie wavelength of the system, which is negligibly small for macroscopic bodies, becomes of the same order of magnitude as the typical size of the system. On the other hand, when the velocities involved in the problem are comparable to the speed of light, the special theory of relativity has to be invoked in order to accurately explain the dynamics of the system.

One of the most basic paradigms of quantum mechanics, and one that profoundly challenges our common-sensical principles, is the division of all fundamental particles of nature

into only two categories. In fact, every single elementary particle in the Universe can be classified as either a *boson* or a *fermion*. Bosons are particles with integer spin, that is, they have an instrinsic angular momentum which is always an integral multiple of $\hbar$. Examples of bosons include photons, phonons, magnons, ^{4}He atoms, etc. Fermions, on the other hand, are half-integer spin particles, that is, their intrinsic angular momentum can only assume values which are integer-plus-half units of $\hbar$. Most of the fundamental particles that constitute the building blocks of matter, as electrons, protons and neutrons, are fermions. The quantum mechanical behavior of a composite system is determined by the type and number of elementary particles it is composed of. A system comprised only of bosons will also possess bosonic behavior, since the addition of any number of integers always results in another integer. On the other hand, the overall character of a fermionic system depends on the particular number of fermions involved, since the summation of half-integer numbers can result in either an integer or a half-integer. For instance, to tell whether an atom is a boson of a fermion, one must count the amount of protons, neutrons and electrons making up that atom. Since these are all spin-1/2 fermions, adding up an odd number of them will make an atom that is a fermion (half-integer spin), whereas an even total number of particles will result in an atom that is a boson (integer spin). Clearly, in the particular case of neutral atoms ($N_{\text{protons}} = N_{\text{electrons}}$), it is the total number of neutrons in the nucleus that decides whether the overall quantum mechanical behavior of the system will be bosonic or fermionic.

Another important difference between fermions and bosons is the symmetry of the wave function describing systems of indistinguishable particles (this is discussed in much more detail in the Appendix A of this thesis). In fact, not all many-body wave functions that satisfy Schroedinger's equation are acceptable representations of quantum mechanical systems. The wave function describing a system composed of bosons must be symmetric with respect to the interchange of any two identical particles. On the other hand, fermionic systems must have anti-symmetric wave functions, meaning that the interchange of any two fermions in the system must result in the appearence of an overall minus sign. Notice that, in both cases, the wave functions are such that any two configurations that differ only by

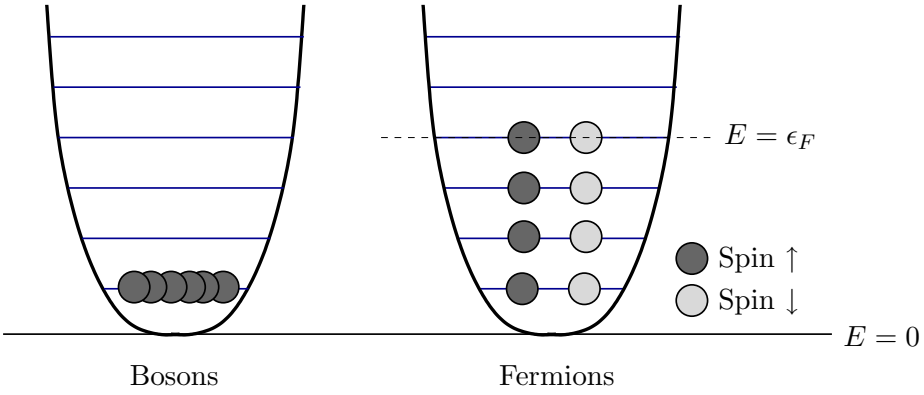

Figure 1.1: Bosonic and fermionic particles occupying the lowest energy levels of a harmonic potential well at zero-temperature. The Fermi energy ϵ_F is defined as the energy of the last occupied quantum state.

an interchange of two particles are still regarded as one and the same state, since an overall minus sign constitutes simply a global phase. However, these symmetry requirements have striking consequences on how the available quantum mechanical states are populated by fermions and bosons. Since bosonic wave functions are completely symmetric under particle exchange, any number of bosons can occupy a certain quantum state. In fact, if the temperature of the system is dropped below a certain critical value, the particles will be pushed *en masse* into the lowest possible energy state, resulting in a macroscopic occupation of the ground state known as Bose-Einstein condenstation. On the other hand, the fact that fermionic wave functions change sign under particle exchange implies that no two identical fermions can occupy the same quantum state (this would lead to a vanishing wave function). This is known as the Pauli exclusion principle, which is one of the most important results of modern physics, and is the ultimate responsible for the stability of matter as we know it. In the limit of absolute zero temperature, fermions will fill the lowest available quantum states with exactly one particle per state, resulting in an arrangement known as the Fermi sea. A schematic view of the zero-temperature occupation of available quantum energy states by fermions and bosons is shown in Fig. 1.1 in the case of a parabolic (harmonic) potential.

The quantum mechanical behavior of fermions and bosons has been extensively studied for almost a century now, and the physics of both systems is currently very well understood. Bose-Einstein statistics has been successfully used to predict the occurrence of a

macroscopic occupation of the ground state, known as Bose-Einstein condensation (BEC), which manifests itself in many different areas of physics, ranging from condensed matter to atomic, molecular and optical (AMO) physics. On the other hand, Fermi-Dirac statistics has also been applied to a broad range of physical problems involving fermionic particles, as for example electrons in metal, equilibrium of white dwarf stars, band structure of semiconductors, etc. However, as mentioned before, while a system of bosons can only behave as a boson, a system comprised of fermions can display either a bosonic or fermionic behavior, depending on the total number of fermions involved. This opens up the exciting possibility of exploring the connection between the Bose and Fermi statistics in the same physical system. In fact, it turns out that for most systems that exhibit Bose-Einstein condensation, it is actually a pair of fermions, rather than a boson, that condenses. This is not surprising, given that the constituents of visible matter are all spin-1/2 fermions, and a pair of particles is the smallest number of fermions one can use to create a composite boson. This raises the question of whether or not it is possible to observe the bosonic degrees of freedom emerge from the underlying fermionic degrees of freedom. In particular, it would be interesting to know under exactly what experimental conditions one could expect such an interplay between Fermi and Bose statistics to become significant.

An answer to this question started to be formulated in the early eighties and, since then, a great deal of theoretical and experimental effort has gone into trying to understand the coexistence of bosonic and fermionic degrees of freedom in the same system. The problem gained further impetus in the late eighties with the discovery of high-critical-temperature superconductors (high-T_c's) and, most recently, in the context of cold atomic gases. A quick discussion of these physical systems, as well as their relation to the problem of the Fermi-Bose interplay, will be presented in what follows.

1.1.1 High-T_c Superconductors

Superconductivity is a remarkable property possessed by most ordinary metals by which they loose all measurable traces of electrical resistivity when cooled below a well-defined critical temperature T_c, which depends on the external magnetic field in which the sample is

placed. At the same time, currents are set up in the metal in such a way that the magnetic field vanishes inside the material irrespective of the existence of an applied external field[1]. This results in all magnetic field lines being expelled from the bulk of the superconductor, a phenomenon known as Meissner effect. This superconducting state exists as long as the temperature is kept below T_c and the external field is sufficiently small.

Although superconductivity was first discovered by Kammerlingh Onnes in 1911 [1], it was not until 1957 that a successful microscopic theory of the phenomenon was finally proposed by Bardeen, Cooper and Schrieffer, in what is known today as the BCS theory [2]. The essence of the microscopic explanation is that a very weak interaction between the conduction electrons of the metal can, at sufficiently low temperatures, lead to quantum states characterized by a highly correlated motion of all these electrons. In fact, this conclusion was based on a previous result by Cooper [3], who showed that an arbitrarily small attractive interaction between two electrons above a filled Fermi sea would be sufficient to create a bound state, resulting in electronic pairs (now known as Cooper pairs) that could move without resistance in the presence of a driving electric field. The BCS theory consisted then of a many-body extension of the Cooper problem, in which the ground-state wave function was constructed from pairs of electrons, and the attractive interaction between the electrons was assumed to arise from the exchange of phonons (quanta of lattice vibrations). The vanishing of electrical resistivity in superconductors can be accounted for by recalling that a Cooper pair, being a combination of two fermions, effectively behaves as a bosonic "molecule" and, therefore, can undergo Bose-Einstein condensation below some critical temperature. This way, the superconducting electrons can be described as a highly correlated matter wave, which is able to propagate without being scattered by the lattice. The BCS theory was successfully used to explain most of the properties presented by the superconductor materials known at the time, including the Meissner effect, the existence of a critical magnetic field, the discontinuity in the specific heat, the appearance of an energy

[1]The situation is slightly different in the so-called type-II superconductors, where magnetic flux can penetrate the material as an array of *vortices*, while the rest of the sample remains in the superconducting state. This is commonly referred to as the Abrikosov phase.

gap in the excitation spectrum, among others. Also, the value of the superconducting critical temperature T_c predicted by BCS was fairly well obeyed by all the so-called conventional (or low-T_c) superconductors.

However, in 1986, Bednorz and Müller [4] discovered a new class of materials that could superconduct at temperatures much higher than the ones predicted by BCS (and observed for metals), which became known as unconventional (or high-T_c) superconductors. Most of the high-T_c materials known up to date are ceramic compounds, with a typical structure consisting of copper-oxide layers spaced by atoms of one or more chemical elements, the most common being barium, yttrium and lanthanum. One of the most striking properties of these materials, besides their elevated critical temperature, is their extremely short coherence length (or pair size) ξ_0, which is typically two to three orders of magnitude smaller than in the case of low-T_c superconductors. In fact, these systems have a pair size ξ_0 comparable to the avarage distance k_F^{-1} between the charge carriers in the material. Therefore, they are believed to lie in an interesting intermediate regime between the limit of large and overlapping Cooper pairs ($k_F\xi_0 \gg 1$) found in the BCS (conventional) superconductors, and the opposite limit of Bose condensation of composite bosons ($k_F\xi_0 \ll 1$) consisting of tightly bound fermion pairs. While these two limiting cases are well understood, the study of the crossover region is still in its infancy. And this is precisely one of the main objectives of this thesis: to analyze the evolution from the BCS limit of weakly interacting fermionic pairs to the BEC limit of strongly coupled bosonic dimers in the context of unconventional superconductivity.

In spite of intense research activity, the physics of high-T_c superconductors is still quite poorly understood. Therefore, one of the goals of studying the BCS-to-BEC evolution in these materials is to shed some light on what happens in the intermediate pair size regime ($k_F\xi_0 \sim 1$) in which these systems are believed to lie, and hopefully gain some further insight into the mechanism responsible for their high critical temperatures. However, the challenge is not simply to find a reasonable formula that predicts the uniquely high values for the superconducting transition temperature in the cuprates. Rather, superconductivity is but one aspect of the complex phase diagram exhibited by this class of materials, as shown

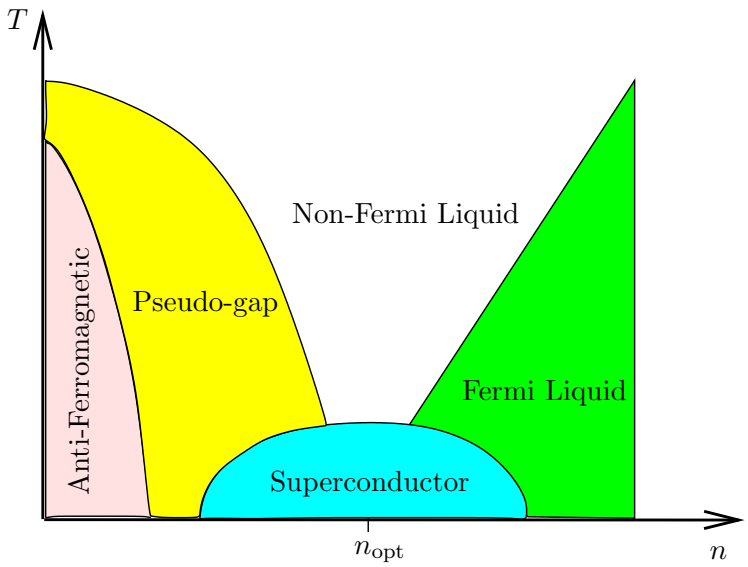

Figure 1.2: Phase diagram of temperature vs. doping level for a typical cuprate material.

schematically in Fig. 1.2. One should notice that, depending on the temperature and the level of doping, the cuprates can be insulators, metals or superconductors. Furthermore, there exists an optimal carrier concentration (denoted by n_{opt} in the figure) that leads to a maximum value of the critical temperature.

In the following two chapters, the zero-temperature BCS-to-BEC evolution in superconductors that exhibit d-wave pairing symmetry will be studied as a function of carrier concentration and fixed inter-particle interaction strength. The main result of this study is that, contrary to the smooth crossover observed in s-wave systems, there is a quantum phase transition between the BCS and BEC ground states of a two-dimensional d-wave superconductor. The occurrence of this phase transition is demonstrated by the calculation of several spectroscopic and thermodynamic properties of the system, such as its momentum distribution, electronic compressibility, superfluid density, and thermal conductivity.

1.1.2 Cold Atomic Gases

The study of ultra-cold atomic systems is a relatively recent area of physics, but experiments with highly degenerate quantum gases have provided researchers with valuable tools to explore exotic properties of matter in the extreme quantum mechanical limit. One of the most important breakthroughs in this field occurred in 1995, when a Bose-Einstein condensate

was produced for the first time in laboratory using ultra-cold alkali atoms. This experiment concluded a 15-year long quest for the BEC, which had been initially pursued in a vapor of spin-polarized Hydrogen atoms, as this system was believed to closely represent the original concept of Bose and Einstein due to the possibility of attaining extremely weak inter-atomic interactions. Somewhat later, developments in laser cooling and trapping, together with improvements in magnetic confinement techniques, allowed the BEC to be achieved in a vapor of alkali atoms (^{7}Li, ^{23}Na and ^{87}Rb in the first three pioneering experiments).

The successful realization of Bose-Einstein condensation in dilute atomic gases has triggered a great deal of activity in trying to cool fermionic atoms to quantum degeneracy. As discussed previously, one of the most appealing aspects of such experiments is the possibility of accessing the interplay between Fermi and Bose statistics in the same system. Several groups have already been able to reach Fermi degeneracy in atoms of ^{40}K and ^{6}Li by cooling the gas to temperatures down to a fraction of the Fermi temperature, using trapping and cooling techniques similar to those employed in the production of BECs. These systems present a unique opportunity to create well-controlled and accessible environments in which the strength of the inter-particle interaction can be varied with extreme precision by means of so-called Feshbach resonances. Such resonances occur when the energy of two free colliding atoms becomes degenerate to the energy of a weakly bound molecular state, which can be accomplished by varying the intensity of an externally applied magnetic field. The field dependence of the resonance allows precise tuning of the atom-atom interaction, which is usually characterized by a single parameter, the s-wave scattering length a_s. This mechanism constitutes a key ingredient in the recent experiments with degenerate Fermi atoms.

One of the main goals of ultracold gas research is to use this ability in controlling the interaction strength to drive the system continuously from a BCS-type limit of large and overlapping pairs of weakly attracting atoms in momentum space, to an opposite BEC regime of tightly bound and strongly interacting bosonic molecules. This BCS-to-BEC crossover from BCS-type superfluidity to Bose-Einstein condensation, which is schematically illustrated in Fig. 1.3, has attracted the interest of researchers long before the experiments

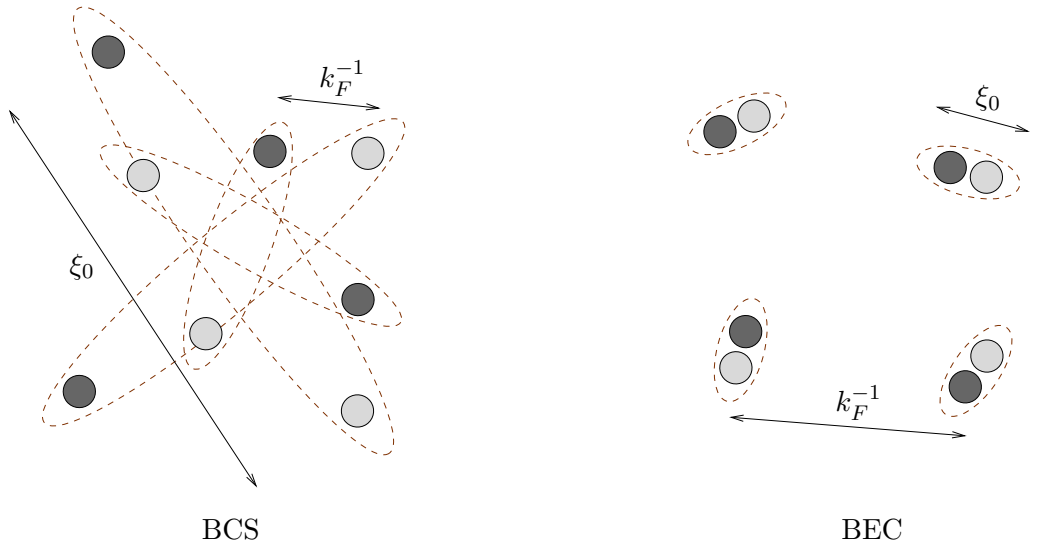

Figure 1.3: Schematic picture of the BCS ($\xi_0 \gg k_F^{-1}$) and BEC ($\xi_0 \ll k_F^{-1}$) regimes, where ξ_0 and k_F^{-1} are the typical coherence length (pair size) and inter-particle spacing, respectively.

with cold atoms became possible, specially in connection with high-T_c superconductivity. In fact, in a seminal paper of 1980 [5], Tony Leggett suggested that these two pictures were but limiting cases of a more general theory, the difference between them being simply how strongly the fermions attract each other. In this more general picture, the fermionic and bosonic degrees of freedom are expected to play equally important roles in the region of intermediate interaction strengths, whereas only the fermionic (bosonic) nature of the particles dominates the behavior of the system as the limit of weak (strong) coupling is approached.

1.2 Outline of the Thesis

The remaining of this thesis is organized as follows. Chapter II is dedicated to the discussion of a possible quantum phase transition in the BCS-to-BEC evolution of d-wave superconductors as a function of carrier concentration in two dimensions. The functional integral technique, which is the main mathematical tool used in this work, will be presented in this chapter. It will be applied to the derivation of the finite-temperature BCS equations of superconductivity, which will be shown to be merely saddle point (mean field) approximations to a more general and complete formulation. Then, in Chapter III, Gaussian fluctuations

about this saddle point solution will be included in the calculation, and the effect of this correction on the description of the system at low ($T \approx 0$) and high ($T \approx T_c$) temperatures will be analyzed. Finally, in Chapter IV, the same formalism will be applied to the study of a completely different physical system, namely, cold gases of spin-polarized fermionic atoms that exhibit p-wave pairing symmetry. We will argue that, contrary to what has been predicted (and observed) for s-wave gases, a quantum phase transition should occur as the inter-atomic interaction strength (characterized by the two-body bound state energy) is varied between the BCS (weak coupling) and BEC (strong coupling) regimes in the case of two-dimensional p-wave systems.

Four appendices are provided at the end of the thesis. The first one presents some fundamentals of the theory of second quantized operators. It constitutes a rather elementary treatment of the subject, and should be skipped by those already familiar with this formalism. Appendix B introduces the Feynman path integral technique, which is discussed in enough detail to make it accessible even to those completely unacquainted with the method. It also serves as a reference to the more powerful functional integral technique presented in Appendix C. A detailed discussion of bosonic and fermionic coherent states, which is pre-requisite to understanding functional integration, is also included in this appendix. Finally, Appendix D contains an overview of Matsubara sums, which appear frequently in finite temperature field-theoretical calcualtions, and are used several times in this work. The bibliographic references for all the thesis are listed on the final pages.

CHAPTER II

BCS-TO-BEC EVOLUTION IN D-WAVE SUPERCONDUCTORS

2.1 Introduction

The problem of the evolution from the BCS regime of large overlapping Cooper pairs to the BEC regime of tightly bound bosonic molecules has attracted the attention of researchers for many years. In particular, it has drawn renewed interest since the beginning of the last decade, due to the discovery of *high critical temperature superconductors*. The relationship between these two problems comes from the fact that the coherence length (or pair size) ξ_0 for the high-T_c materials is comparable to their average interparticle spacing (mean distance between charge carriers). In fact, the dimensionless parameter $k_F\xi_0$ was estimated to be as small as 10 for $La_{1.85}Sr_{0.15}CuO_4$, and approximately 5 for $YBa_2Cu_3O_7$ [6], in clear contrast to the traditional BCS superconductors, that have $k_F\xi_0 \sim 10^3 - 10^4$. This led to the suggestion that the high-T_c compounds are in the intermediate regime between Cooper pairs and composite bosons, which prompted further investigation of the transition region in order to better understand the physics behind the behavior of those materials. Nevertheless, despite years of intense experimental and theoretical activities, the development of a consistent theory of high-T_c superconductivity is still lacking, and the explanation of most of the properties of these materials remains an open and important problem.

One of the earliest attempts to study the BCS-to-BEC evolution was made by Eagles [7], who used BCS theory to explain some experimental results on superconductivity in Zr-doped $SrTiO_3$ at low carrier concentrations [8]. Assuming a constant attraction between electrons, the author numerically solved the simultaneous equations for the BCS order parameter Δ_0 and chemical potential μ at $T = 0$ for varying carrier concentrations. He also calculated the BCS critical temperature T_c as a function of carrier density, and discussed the possibility

that, at low concentrations, T_c might be better interpreted as a pairing temperature rather than as a superconducting transition temperature. The author then concluded that, in the case of three-dimensional systems, there is a critical value of the electron-electron interaction below which the BCS-to-BEC crossover does not occur. However, for two-dimensional films, he found that pairing without superconductivity might be attainable for any attractive interaction, due to the possibility of approximating the density of states by a constant when all carriers are in the lowest quantum state with respect to motion in the direction of the thickness.

The next step toward a better understanding of the BCS-to-BEC evolution was probably taken by Leggett [9]. Motivated by the problem of Cooper pairing in superfluid ^{3}He, the author used the variational ground-state wavefunction approach to study a simple model of fermions interacting via an isotropic (s-wave) attractive potential. He considered the case of three-dimensional systems at $T = 0$, and used the dimensionless parameter $1/k_F a_\ell$, where a_ℓ is the two-body scattering length and k_F is the Fermi momentum, as a measure of the effective interaction strength between the electrons. He then found that the point $1/k_F a_\ell = 0$, which corresponds to the onset of a two-body bound state formation, separates a BCS ground state of overlapping Cooper pairs ($1/k_F a_\ell \to -\infty$) from a Bose ground state of diatomic molecules ($1/k_F a_\ell \to +\infty$). However, he showed that this crossover happens smoothly as a function of interaction strength for an s-wave potential, and no phase transition occurs when the system is driven from one limit to the other.

Later on, the problem of the BCS-to-BEC evolution was studied by Nozières and Schmitt-Rink [10], who also considered a three-dimensional system of attractive fermions, but used a separable s-wave interparticle potential in k-space. They analyzed both the continuum and lattice models, the latter being tackled via the attractive Hubbard model with nearest-neighbor hopping. By using a diagrammatic technique, the authors also calculated the contribution from pair fluctuations to the thermodynamic potential, which led to a generalization of Leggett's results to finite temperatures. They obtained a transition temperature T_c (including effects of fluctuations in the order parameter) which evolved smoothly as a function of the attractive coupling from the BCS to the Bose limit, thus

concluding that there is no phase transition in the evolution from weak to strong coupling superconductivity in the case of s-wave interaction.

Many other theoretical papers that followed these three pioneer works investigated the BCS-to-BEC evolution in different contexts and situations. Sá de Melo *et al* [11] applied functional integral techniques to a system of fermions interacting via a zero-range (contact) s-wave potential in three dimensions. They showed that the mean field results become increasingly inadequate to describe the normal state properties of the system as the coupling increases. By including Gaussian fluctuations about the saddle point solution, they calculated the transition temperature T_c valid for all coupling, and described the evolution of the collective modes at zero temperature.

In Ref. [12], Andrenacci *et al* studied a three-dimensional continuum model of fermions interacting via a separable s-wave potential. They also examined the BCS-to-BEC evolution problem in a two-dimensional lattice by solving the extended Hubbard model for both s- and d-wave pairing. The issue of anisotropic superconductors was taken up by Wallington and Annett [13], who used functional integral techniques to study the case of mixed (s and d) symmetry states on a quasi-two-dimensional lattice at finite temperatures. More recently, Duncan and Sá de Melo [14] analyzed the spectroscopic and thermodynamic properties of d-wave superconductors within the saddle point (mean field) approximation for a continuum model in two dimensions, while Loktev and Turkowski, in a review paper [15], considered various types of indirect boson-exchange attractive interactions in two dimensions at $T = 0$.

Several different techniques were applied to the theoretical study of the BCS-to-BEC evolution. For example, in Ref. [16], a two-dimensional system of attractive fermions in the singlet d-wave channel was analyzed via a statistical Ginzburg-Landau theory. A study of the $T = 0$ collective mode spectrum of the two- and three-dimensional attractive Hubbard model was performed in Ref. [17] using a generalized random phase approximation (RPA) formulation. This same model was examined in Ref. [18] via quantum Monte-Carlo simulations in two dimensions, while its normal phase was analyzed within the dynamical mean field theory (DMFT) framework in Ref. [19]. Finally, a diagrammatic technique based on repeated Fourier transformation of the Green's functions of the system was used in Ref. [20]

to study three-dimensional interacting Fermi systems in the BCS-to-BEC crossover region.

The discovery of high-T_c superconductors has also spurred a great deal of experimental activity to investigate the transition from BCS superconductivity to Bose-Einstein condensation. One of the most important issues associated with the cuprate materials consists in the determination of the symmetry of the order parameter. Although a variety of experiments have shown that hole-doped cuprates possess a predominantly d-wave gap, there is evidence that pure s-wave pairing or even mixed $s + id$ symmetries can exist in some materials at certain doping levels [21]. In Ref. [22], scanning tunneling spectroscopy studies on $YBa_2Cu_3O_7$ revealed a crossover from d-wave pairing in the underdoped limit to $s + id$-wave pairing in the overdoped limit, whereas in Ref. [23], a d- to s-wave pairing transition was observed on $Pr_{2-x}Ce_xCuO_{4-y}$ and $Nd_{2-x}Ce_xCuO_{4-y}$ via magnetic penetration depth measurements.

A major challenge to the study of the BCS-to-BEC evolution in condensed matter systems is the precise manipulation of the carrier concentration without doping. One promising solution (despite some sad recent events [24] that decelerated further developments in the area) is presented by the *field effect transistors* (FETs), by means of which the charge density of some high-T_c oxide superconductors can be tuned by the application of an external electric field, inducing a reversible insulator-superconductor quantum phase transition [25]. Since most of the properties of the high-T_c materials are doping dependent, the possibility of driving the system from high to low densities at the turn of a knob becomes very appealing. Furthermore, the advantages of this procedure over chemical doping are obvious, since it makes unnecessary to prepare a new sample for each different data point in the experiment, not to mention other spurious effects (such as disorder) that could be otherwise introduced by the doping atoms.

Although there has been a vast amount of theoretical and experimental research dedicated to the subject of the BCS-to-BEC evolution, not much has been done in relation to d-wave superconductivity in continuum models and, in particular, to the analysis of fluctuations in the order parameter about the saddle point (mean field) solution in the case of anisotropic pairing. Therefore, in this chapter, our functional integral formulation of the

BCS-to-BEC problem in two-dimensional d-wave superconductors will be presented. We study spectroscopic properties (excitation spectrum and momentum distribution), thermodynamic quantities (electronic compressibility and superfluid density) and transport properties (thermal conductivity) as functions of both carrier density and interaction strength. Anticipating some of the results to be shown next, we find that a quantum phase transition occurs when the chemical potential crosses the bottom of the band, which leads to a logarithmic singularity in the compressibility at a critical concentration for fixed interaction (or at a critical interaction for fixed concentration) and to non-analytic behaviors of temperature derivatives of the superfluid density and thermal conductivity. The analysis of Gaussian fluctuations about the saddle point solution will be deferred to the next chapter.

The remaining of this chapter is organized as follows. In Section 2.2, the Hamiltonian of the system is described, and an approximate expression for interaction potential is derived. In Section 2.3, the functional integral analysis of the BCS-to-BEC evolution is performed, and the order parameter and number equations are obtained at the saddle point level of approximation. Then, in Section 2.4, our approach to the solution of these equations via numerical methods is outlined, and all our results for the relevant properties of d-wave superconductors across the BCS-to-BEC transition region are presented and discussed. Finally, in Section 2.5, our conclusions are summarized.

2.2 Hamiltonian and Interaction Potential

We study a two-dimensional continuum model of attractive fermions of mass m and density $n = k_F^2/2\pi$, where k_F is the Fermi momentum. The system is described by the Hamiltonian

$$\mathcal{H} = \sum_{\mathbf{k},\sigma} \epsilon_{\mathbf{k}} \psi^\dagger_{\mathbf{k},\sigma} \psi_{\mathbf{k},\sigma} + \sum_{\mathbf{k},\mathbf{k}',\mathbf{q}} V_{\mathbf{k}\mathbf{k}'} b^\dagger_{\mathbf{k}\mathbf{q}} b_{\mathbf{k}'\mathbf{q}}, \tag{2.1}$$

where $b_{\mathbf{k}\mathbf{q}} = \psi_{-\mathbf{k}+\mathbf{q}/2,\downarrow} \psi_{\mathbf{k}+\mathbf{q}/2,\uparrow}$ is the pairing operator and $\epsilon_{\mathbf{k}} = k^2/2m$ is the free-particle dispersion relation, and we have used $\hbar = 1$. The interaction described by the second term in this Hamiltonian is shown schematically in Fig. 2.1, which represents the scattering of two electrons with opposite spins and total momentum $\mathbf{q}$ (conserved in the process).

We now explain in some detail how an approximate expression for the electron-electron

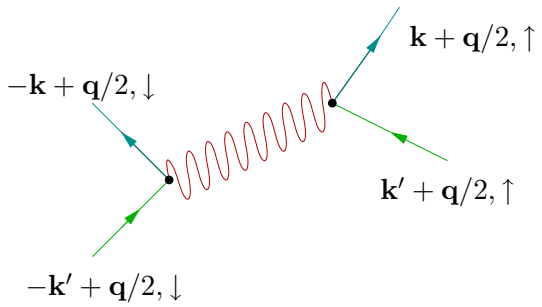

Figure 2.1: Scattering of two electrons with opposite spins and total momentum $\mathbf{q}$.

interaction can be obtained. We start by using the Fourier expansion of a plane wave in two dimensions,

$$e^{i\mathbf{k}\cdot\mathbf{r}} = \sum_{\ell=-\infty}^{\infty} i^{\ell}\, J_{\ell}(kr)\, e^{i\ell\phi}, \tag{2.2}$$

where $\phi = \arccos(\hat{\mathbf{k}}\cdot\hat{\mathbf{r}})$ and $J_{\ell}(kr)$ is a Bessel function of order ℓ, into the matrix element $V_{\mathbf{k}\mathbf{k}'}$ of the interaction potential in k-space. This leads to

$$V_{\mathbf{k}\mathbf{k}'} = \langle \mathbf{k}|V|\mathbf{k}'\rangle = \sum_{\ell=-\infty}^{\infty} e^{i\ell\theta_{\mathbf{k}\mathbf{k}'}}\, V_{kk'}^{(\ell)}, \tag{2.3}$$

where $\theta_{\mathbf{k}\mathbf{k}'} = \arccos(\hat{\mathbf{k}}\cdot\hat{\mathbf{k}}')$ is the angle between the vectors $\mathbf{k}$ and $\mathbf{k}'$. The k-dependent coefficients $V_{kk'}^{(\ell)}$ are related to the real space potential $V(r)$ through a Bessel transform,

$$V_{kk'}^{(\ell)} = 2\pi \int_0^{\infty} dr\, r\, J_{\ell}(kr) J_{\ell}(k'r) V(r), \tag{2.4}$$

where the index ℓ labels angular momentum states in two spatial dimensions, with $\ell = 0, \pm 1, \pm 2, \ldots$ corresponding to $s, p, d, \ldots$ channels, respectively.

It is instructive to analyze the behavior of $V_{kk'}^{(\ell)}$ in the limits of large and small k. In the long wavelength limit ($k \to 0$), one can show that the dependence of the potential on k and k' becomes exactly separable. In fact, for $kr \ll 1$ and $k'r \ll 1$, the following asymptotic expression for the Bessel function of order n becomes valid:

$$J_n(x) \approx \frac{1}{n!}\left(\frac{x}{2}\right)^n, \quad \text{for } x \ll 1. \tag{2.5}$$

Using this approximation in Eq.(2.4), one obtains:

$$V_{kk'}^{(\ell)} = \frac{2\pi}{(2^{\ell}\ell!)^2} k^{\ell}(k')^{\ell} \int_0^{\infty} dr\, r^{2\ell+1}\, V(r). \tag{2.6}$$

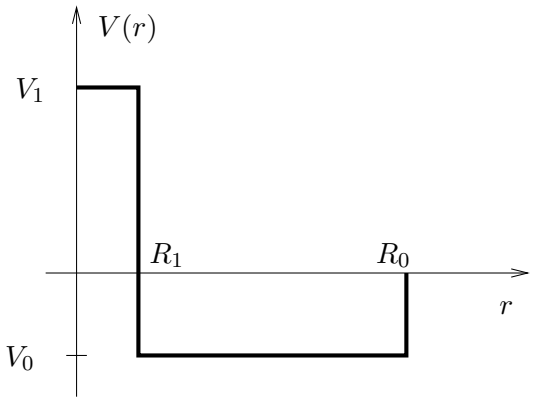

Figure 2.2: Plot of a possible real space interatomic potential $V(r)$.

Notice that $V_{kk'}^{(\ell)} = C_\ell k^\ell (k')^\ell$, with the coefficient C_ℓ dependent only on the particular choice of the real space potential. In the opposite limit of short wavelengths ($kr \gg 1$ and $k'r \gg 1$), the k and k' dependences of the potential will not be as simply separable as in the long wavelength limit. In fact, one can follow the same procedure and use an asymptotic expression for the Bessel function (this time for large arguments),

$$J_n(x) \approx \left(\frac{2}{\pi x}\right)^{1/2} \cos\left(x - \frac{n\pi}{2} - \frac{\pi}{4}\right), \quad \text{for } x \gg 1, \tag{2.7}$$

in the equation for the coefficients $V_{kk'}^{(\ell)}$. This results in

$$V_{kk'}^{(\ell)} = \frac{4}{k^{1/2}(k')^{1/2}} \int_0^\infty dr\, V(r) \cos\left(kr - \frac{\ell\pi}{2} - \frac{\pi}{4}\right) \cos\left(k'r - \frac{\ell\pi}{2} - \frac{\pi}{4}\right), \tag{2.8}$$

which is clearly not separable. In fact, $V_{kk'}^{(\ell)}$ mixes different values of k and k', and shows an oscillatory behavior dependent on the exact form of $V(r)$, with a decaying envelope that is always proportional to $k^{-1/2}(k')^{-1/2}$.

A possible choice of the real space potential that captures the essence of the interparticle interactions, but at the same time is simple enough to allow analytic manipulations, is given by

$$V(r) = V_1 \Theta(R_1 - r) + V_0 \Theta(r - R_1)\Theta(R_0 - r), \tag{2.9}$$

which is plotted in Fig. 2.2. This potential is repulsive at short distances $r < R_1$, attractive at intermediate distances $R_1 < r < R_0$, and vanishes for $r > R_0$, provided that $V_1 > 0$ and $V_0 < 0$. This class of potentials also includes as particular cases the delta-function

interaction with zero range ($V_1 \to -\infty$, $V_0 = 0$ and $R_0 = R_1 = 0$) and the purely attractive potential with range R_0 ($V_1 < 0$, $V_0 = 0$ and $R_0 = R_1$). Using this as the real space potential in Eq.(2.6), the long wavelength limit of the coefficient $V_{kk'}^{(\ell)}$ becomes

$$V_{kk'}^{(\ell)} = \frac{2\pi}{(2^\ell \ell!)^2} \frac{1}{2\ell+2} k^\ell \, (k')^\ell \left[(V_1 - V_0) R_1^{2\ell+2} + V_0 R_0^{2\ell+2} \right]. \tag{2.10}$$

Under these circumstances, it is generally not possible to find an interaction potential whose k and k' dependences are always exactly separable. Nevertheless, we choose to study an interaction that contains most of the general features described above. For this purpose, we use the following separable function in k-space,

$$V_{\mathbf{k}\mathbf{k}'} = -\lambda \Gamma(\mathbf{k}) \Gamma(\mathbf{k}'), \tag{2.11}$$

where $\lambda > 0$ is the interaction strength, and $\Gamma(\mathbf{k})$ is defined as

$$\Gamma(\mathbf{k}) = h(k) \, g(\hat{\mathbf{k}}). \tag{2.12}$$

The function $h(k)$, which depends only on the magnitude k of the wave-vector $\mathbf{k}$ and is given by

$$h(k) = \frac{(k/k_1)^\ell}{(1 + k/k_0)^{\ell+1/2}}, \tag{2.13}$$

controls the range of the interaction, with $R_0 \sim k_0^{-1}$ playing the role of the interaction range, and k_1 setting the scale at low momenta. Notice that the constants k_0 and k_1 are not momentum cutoffs, but merely set the scales in the short and long wavelength limits. This function indeed reduces to $h(k) \sim k^\ell$ for small k, and behaves as $h(k) \sim k^{-1/2}$ for large k, which guarantees the correct behavior expected for $V_{kk'}^{(\ell)}$ according to the previous analysis. The angular function $g(\hat{\mathbf{k}})$, which depends only on the direction of the vector $\mathbf{k}$, is obtained by retaining only the $\pm\ell$ terms in Eq.(2.3), which results in

$$g(\hat{\mathbf{k}}) = \cos(\ell\varphi), \tag{2.14}$$

where φ is the momentum angle in polar coordinates. Physically, this amounts to isolating only the contribution from the ℓ^{th} angular momentum channel to the scattering process responsible for the interaction between the electrons. In particular, in the case of d-wave

pairing ($\ell = 2$) that will be discussed in this chapter, the function $\Gamma(\mathbf{k})$ becomes

$$\Gamma(\mathbf{k}) = \frac{(k/k_1)^2}{(1 + k/k_0)^{5/2}} \cos(2\varphi). \tag{2.15}$$

In the limit of small momenta, this approach is identical to the T-matrix formalism [9], but has the added advantage of making unnecessary to introduce a scattering length as a relevant parameter, which can be quite problematic in two dimensions [26].

2.3 Effective Action and Saddle Point Equations

In this section, we begin the analysis of the functional integral formulation of the BCS-to-BEC crossover problem in d-wave superconductors. This technique consists of a very powerful field-theoretical tool, which has been vastly applied to numerous problems in the areas of quantum many-body systems and strongly-correlated particles. For those not familiar with the method, a detailed review has been provided in Appendix C of this thesis, which is mostly based on Ref. [27]. A more advanced reference is Popov [28], which also considers many applications to physical systems.

Roughly speaking, the method of functional integration consists in a generalization of the Feynman path integral, in which the grand-canonical partition function of a system is written in terms of integrals over fermionic or bosonic coherent states, instead of the usual momentum and position eigenstates. And since the coherent states form a basis of eigenvectors of the annihilation operators in Fock space, this technique provides a suitable framework to treat general many-particle Hamiltonians expressed in second quantized form. Furthermore, one of the merits of this approach is that, in addition to recovering previously known results within a single formalism, one is able to go beyond and gain further insight into the physics of the problem. In particular, by including fluctuations about the saddle point solutions, the method leads to the determination of the collective modes of the system, which become extremely important at finite temperatures. In the present case, for example, the functional integral formulation will not only lead to the derivation of the BCS equations of superconductivity, but will also allow us to go beyond the mean field solutions and study the corrections to these equations due to Gaussian fluctuations.

For a fermionic system in equilibrium with both a particle and a thermal reservoir, the grand-canonical partition function can be written as a functional integral over the Fermi field ψ with action $S[\psi^\dagger, \psi]$ as

$$\mathcal{Z} = \oint_{\psi(0)=-\psi(\beta)} \mathcal{D}[\psi^\dagger, \psi]\, e^{-S[\psi^\dagger,\psi]}, \tag{2.16}$$

where the constraint $\psi(0) = -\psi(\beta)$ implies that the integration is over fermionic (Grassman) variables satisfying anti-periodic boundary conditions, and the Euclidian action $S[\psi^\dagger, \psi]$ is given by

$$S[\psi^\dagger, \psi] = \int_0^\beta d\tau \left[\sum_{\mathbf{k},\sigma} \psi^\dagger_{\mathbf{k}\sigma}(\partial_\tau - \mu)\psi_{\mathbf{k}\sigma} + \mathcal{H}(\psi^\dagger, \psi) \right], \tag{2.17}$$

where μ is the chemical potential and $\beta = T^{-1}$, where T is the temperature. We adopt a system of units in which $k_B = \hbar = 1$.

Before proceeding, it is convenient to express the Hamiltonian in a slightly different way. Using the separable form of the interparticle potential, $V_{\mathbf{k}\mathbf{k}'} = -\lambda\Gamma(\mathbf{k})\Gamma(\mathbf{k}')$, one can rewrite the Hamiltonian given in Eq.(2.1) as

$$\mathcal{H} = \sum_{\mathbf{k},\sigma} \epsilon_{\mathbf{k}} \psi^\dagger_{\mathbf{k}\sigma}\psi_{\mathbf{k}\sigma} - \lambda \sum_{\mathbf{q}} \zeta^\dagger_{\mathbf{q}}\zeta_{\mathbf{q}}, \tag{2.18}$$

where the auxiliary function $\zeta_{\mathbf{q}}$ is defined as

$$\zeta_{\mathbf{q}} = \sum_{\mathbf{k}} \Gamma(\mathbf{k})\psi_{-\mathbf{k}+\mathbf{q}/2,\downarrow}\, \psi_{\mathbf{k}+\mathbf{q}/2,\uparrow}. \tag{2.19}$$

Using these expressions in Eq.(2.17), and then plugging the action back into Eq.(2.16), the functional integral equation for the partition function becomes

$$\mathcal{Z} = \oint_{\psi(0)=-\psi(\beta)} \mathcal{D}[\psi^\dagger, \psi]\, e^{-\int_0^\beta d\tau \sum_{\mathbf{k},\sigma} \psi^\dagger_{\mathbf{k}\sigma}(\partial_\tau + \xi_{\mathbf{k}})\psi_{\mathbf{k}\sigma}}\, e^{\lambda \int_0^\beta d\tau \sum_{\mathbf{q}} \zeta^\dagger_{\mathbf{q}}\zeta_{\mathbf{q}}}, \tag{2.20}$$

where the definition $\xi_{\mathbf{k}} = \epsilon_{\mathbf{k}} - \mu$ was used.

This expression can be further simplified by means of the so-called Hubbard-Stratonovich transformation, which consists in introducing an auxiliary field $\phi_{\mathbf{q}}(\tau)$ which couples to $\psi^\dagger\psi^\dagger$. This procedure renders the action quadratic in the fermion fields, enabling one to integrate out the fermionic degrees of freedom. In the present case, this transformation can be

implemented by rewriting the second exponential in the integrand of Eq.(2.20) in terms of a functional Gaussian integral[1] over the (bosonic) field ϕ, that is,

$$e^{\lambda\int_0^\beta d\tau\sum_{\mathbf{q}}\zeta^\dagger_{\mathbf{q}}\zeta_{\mathbf{q}}}=\int\mathcal{D}[\phi^*,\phi]\,e^{\int_0^\beta d\tau\sum_{\mathbf{q}}\left(-\frac{1}{\lambda}|\phi_{\mathbf{q}}|^2+\zeta^\dagger_{\mathbf{q}}\phi_{\mathbf{q}}+\zeta_{\mathbf{q}}\phi^*_{\mathbf{q}}\right)}. \tag{2.21}$$

Substituting this relation back into the equation for the partition function, swapping the bosonic and fermionic functional integrations, and using the definition Eq.(2.19) of $\zeta_{\mathbf{q}}$ in terms of the fermionic fields ψ, the partition function can be written (in full form) as

$$\begin{aligned}\mathcal{Z}=&\int\mathcal{D}[\phi^*,\phi]\,\exp\left[-\frac{1}{\lambda}\int_0^\beta d\tau\sum_{\mathbf{q}}|\phi_{\mathbf{q}}|^2\right]\times\\ &\times\oint_{\psi(0)=-\psi(\beta)}\mathcal{D}[\psi^\dagger,\psi]\,\exp\left[-\int_0^\beta d\tau\sum_{\mathbf{k},\mathbf{k}',\sigma}\psi^\dagger_{\mathbf{k}\sigma}(\partial_\tau+\xi_{\mathbf{k}})\psi_{\mathbf{k}'\sigma}\delta_{\mathbf{k}\mathbf{k}'}+\right.\\ &\left.+\int_0^\beta d\tau\sum_{\mathbf{k},\mathbf{q}}\Gamma(\mathbf{k})\left(\psi^\dagger_{\mathbf{k}+\mathbf{q}/2,\uparrow}\psi^\dagger_{-\mathbf{k}+\mathbf{q}/2,\downarrow}\phi_{\mathbf{q}}+\psi_{-\mathbf{k}+\mathbf{q}/2,\downarrow}\psi_{\mathbf{k}+\mathbf{q}/2,\uparrow}\phi^*_{\mathbf{q}}\right)\right].\end{aligned} \tag{2.22}$$

In order to cast this expression in a more convenient way, the integrand of the fermionic functional integral can be written in matrix form. In order to do so, two properties of the Fermi field $\psi_{\mathbf{k}\sigma}$ have to be used:

(i) Anti-commutation relation: $\{\psi^\dagger_{\mathbf{k}\sigma}(\tau),\psi_{\mathbf{k}'\sigma}(\tau)\}=\delta_{\mathbf{k}\mathbf{k}'}$.

Using this, one can write

$$\sum_{\mathbf{k},\mathbf{k}'}\psi^\dagger_{\mathbf{k}\sigma}(\tau)\xi_{\mathbf{k}}\psi_{\mathbf{k}'\sigma}(\tau)=\sum_{\mathbf{k}}\xi_{\mathbf{k}}-\sum_{\mathbf{k},\mathbf{k}'}\psi_{\mathbf{k}'\sigma}(\tau)\xi_{\mathbf{k}}\psi^\dagger_{\mathbf{k}\sigma}(\tau). \tag{2.23}$$

(ii) Imaginary-time boundary condition: $\psi_{\mathbf{k}\sigma}(\beta)=-\psi_{\mathbf{k}\sigma}(0)$.

Integrating by parts, one can conclude from this property that

$$\int_0^\beta d\tau\,\psi^\dagger_{\mathbf{k}\sigma}(\tau)\partial_\tau\psi_{\mathbf{k}\sigma}(\tau)=\int_0^\beta d\tau\,\psi_{\mathbf{k}\sigma}(\tau)\partial_\tau\psi^\dagger_{\mathbf{k}\sigma}(\tau). \tag{2.24}$$

With the help of these properties, and using the following variable transformation,

$$\begin{cases}\mathbf{k}+\mathbf{q}/2\to\mathbf{k}'\\ \mathbf{k}-\mathbf{q}/2\to\mathbf{k},\end{cases} \tag{2.25}$$

[1]Such Gaussian integrals are also discussed in Appendix C.

one can show by direct inspection that the expression for the partition function given by Eq.(2.22) reduces to

$$\mathcal{Z} = \int \mathcal{D}[\phi^*, \phi]\, e^{-\int_0^\beta d\tau \sum_{\mathbf{k}} \left(\frac{1}{\lambda} |\phi_{\mathbf{k}}(\tau)|^2 + \xi_{\mathbf{k}} \right)} \oint_{\psi(0) = -\psi(\beta)} \mathcal{D}[\psi^\dagger, \psi]\, e^{\int_0^\beta d\tau \sum_{\mathbf{k},\mathbf{k}'} \mathbf{v}^\dagger_{\mathbf{k}}(\tau)\, \mathbf{G}^{-1}_{\mathbf{k},\mathbf{k}'}(\tau)\, \mathbf{v}_{\mathbf{k}'}(\tau)}, \quad (2.26)$$

where the matrix $\mathbf{G}^{-1}_{\mathbf{k},\mathbf{k}'}(\tau)$, which is known as the (inverse) Nambu propagator, is given by

$$\mathbf{G}^{-1}_{\mathbf{k},\mathbf{k}'}(\tau) = \begin{pmatrix} -(\partial_\tau + \xi_{\mathbf{k}})\delta_{\mathbf{k}\mathbf{k}'} & \Gamma\left(\frac{\mathbf{k}+\mathbf{k}'}{2}\right) \phi_{\mathbf{k}-\mathbf{k}'}(\tau) \\ \Gamma\left(\frac{\mathbf{k}+\mathbf{k}'}{2}\right) \phi^*_{\mathbf{k}'-\mathbf{k}}(\tau) & -(\partial_\tau - \xi_{\mathbf{k}})\delta_{\mathbf{k}\mathbf{k}'} \end{pmatrix}, \quad (2.27)$$

while the two-dimensional vector $\mathbf{v}_{\mathbf{k}}(\tau)$ is defined as

$$\mathbf{v}_{\mathbf{k}}(\tau) = \begin{pmatrix} \psi_{\mathbf{k}\uparrow}(\tau) \\ \psi^\dagger_{-\mathbf{k}\downarrow}(\tau) \end{pmatrix}. \quad (2.28)$$

Finally, as mentioned before, the introduction of the Hubbard-Stratonovich field allows the integral with respect to the fermionic variables to be performed. In fact, the functional integration over the ψ-field in Eq.(2.26) can be evaluated exactly by means of a Gaussian integral for Grassman variables, resulting simply in $\det \mathbf{G}^{-1}_{\mathbf{k},\mathbf{k}'}(\tau)$. Plugging this result back into Eq.(2.26), and using the fact that, for an arbitrary matrix $\mathbf{A}$,

$$\ln(\det \mathbf{A}) = \mathrm{tr}(\ln \mathbf{A}), \quad (2.29)$$

the grand-canonical partition function of the system can be written only in terms of the bosonic field ϕ as

$$\mathcal{Z} = \int \mathcal{D}[\phi^*, \phi]\, e^{-S_{\mathrm{eff}}[\phi^*, \phi]}, \quad (2.30)$$

with the effective action $S_{\mathrm{eff}}[\phi^*, \phi]$ given by

$$S_{\mathrm{eff}}[\phi^*, \phi] = \int_0^\beta d\tau \sum_{\mathbf{k}} \left(\frac{1}{\lambda} |\phi_{\mathbf{k}}(\tau)|^2 + \xi_{\mathbf{k}} \right) - \mathbf{Tr} \left(\ln \mathbf{G}^{-1}_{\mathbf{k},\mathbf{k}'}(\tau) \right), \quad (2.31)$$

where the notation **Tr** indicates not only the trace over matrix elements, but also over momentum and time coordinates, that is, $\mathbf{Tr} \rightarrow \int_0^\beta d\tau \sum_{\mathbf{k},\mathbf{k}'} \mathrm{tr}$.

2.3.1 Order Parameter Equation

As discussed earlier, one of the advantages of the functional integral formalism is that it allows the recovery of some known results within the same framework. In fact, the BCS order parameter equation can be immediately derived from the effective action obtained above by considering a static and uniform saddle point $\phi_{\mathbf{k}}(\tau) = \Delta_0$ of the functional integral given by Eq.(2.30), which satisfies the stationarity condition

$$\left.\frac{\delta S_{\text{eff}}}{\delta \phi^*_{\mathbf{q}}(\tau')}\right|_{\Delta_0} = 0. \tag{2.32}$$

Using the fact that, for an arbitrary matrix $\mathbf{A}$ that depends on the variable x,

$$\text{tr}\left(\frac{\partial}{\partial x}\ln \mathbf{A}(x)\right) = \text{tr}\left(\mathbf{A}^{-1}(x)\frac{\partial}{\partial x}\mathbf{A}(x)\right), \tag{2.33}$$

and applying the stationarity condition to the effective action $S_{\text{eff}}[\phi^*, \phi]$ given by Eq.(2.31), one obtains

$$\int_0^\beta d\tau \left\{ \sum_{\mathbf{k}} \frac{1}{\lambda}\phi_{\mathbf{k}}(\tau)\delta_{\mathbf{k},\mathbf{q}} - \sum_{\mathbf{k},\mathbf{k}'} \text{tr}\left[\mathbf{G}_{\mathbf{k},\mathbf{k}'}(\tau)\frac{\delta}{\delta\phi^*_{\mathbf{q}}(\tau')}\mathbf{G}^{-1}_{\mathbf{k},\mathbf{k}'}(\tau)\right]\right\}_{\Delta_0} = 0. \tag{2.34}$$

The evaluation of the integral over τ in this equation can be substantially simplified by Fourier transforming from time τ to Matsubara frequencies ω_n. This transformation results in the replacement of the integral by a so-called Matsubara sum over ω_n. These frequency (or Matsubara) sums, which are very common in many-body physics calculations, are discussed in the Appendix D of this thesis, and are treated in more detail in Ref. [29]. The matrices $\mathbf{G}_{\mathbf{k},\mathbf{k}'}(\tau)$ and $\mathbf{G}^{-1}_{\mathbf{k},\mathbf{k}'}(\tau)$ can be Fourier transformed by means of the relations

$$\begin{cases} \mathbf{G}_{\mathbf{k},\mathbf{k}'}(\tau) = \sum_{\omega_n} e^{i\omega_n\tau}\,\mathcal{G}_{\mathbf{k},\mathbf{k}'}(i\omega_n); \\ \mathbf{G}^{-1}_{\mathbf{k},\mathbf{k}'}(\tau) = \frac{1}{\beta}\sum_{\omega_n} e^{-i\omega_n\tau}\,\mathcal{G}^{-1}_{\mathbf{k},\mathbf{k}'}(i\omega_n), \end{cases} \tag{2.35}$$

where $\mathcal{G}^{-1}_{\mathbf{k},\mathbf{k}'}(i\omega_n)$ can be obtained from $\mathbf{G}^{-1}_{\mathbf{k},\mathbf{k}'}(\tau)$ by simply replacing $\partial_\tau \to -i\omega_n$, such that its inverse $\mathcal{G}_{\mathbf{k},\mathbf{k}'}(i\omega_n)$ becomes

$$\mathcal{G}_{\mathbf{k},\mathbf{k}'}(i\omega_n) = \frac{1}{(i\omega_n)^2 - E^2_{\mathbf{k}}}\begin{pmatrix} (i\omega_n + \xi_{\mathbf{k}})\delta_{\mathbf{k}\mathbf{k}'} & -\Gamma\left(\frac{\mathbf{k}+\mathbf{k}'}{2}\right)\phi_{\mathbf{k}-\mathbf{k}'}(i\omega_n) \\ -\Gamma\left(\frac{\mathbf{k}+\mathbf{k}'}{2}\right)\phi^*_{\mathbf{k}'-\mathbf{k}}(i\omega_n) & (i\omega_n - \xi_{\mathbf{k}})\delta_{\mathbf{k}\mathbf{k}'} \end{pmatrix}. \tag{2.36}$$

The quantity $E_{\mathbf{k}} = \sqrt{\xi_{\mathbf{k}}^2 + \Delta_{\mathbf{k}}^2}$ is the quasiparticle excitation energy, where $\Delta_{\mathbf{k}} = \Delta_0 \Gamma(\mathbf{k})$ plays the role of the order parameter function. Fourier transforming Eq.(2.34) to Matsubara frequencies, using the matrices $\mathcal{G}_{\mathbf{k},\mathbf{k}'}(i\omega_n)$ and $\mathcal{G}^{-1}_{\mathbf{k},\mathbf{k}'}(i\omega_n)$, and performing the necessary matrix operations (including the trace over Nambu indices), one finds

$$\frac{\beta}{\lambda} = -\sum_{\mathbf{k}} \Gamma^2(\mathbf{k}) \sum_{\omega_n} \frac{1}{(i\omega_n)^2 - E_{\mathbf{k}}^2}. \tag{2.37}$$

Finally, the remaining Matsubara sum over ω_n can be evaluated with the help of the following result (which is derived in Appendix D),

$$\sum_{\omega_n} \frac{1}{i\omega_n \pm E_{\mathbf{k}}} = \frac{\beta}{2} \left[1 \pm \tanh\left(\frac{\beta E_{\mathbf{k}}}{2} \right) \right], \tag{2.38}$$

leading to the well-known [30] order parameter equation for the case of a separable interparticle potential in k-space,

$$\frac{1}{\lambda} = \sum_{\mathbf{k}} \frac{\Gamma^2(\mathbf{k})}{2E_{\mathbf{k}}} \tanh\left(\frac{\beta E_{\mathbf{k}}}{2} \right). \tag{2.39}$$

2.3.2 Number Equation

The BCS equation for the number of charge carriers in the system can also be obtained from this functional integral formalism at the saddle point level of approximation. The starting point of this calculation is the saddle point approximation for the grand-canonical partition function, which can be shown to be

$$\mathcal{Z}_0 = e^{-S_{\text{eff}}[\Delta_0]}, \tag{2.40}$$

where $S_{\text{eff}}[\Delta_0]$ is obtained from the effective action $S_{\text{eff}}[\phi^*, \phi]$ derived above by taking $\phi_{\mathbf{k}}(\tau) = \Delta_0 \delta_{\mathbf{k},0}$. The resulting thermodynamic potential, $\Omega_0 = -\beta^{-1} \ln \mathcal{Z}_0 = S_{\text{eff}}[\Delta_0]/\beta$, leads to the following saddle point (mean field) expression for the number of particles

$$N_0 = -\left(\frac{\partial \Omega_0}{\partial \mu} \right)_T = -\frac{1}{\beta} \frac{\partial}{\partial \mu} S_{\text{eff}}[\Delta_0], \tag{2.41}$$

which can be rewritten, after substituting the saddle point action $S_{\text{eff}}[\Delta_0]$, as

$$N_0 = -\frac{1}{\beta} \frac{\partial}{\partial \mu} \left\{ \int_0^\beta d\tau \sum_{\mathbf{k}} \left(\frac{1}{\lambda} \Delta_0^2 + \xi_{\mathbf{k}} \right) - \mathbf{Tr} \left(\ln \mathbf{G}^{(0)-1}_{\mathbf{k},\mathbf{k}'}(\tau) \right) \right\}, \tag{2.42}$$

where the matrix $\mathbf{G}^{(0)-1}_{\mathbf{k},\mathbf{k}'}(\tau)$ can be derived from $\mathbf{G}^{-1}_{\mathbf{k},\mathbf{k}'}(\tau)$ through the same procedure of taking $\phi_{\mathbf{k}}(\tau) = \Delta_0 \delta_{\mathbf{k},0}$. Using Eq.(2.33) to work out the derivative of the logarithm of a matrix, applying Eq.(2.35) to perform the Fourier transformation from time to Matsubara frequencies, and evaluating the required matrix operations and the trace over Nambu indices, one finds

$$N_0 = \sum_{\mathbf{k}} \left\{ 1 + \frac{2\xi_{\mathbf{k}}}{\beta} \sum_{\omega_n} \frac{1}{(i\omega_n)^2 - E^2_{\mathbf{k}}} \right\}. \tag{2.43}$$

Performing the frequency sum, this finally becomes the BCS number equation, which is more appropriately written as

$$N_0 = 2 \sum_{\mathbf{k}} n_{\mathbf{k}}, \tag{2.44}$$

where $n_{\mathbf{k}}$ is known as the momentum distribution, and is given by

$$n_{\mathbf{k}} = \frac{1}{2} \left[1 - \frac{\xi_{\mathbf{k}}}{E_{\mathbf{k}}} \tanh \left(\frac{\beta E_{\mathbf{k}}}{2} \right) \right]. \tag{2.45}$$

Instead of proceeding with the functional integral analysis of the problem, the remaining of this chapter will be dedicated to the presentation and discussion of the results that can be obtained at the saddle point level of approximation. In what follows, the zero-temperature order parameter and number equations will be solved numerically for Δ_0 and μ as functions of carrier density and interaction strength, and some spectroscopic and thermodynamic properties of d-wave superconductors in the BCS-to-BEC crossover region will be examined. The analysis of fluctuations about the saddle point solution, as well as finite temperature corrections, will be postponed to the next chapter.

2.4 Numerical Calculations

When solving a problem via numerical methods, one always has to deal beforehand with the issue of the scaling of variables. Since real quantities and parameters are usually cumbersome to manipulate with a computer, one has to devise a conversion scheme that allows standard physical values to be represented as simple and manageable numbers.

The scaling scheme we adopted in all calculations presented in this chapter is based on the diluteness condition, that is, the assumption that the BCS-to-BEC evolution can be

safely analyzed provided that the system is dilute enough ($k_F^2 \ll k_0^2$), i.e., the square of the interparticle spacing ($\sim k_F^{-1}$) is much larger than the square of the interaction range ($\sim k_0^{-1}$). This condition implies that there must be a maximum density $n_{\max}$ above which the distances between particles become comparable to the potential range, and the system ceases to be dilute. And since the carrier density n and the Fermi momentum k_F are related via $n = k_F^2/2\pi$, this leads to a maximum Fermi momentum of $k_{F_{\max}} = \sqrt{2\pi n_{\max}}$. Therefore, it becomes natural (and, as it turns out, convenient) to scale all energies with respect to $\epsilon_{F_{\max}} = k_{F_{\max}}^2/2m$, defining the dimensionless single-particle energy $\tilde{\epsilon}_{\mathbf{k}}$ as

$$\tilde{\epsilon}_{\mathbf{k}} = \frac{\epsilon_{\mathbf{k}}}{\epsilon_{F_{\max}}}, \tag{2.46}$$

and to scale all momenta with respect to $k_{F_{\max}}$, introducing the dimensionless wave-number $\tilde{k}$ defined as

$$\tilde{k} = \frac{k}{k_{F_{\max}}}, \tag{2.47}$$

such that $\tilde{\epsilon}_{\mathbf{k}} = \tilde{k}^2$. Therefore, the chemical potential and order parameter will be replaced by the scaled variables $\tilde{\mu} = \mu/\epsilon_{F_{\max}}$ and $\tilde{\Delta}_{\mathbf{k}} = \Delta_{\mathbf{k}}/\epsilon_{F_{\max}}$, respectively, such that the dimensionless excitation energy $\tilde{E}_{\tilde{\mathbf{k}}}$ will be

$$\tilde{E}_{\tilde{\mathbf{k}}} = \frac{E_{\mathbf{k}}}{\epsilon_{F_{\max}}} = \sqrt{(\tilde{k}^2 - \tilde{\mu})^2 + \tilde{\Delta}_{\tilde{\mathbf{k}}}^2}. \tag{2.48}$$

The next step is to rewrite the saddle point equations derived in the last section in dimensionless form. The summations over $\mathbf{k}$ can be converted into two-dimensional integrals with respect to the variables k and φ (polar coordinates) by means of the transformation

$$\sum_{\mathbf{k}} \rightarrow \frac{L^2}{(2\pi)^2} \int_0^{2\pi} d\varphi \int_0^{\infty} dk\, k, \tag{2.49}$$

where L^2 is the two-dimensional "volume" of the system. After appropriately scaling all variables in Eq.(2.44), the zero-temperature number equation can be written in terms of the dimensionless density $\tilde{n}$ as

$$\tilde{n} \equiv 2\pi \frac{n}{n_{\max}} = \int_0^{2\pi} d\varphi \int_0^{\infty} d\tilde{k}\, \tilde{k} \left[1 - \frac{\tilde{k}^2 - \tilde{\mu}}{\sqrt{(\tilde{k}^2 - \tilde{\mu})^2 + \tilde{\Delta}_0^2 \Gamma^2(\tilde{\mathbf{k}})}} \right]. \tag{2.50}$$

Meanwhile, starting with Eq.(2.39) and following the same procedure, the order parameter equation at $T = 0$ can be cast in terms of the dimensionless interaction strength $\tilde{\lambda}$ as

$$\frac{1}{\tilde{\lambda}} \equiv \frac{1}{g_{2\mathrm{D}}\,\lambda} = \frac{1}{\pi}\int_0^{2\pi} d\varphi \int_0^{\infty} d\tilde{k}\,\tilde{k}\,\frac{\Gamma^2(\tilde{\mathbf{k}})}{2\sqrt{(\tilde{k}^2-\tilde{\mu})^2+\tilde{\Delta}_0^2\Gamma^2(\tilde{\mathbf{k}})}}, \tag{2.51}$$

where $g_{2\mathrm{D}} = mL^2/2\pi$ is the density of states in two dimensions (number of available states per unit energy and per spin degree of freedom). Clearly, the scaling factor $\epsilon_{F_{\max}}$ remains a free parameter of the theory, and can be used afterward to fit our results to the specific material that the theory is being used to model. In particular, this number can be estimated from experimental data regarding the maximum density of charge carriers $n_{\max}$ in the system, which itself can be inferred from the doping level together with geometrical information about the structure of the material.

A note of caution is in order here: in the following sections, the tilde over the scaled variables will be dropped for the sake of notational simplicity, but the scaling scheme discussed above will be implicit in our calculations, and all quantities are to be understood as their dimensionless counterparts.

2.4.1 Chemical Potential and Order Parameter Amplitude

The scaled saddle point equations (2.50) and (2.51) derived in the previous section determine the carrier density n and the interaction strength λ as functions of the chemical potential μ and the order parameter amplitude Δ_0. However, they can also be inverted in such a way that, given fixed values of n and λ, they uniquely determine a pair (μ, Δ_0). Therefore, the BCS-to-BEC evolution can be studied either as a function of density (at fixed interaction strength) or as a function of coupling (at fixed density).

We consider first the case where λ is fixed and the quantities μ and Δ_0 are calculated for varying n. The parameter k_0 (see Eq.(2.13)) is chosen to be equal to 10, which is consistent with the diluteness condition discussed above, and the parameter k_1 is made equal to k_0 for simplicity. The numerical solutions for the chemical potential μ and the order parameter amplitude Δ_0 are shown in Fig. 2.3 for $\lambda = 8.0019$ and $k_0 = k_1 = 10$ as functions of the carrier density n. The insets represent the same quantities in the case of s-wave symmetry.

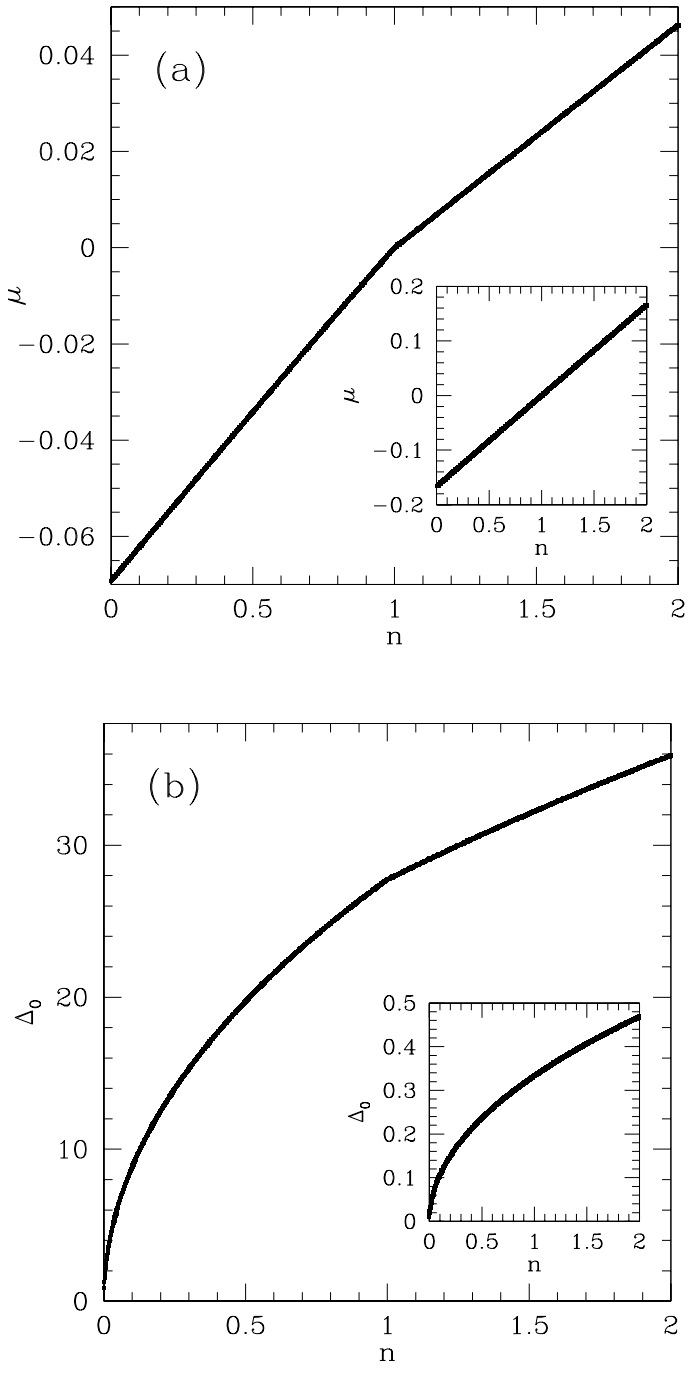

Figure 2.3: (a) Chemical potential μ and (b) order parameter amplitude Δ_0 (in units of $\epsilon_{F_{\max}}$) as functions of density n (in units of $n_{\max}/2\pi$) at fixed interaction strength $\lambda = 8.0019$ (in units of $g_{2\mathrm{D}}^{-1}$) for the case of d-wave symmetry. Notice that the chemical potential changes sign at $n = 1$. *Insets:* The same quantities in the case of s-wave symmetry ($\lambda = 0.30703$).

The first relevant thing to observe is the presence of a kink in both the chemical potential and order parameter amplitude when the carrier density crosses $n = 1$. This kink is in fact a plateau on the graphs of μ and Δ_0, that is, it represents a region of zero derivative with respect to n, and happens at a certain critical value $n = n_c = 1$. One can actually show that, for d-wave symmetry and fixed interaction, $\mu(n)$ and $\Delta_0(n)$ have continuous first derivatives with respect to n, but their second derivatives are discontinuous at $n = n_c$. Furthermore, this discontinuity happens exactly when the chemical potential changes sign, which can be interpreted as indicative of the appearance of a two-body bound state. As shown later, this behavior will have important consequences to the electronic compressibility of the system, which is related to $\partial n/\partial\mu$ and, therefore, diverges at $n = n_c$.

On the other hand, this feature is not observed for s-wave symmetry ($\ell = 0$), which is shown on the insets of Fig. 2.3. In this case, both $\mu(n)$ and $\Delta_0(n)$ are smooth functions of n, and both their first and second derivatives with respect to the carrier density can be shown to be always continuous.

We next analyze the BCS-to-BEC evolution at constant carrier density and varying interaction strength. We fix $n = 1$ and calculate $\mu(\lambda)$ and $\Delta_0(\lambda)$ using the same method of numerically inverting the saddle point equations in order to obtain a unique pair (μ, Δ_0) for given values of n and λ. Our results are shown in Fig. 2.4 for $k_0 = k_1 = 10$ in the d-wave case, together with the corresponding s-wave results (insets). As expected, both quantities still exhibit a kink at a certain critical value of the interparticle interaction strength $\lambda = \lambda_c = 8.00191$, which is actually even more pronounced in this case than on the plots of μ and Δ_0 as functions of n. This feature is again absent from the s-wave plots, in which μ and Δ_0 are smooth for all λ. Analogously, in the case of d-wave symmetry, the functions $\mu(\lambda)$ and $\Delta_0(\lambda)$ can be shown to have continuous first derivatives and discontinuous second derivatives with respect to λ. On the other hand, both the first and second derivatives of these functions with respect to λ are continuous in the s-wave case.

These results indicate a fundamental difference in the behavior of the d-wave system in comparison to the corresponding s-wave case. This suggestion will be further confirmed

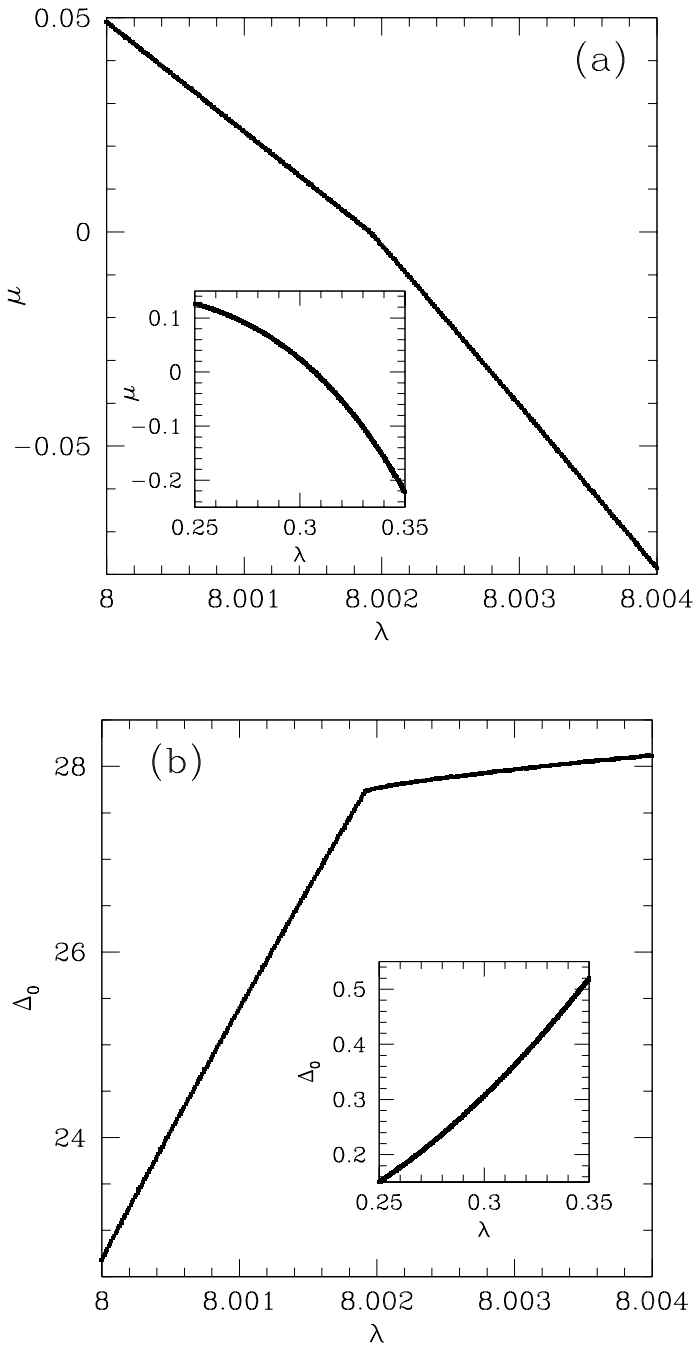

Figure 2.4: (a) Chemical potential μ and (b) order parameter amplitude Δ_0 (in units of $\epsilon_{F_{\max}}$) as functions of the interaction strength λ (in units of g_{2D}^{-1}) at fixed carrier density $n = 1$ (in units of $n_{\max}/2\pi$) for the case of d-wave symmetry. *Insets:* The same quantities in the case of s-wave symmetry.

in the next sections by calculations of the quasiparticle excitation spectrum, momentum distribution and electronic compressibility, which show that the $\mu = 0$ point is indeed special to the physics of d-wave superconductors, and separates a gapless spectrum at $\mu > 0$ from a fully gapped spectrum at $\mu < 0$.

2.4.2 Phase Diagram and Quasiparticle Excitation Spectrum

The first important spectroscopic quantity to be analyzed is the single-particle excitation spectrum $E_{\mathbf{k}}$, which is given by

$$E_{\mathbf{k}} = \sqrt{\xi_{\mathbf{k}}^2 + \Delta_{\mathbf{k}}^2}, \tag{2.52}$$

where $\xi_{\mathbf{k}} = \epsilon_{\mathbf{k}} - \mu$ and $\Delta_{\mathbf{k}} = \Delta_0 \Gamma(\mathbf{k})$. For $\mu > 0$, including the BCS limit, the d-wave excitation spectrum is gapless at $k_\mu \equiv \sqrt{\mu}$ along the special directions $\varphi = \{\pm\pi/4, \pm 3\pi/4\}$. In other words, the quasiparticle excitation energy has nodes at these particular locations in k-space called *Dirac points*, near which $E_{\mathbf{k}}$ disperses linealy with momentum. When μ reaches zero, the minimum value of the energy gap occurs at the single point $\mathbf{k} = 0$ and is given by $E_{\mathbf{k}=0} = |\Delta_{\mathbf{k}=0}| = \Delta_0 \Gamma(\mathbf{k} = 0)$, which also vanishes due to the k^2 dependence of the function $\Gamma(\mathbf{k})$ for d-wave symmetry. In this case, the excitation spectrum behaves quadratically for small momenta at any given angle φ, since $\Delta_{\mathbf{k}} \sim \Delta_0 k^2 \cos(2\varphi)$ and $\epsilon_{\mathbf{k}} = k^2$. The shrinking of the energy gap to zero at $\mathbf{k} = 0$ is a consequence of the diminishing pairing interaction for $\mu \to 0$. Finally, as soon as $\mu < 0$, including the BEC limit, a full gap in the excitation spectrum appears, but the minimum gap remains at $\mathbf{k} = 0$ with the value $E_{\mathbf{k}=0} = |\mu| > 0$. Thus, the $\mu = 0$ line separates a gapless d-wave superconductor ($\mu > 0$) from a fully gapped d-wave superconductor ($\mu < 0$), as illustrated in Fig. 2.5 by the plots of $\pm E_{\mathbf{k}}$ as a function of $\mathbf{k}$ for three different values of μ. Notice the collapse of the four Dirac cones to the single point $\mathbf{k} = 0$ and the appearance of a full gap to the addition of quasiparticles at $\mu = 0$.

It is important to point out that the behavior of the excitation spectrum for s-wave systems is completely different from the one described above, and the point $\mu = 0$ does not separate a gapless from a gapped regime. In fact, for $\mu > 0$, the excitation spectrum in this case has a gap $E_{\mathbf{k}_\mu} = |\Delta_{\mathbf{k}_\mu}|$ at $k = k_\mu$ for any angle φ. When the chemical potential becomes

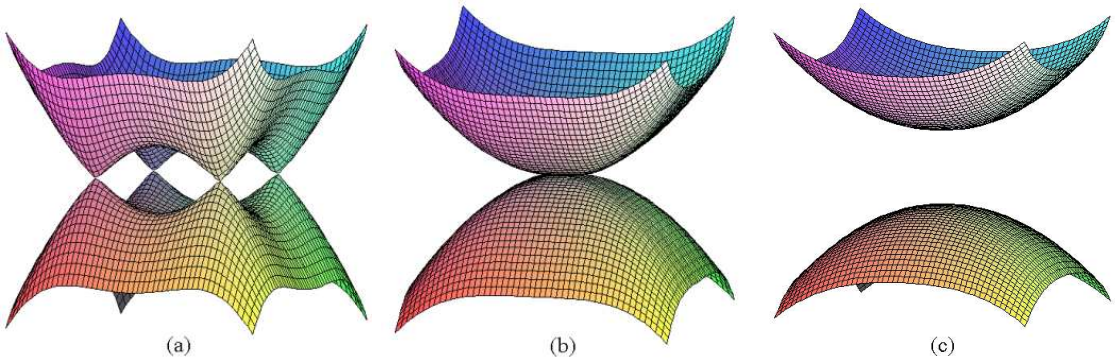

Figure 2.5: Plot of $\pm E_{\mathbf{k}}$ as a function of $\mathbf{k}$ for (a) $\mu > 0$, (b) $\mu = 0$ and (c) $\mu < 0$. Notice the collapse of the Dirac cones to the point $\mathbf{k} = 0$ that occurs at $\mu = 0$.

negative towards the BEC limit, the energy gap has a minimum at $\mathbf{k} = 0$, but remains always positive with value $E_{\mathbf{k}=0} = \left(\mu^2 + \Delta_0^2\right)^{1/2}$. Therefore, the excitation spectrum is always gapped for all values of μ in the case of s-wave symmetry.

The carrier density versus interaction strength phase diagram for this system can be constructed by making $\mu = 0$ and solving the (dimensionless) saddle point equations (2.50) and (2.51) for n (and Δ_0) given a certain value of λ. This leads to the results plotted in Figs. 2.6-a (d-wave case) and 2.6-b (s-wave case), where the solid line corresponds to the *loci* of points on the $n \times \lambda$ plane at which $\mu = 0$.

The most striking conclusion that can be drawn from these graphs is the fact that, at low enough densities, an s-wave system can have a negative chemical potential for arbitrarily small interactions. This implies that the appearance of a two-body bound state in this case can occur for any coupling. On the other hand, the low density limit of a d-wave system is qualitatively different, since the chemical potential does not become negative below a certain value of the interparticle interaction (which was found to be exactly $\lambda_{\min} = 8$). This indicates that the appearance of a two-body bound state in a two-dimensional d-wave system requires a finite coupling, which is similar to the situation found in three-dimensional systems with isotropic coupling, as originally pointed out by Eagles [7] and further confirmed by Engelbrecht *et al* in the case of a contact s-wave interaction potential [31].

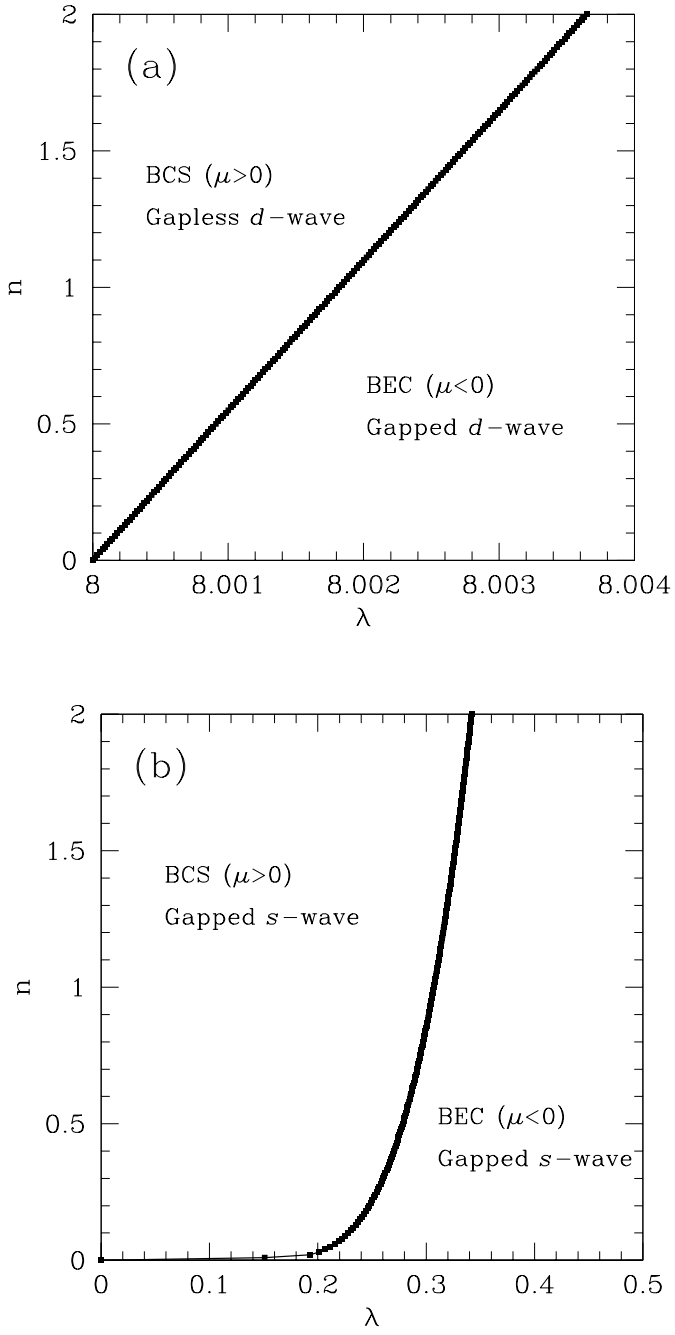

Figure 2.6: Phase diagram of carrier density n (in units of $n_{\max}/2\pi$) versus interaction strength λ (in units of $g_{2\mathrm{D}}^{-1}$) in the case of (a) d-wave and (b) s-wave symmetries. The solid line ($\mu = 0$) separates a BCS regime ($\mu > 0$) from a BEC regime ($\mu < 0$) on the $n \times \lambda$ plane.

2.4.3 Momentum Distribution and Electronic Compressibility

We next analyze the behavior of the momentum distribution $n_{\mathbf{k}}$ for a d-wave superconductor across the BCS-to-BEC transition region. According to Eq.(2.45), this quantity reduces at zero temperature to

$$n_{\mathbf{k}} = \frac{1}{2}\left(1 - \frac{\xi_{\mathbf{k}}}{E_{\mathbf{k}}}\right) = \frac{1}{2}\left(1 - \frac{\epsilon_{\mathbf{k}} - \mu}{\sqrt{(\epsilon_{\mathbf{k}} - \mu)^2 + \Delta_{\mathbf{k}}^2}}\right). \tag{2.53}$$

In Fig. 2.7, we show three-dimensional plots of the momentum distribution as a function of $\mathbf{k} = (k_x, k_y)$ for three different values of μ, together with the corresponding contour plots. The important feature that one should notice is the presence of four Dirac points along the special directions $\varphi = \{\pm\pi/4, \pm 3\pi/4\}$ and $k = k_\mu$. When the chemical potential crosses zero, these points collapse at $\mathbf{k} = 0$ and the momentum distribution becomes discontinuous for low k, which is accompanied by the appearance of a full gap in the quasiparticle excitation spectrum as soon as $\mu < 0$, as discussed previously.

This massive rearrangement of the momentum distribution at $\mu = 0$ has a dramatic effect on the isothermal electronic compressibility of the system, which is defined as

$$\kappa = -\frac{L^2}{N_0^2}\left(\frac{\partial^2 \Omega}{\partial \mu^2}\right)_T = \frac{1}{n^2}\left(\frac{\partial n}{\partial \mu}\right)_T, \tag{2.54}$$

where $n = N_0/L^2$ is the particle density. At zero temperature and constant coupling, the compressibility $\kappa(n)$ diverges logarithmically in the d-wave case at the critical density $n_c = 1$ (which corresponds to $\mu = 0$), as shown in Fig. 2.8. In fact, in the immediate vicinity of $n = n_c$, the compressibility can be written as

$$\kappa \approx -\gamma_1 \ln|1 - n/n_c| + \gamma_2, \tag{2.55}$$

with the coefficient γ_1 depending only on the sign of μ (notice the asymmetric behavior of κ around $n = n_c$). This result is not very surprising, given that a full gap to the addition of quasiparticles suddenly appears in the excitation spectrum when the chemical potential crosses zero, leading to the divergence of $\partial n/\partial \mu$ at $n = n_c$. This suggests the existence of a quantum critical point along the BCS-to-BEC evolution in d-wave superconductors,

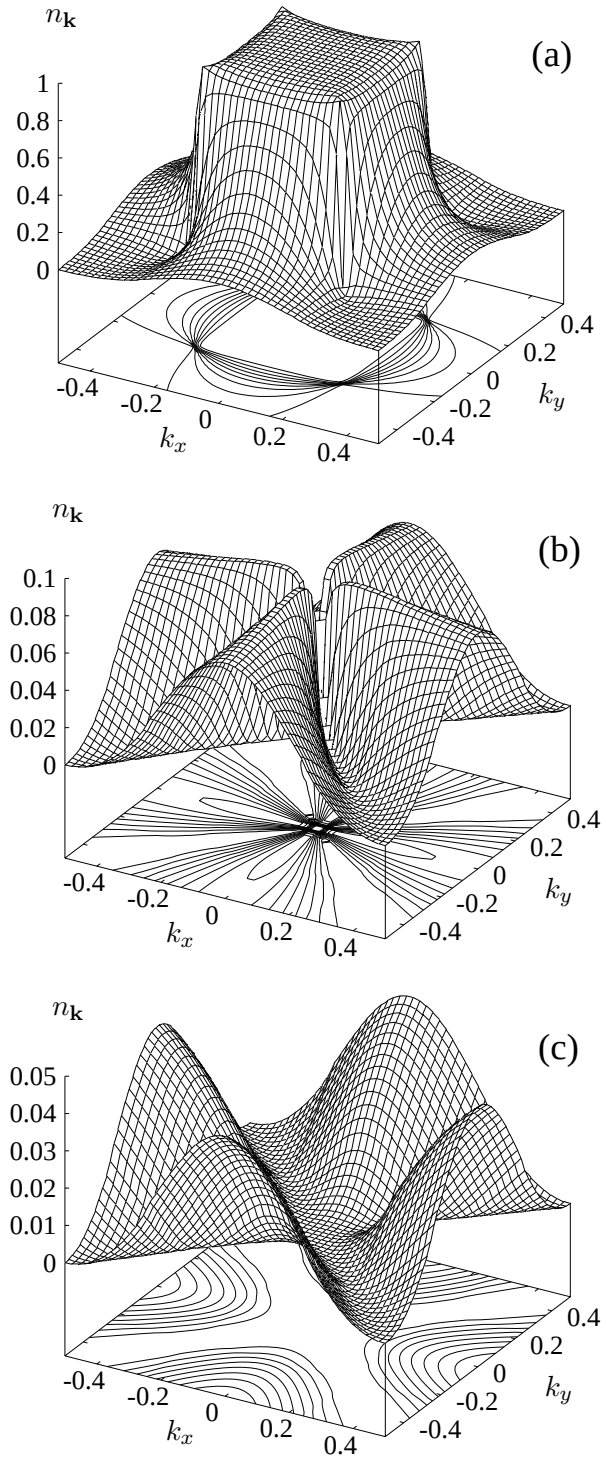

Figure 2.7: Plot of the momentum distribution $n_{\mathbf{k}}$ as a function of $\mathbf{k} = (k_x, k_y)$ in the case of d-wave symmetry for (a) $\mu = 0.1$, (b) $\mu = 0$ and (c) $\mu = -0.1$. Notice the collapse of the four Dirac points when the chemical potential crosses zero.

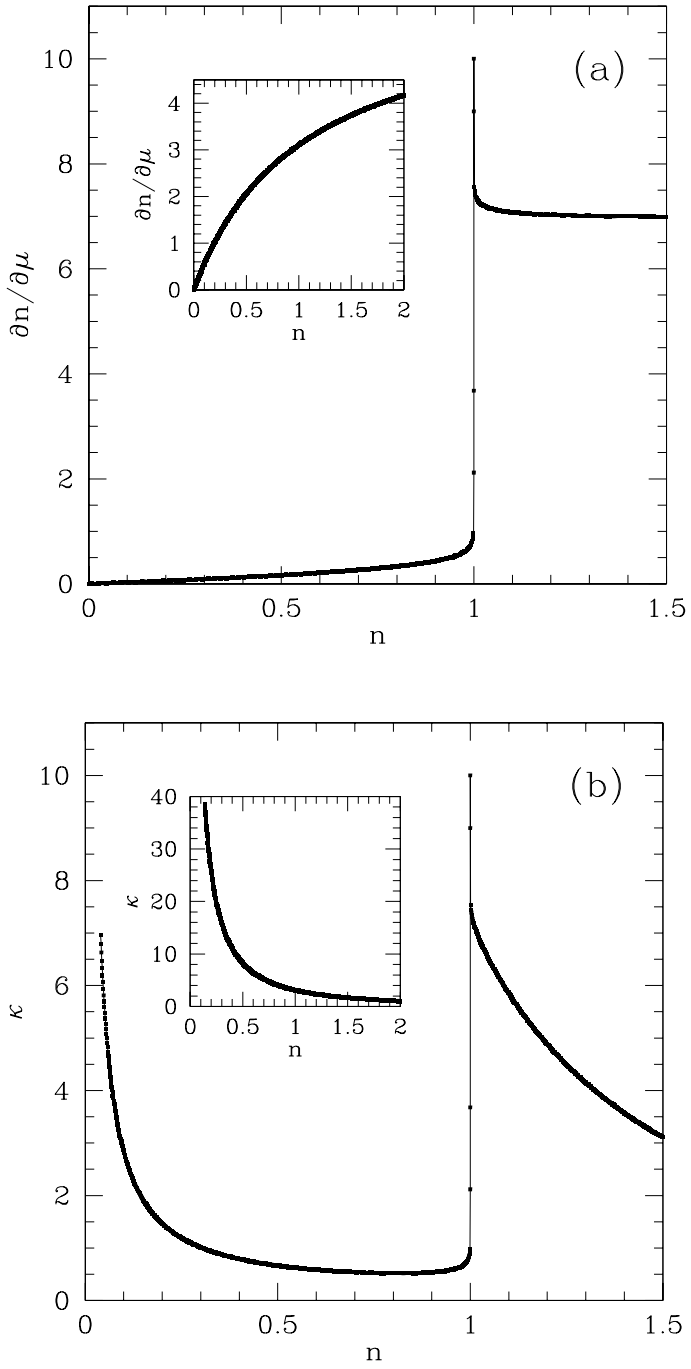

Figure 2.8: Plot of (a) $\partial n/\partial\mu$ (in units of $n_{\max}/2\pi\epsilon_{F_{\max}}$) and (b) the electronic compressibility $\kappa = (\partial n/\partial\mu)/n^2$ (in units of $2\pi/n_{\max}\epsilon_{F_{\max}}$) as functions of particle density n (in units of $n_{\max}/2\pi$) at fixed interaction strength in the case of d-wave symmetry. *Insets:* The corresponding quantities in the s-wave case.

a suggestion that will be further confirmed by the calculation of other properties of these systems. On the other hand, the electronic compressibility of s-wave systems is always a smooth function of n, and does not present any anomalous behavior in the vicinity of $\mu = 0$, as shown in the insets of Fig. 2.8. This is also an expected result, since the ground state energy is a well-behaved function of μ (and n) for s-wave systems, and both the first and second derivatives of the chemical potential with respect to the density are smooth in this case.

This non-analytic behavior of the d-wave electronic compressibility can be better understood by means of the following alternative equation for κ in terms of the momentum distribution,

$$n^2\kappa = \frac{4}{L^2}\sum_{\mathbf{k}} \frac{n_{\mathbf{k}}(1-n_{\mathbf{k}})}{E_{\mathbf{k}}}, \tag{2.56}$$

where $E_{\mathbf{k}}$ is the quasiparticle excitation energy. This expression clearly shows the close relationship between the momentum distribution and the compressibility, and explains how the rearrangement of $n_{\mathbf{k}}$ at $\mu = 0$ (and specially its discontinuity at low k) can be responsible for the divergence of κ at $n = n_c$ for d-wave systems.

Before leaving this section, it is worth discussing a possible analogy that can be made between the BCS-to-BEC evolution just described, in particular the change in topology of the $\pm E_{\mathbf{k}}$ surfaces in k-space when $\mu \to 0$, and the so-called Lifshitz transition in the context of ordinary metals at $T = 0$ and high pressures [32]. In the conventional Lifshitz transition, the Fermi surface of a metal $\epsilon(\mathbf{k}, P) = E_F$ changes its topology as the pressure P is varied. For an isotropic applied pressure, the deviation $\Delta P = P - P_c$ from the critical pressure P_c is proportional to $\Delta\mu = \mu - \mu_c$. A typical manifestation of the Lifshitz transition is the disruption of a "neck" of the Fermi surface, as illustrated in Fig. 2.9. This process leads to a non-analytic behavior of the number of states $\mathcal{N}(\mu)$ inside the Fermi surface, which then behaves in the vicinity of μ_c as

$$\mathcal{N}(\mu) \sim \begin{cases} A(\mu_c) + B|\mu - \mu_c|^{3/2}, & \mu < \mu_c; \\ A(\mu_c), & \mu > \mu_c. \end{cases} \tag{2.57}$$

In this case, the compressibility also presents a non-analyticity at μ_c and has the asymptotic

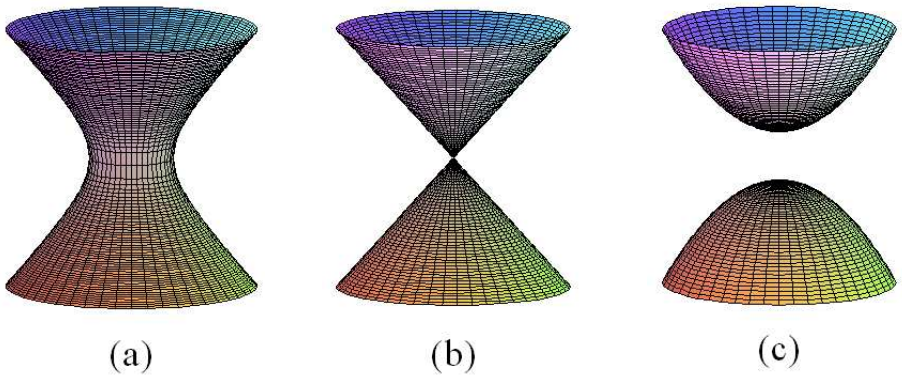

Figure 2.9: Plot of the Fermi surface of a typical metal in k-space undergoing a Lifshitz transition with (a) $P < P_c$, (b) $P = P_c$ and (c) $P > P_c$. Notice the disruption of a "neck" and the change in topology of the Fermi surface as the critical pressure P_c is crossed.

form $\kappa = (3/2)B|\mu - \mu_c|^{1/2}/n_c^2$. However, the quantity that signals a phase transition in this system is not κ, but the thermopower Q, which is proportional to $-\partial \ln(n)/\partial\mu$ and thus behaves as $Q \sim -|\Delta\mu|^{-1/2}$. In the conventional Lifshitz transition, the system lowers its energy by $\Delta E \sim -|\Delta\mu|^{5/2} \sim -|\Delta P|^{5/2}$, and the phase transition is said to be of *second-and-half order* [33].

In the case of d-wave superconductors, there is already a non-analytic and singular behavior in $\partial n/\partial\mu$ (and thus in κ). As discussed above, this singularity is logarithmic, since the system lowers its energy by $\Delta E \sim -|\mu - \mu_c|^2 \ln|\mu - \mu_c|$. This logarithmic contribution originates from the simultaneous collapse of the four Dirac points at $\mathbf{k} = 0$, which produces a gap in the excitation spectrum $E_\mathbf{k}$ and a major discontinuous rearrangement of the momentum distribution $n_\mathbf{k}$ in the ground state as $\mu \to 0$. A direct topological analogy with the standard Lifshitz transition can be drawn from the similarity between this collapse of the Dirac cones at $\mu = \mu_c$ and the corresponding disruption of a "neck" of the Fermi surface at $P = P_c$ in the case of metals.

2.4.4 Superfluid Density

We now turn our attention to the behavior of the superfluid density tensor $\rho_{ij}(T, n)$ at low temperatures across the BCS-to-BEC transition in d-wave superconductors. This quantity is related to the free energy increase produced in response to a phase twist of the superconducting order parameter field $\Delta_\mathbf{k}$. A quick outline of the steps involved in the derivation

of an expression for $\rho_{ij}(T,n)$ will be provided here, but a more detailed discussion can be found, for example, in Ref. [34]. One can start by allowing the order parameter to have a complex part by introducing a phase $\theta_{\mathbf{k}}$, so that $\Delta_{\mathbf{k}} = \Delta^0_{\mathbf{k}} e^{i\theta_{\mathbf{k}}}$. Expanding the effective action S_{eff} in powers of $\theta_{\mathbf{k}}$ about the saddle point with $\theta_{\mathbf{k}} = 0$, the resulting difference $\Delta S = S_{\text{eff}}(\theta_{\mathbf{k}}) - S_{\text{eff}}(\theta_{\mathbf{k}} = 0)$ becomes

$$\Delta S = -\frac{\beta L^2}{2} \sum_{\mathbf{k}} \theta_{\mathbf{k}}\, \theta_{-\mathbf{k}}\, k_i\, k_j\, \rho_{ij}(T), \tag{2.58}$$

with $\rho_{ij}(T)$ being the superfluid density tensor,

$$\rho_{ij}(T) = \frac{1}{L^2} \sum_{\mathbf{k}} \left[2n_{\mathbf{k}} \partial_i \partial_j \xi_{\mathbf{k}} - Y_{\mathbf{k}} \partial_i \xi_{\mathbf{k}} \partial_j \xi_{\mathbf{k}} \right], \tag{2.59}$$

where $n_{\mathbf{k}}$ is the momentum distribution given by Eq.(2.45), ∂_i denotes the partial derivative with respect to k_i, and $Y_{\mathbf{k}}$ is known as the Yoshida distribution, defined as

$$Y_{\mathbf{k}} = \frac{1}{2T} \operatorname{sech}^2 \left(\frac{E_{\mathbf{k}}}{2T} \right). \tag{2.60}$$

One can easily conclude that the off-diagonal elements of $\rho_{ij}(T)$ vanish ($\rho_{xy} = \rho_{yx} = 0$), while the diagonal elements are equal to each other, $\rho_{xx} = \rho_{yy} \equiv \rho(T)$. Furthermore, due to Galilean invariance of our continuum model, the zero-temperature superfluid density becomes $\rho(0) = n/m$, and is well-behaved as the critical point is crossed, while its derivative with respect to the chemical potential, $\partial\rho(0)/\partial\mu = n^2\kappa/m$, diverges at $n = n_c$.

Using our scaling conventions discussed previously, the equation above for the superfluid density tensor can be rewritten in dimensionless form. In fact, expressing energies in units of $\epsilon_{F_{\max}}$ and momenta in units of $k_{F_{\max}}$, using Eq.(2.44) to eliminate the momentum distribution term in favor of the density, and recalling the relation between carrier concentration and Fermi momentum in two dimensions, $n = k_F^2/2\pi$, one obtains

$$\Delta\rho(T) \equiv m\rho(T) - n = -\frac{1}{T} \int_0^{2\pi} d\varphi \int_0^{\infty} dk\, k^3\, \cos^2(\varphi) \operatorname{sech}^2 \left(\frac{E_{\mathbf{k}}}{2T} \right). \tag{2.61}$$

Notice that all quantities in this equation are already dimensionless, although the tildes were omitted for the sake of notational simplicity. The quantity $\Delta\rho(T) \equiv m\rho(T) - n$, which emerges naturally from the calculations, vanishes at $T = 0$ and is always negative

for $T > 0$, consistent with the two-fluid picture of superconductivity [35], according to which the superfluid fraction comprises the whole system at $T = 0$ and is reduced as the temperature is increased, vanishing at the superconducting critical temperature T_c.

Our results for $\Delta\rho(T)$ are shown in Fig. 2.10-a for various carrier concentrations. The temperature range was chosen in such a way that one always has $T \ll \epsilon_F$. This condition is necessary because the finite-temperature saddle point equations, which are used here to calculate the necessary values of μ and Δ_0, break down away from this limit. The derivative of $\Delta\rho(T)$ with respect to temperature at $T = 0$ is also shown in Fig. 2.10-b as a function of particle density. The most important conclusion that can be drawn from these plots is that the zero-temperature slope of the superfluid density is discontinuous at the critical point $n = n_c = 1$, which strengthens our hypothesis of the occurrence of a quantum phase transition in the BCS-to-BEC evolution of d-wave superconductors as a function of density.

We have also calculated $\Delta\rho(T)$ analytically at low temperatures and under the approximation of very short range interactions ($k_0 \to \infty$). In the BCS limit, we found $\Delta\rho(T) = -4\pi k_1^2 T/\Delta_0(n)$, the linear behavior being consistent with the nodal structure of the d-wave symmetry in the gapless phase. At the critical point $n = n_c$ ($\mu = 0$), we obtained $\Delta\rho(T) = -\ln(2) F(\Delta_0(n)/k_1^2) T$, with $F(x) = (1 + x^2)^{-1/2}$. Finally, in the BEC limit, we concluded that $\Delta\rho(T) = -16 F(\Delta_0(n)/k_1^2) \exp(-|\mu|/T)$, the exponential behavior reflecting the appearance of a full gap to the addition of quasiparticles for $n < n_c$.

Finally, it is important to point out that there is an additional contribution to $\Delta\rho(T)$ due to Goldstone modes (which are discussed in the next chapter). These modes are underdamped for $\mu > 0$ due to Landau damping, but are not damped for $\mu < 0$ due to the existence of a gap in the excitation spectrum. In our formulation, this contribution comes as a next order correction, and has the form $\rho_G(T) \sim T^3$ at low temperatures. Therefore, it does not contribute to the discontinuity in the zero-temperature slope of the superfluid density shown in Fig. 2.10-b.

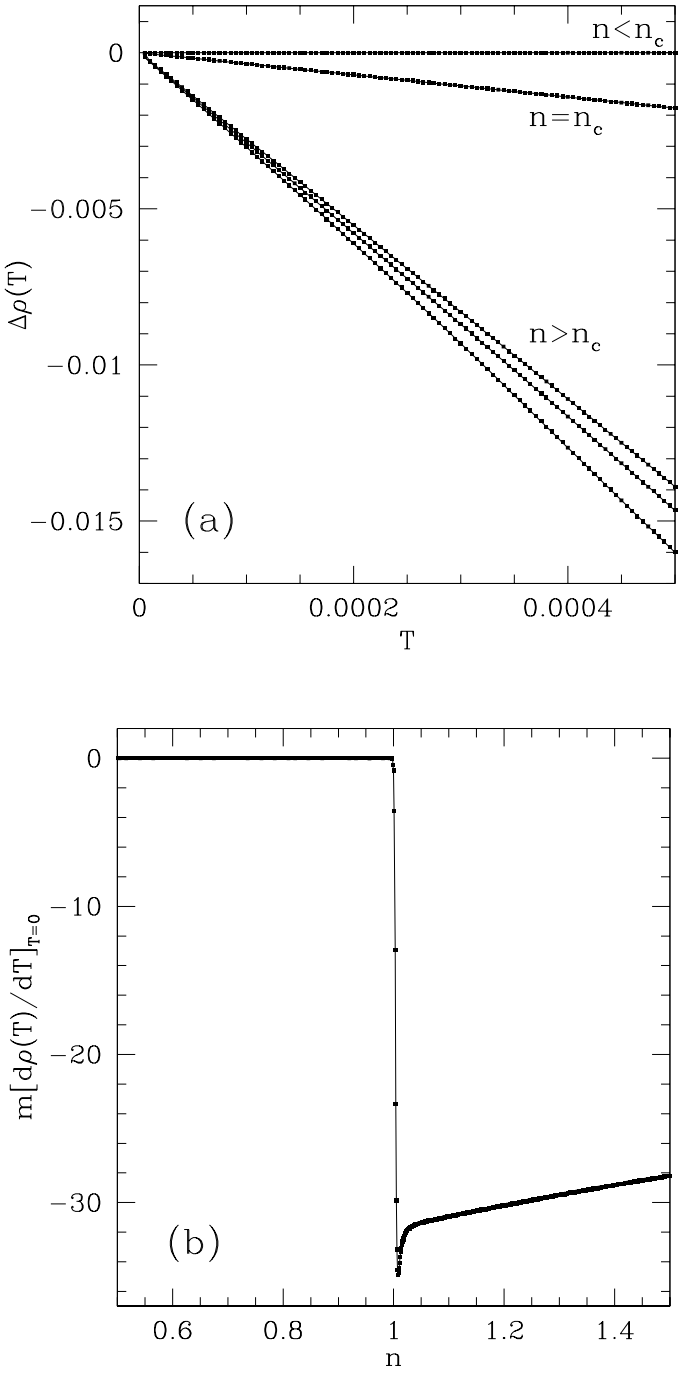

Figure 2.10: (a) Plot of $\Delta\rho(T) \equiv m\rho(T) - n$ (in units of $n_{\max}/2\pi$) as a function of temperature T (in units of $\epsilon_{F_{\max}}$) for several carrier densities around $n = n_c$ in the case of d-wave symmetry. (b) Plot of the superfluid density zero-temperature slope (in units of $n_{\max}/2\pi\epsilon_{F_{\max}}$) as a function of carrier density n (in units of $n_{\max}/2\pi$) in the case of d-wave symmetry.

2.4.5 Electronic Thermal Conductivity

We now start the discussion of the thermal conductivity of d-wave superconductors, which is an example of a non-equilibrium property that, as we will show next, is also affected by the presence of nodes in the spectrum of elementary excitations. The thermal conductivity tensor $\mathcal{K}_{\alpha\beta}$ is defined as the proportionality coefficient between a certain temperature gradient ∇T and the resulting thermal flux $\mathbf{Q}$,

$$Q_\alpha = -\mathcal{K}_{\alpha\beta}\,\partial_\beta T, \tag{2.62}$$

where ∂_β denotes the derivative with respect to x_β, and the thermal flux carried by non-equilibrium excitations in two dimensions is given by the equation

$$\mathbf{Q}(\mathbf{r}) = 2\int \frac{d^2k}{(2\pi)^2}\, E_{\mathbf{k}}(\mathbf{r})\mathbf{v}_{\mathbf{k}}(\mathbf{r})f_{\mathbf{k}}(\mathbf{r}), \tag{2.63}$$

where $\mathbf{v}_{\mathbf{k}} = \partial E_{\mathbf{k}}/\partial\mathbf{k}$ is the quasiparticle velocity in a superconductor, and the coordinate dependence of $E_{\mathbf{k}}$ is due to a possible dependence of the order parameter $\Delta_{\mathbf{k}}$ on temperature, which is itself a function of $\mathbf{r}$. The quantity $f_{\mathbf{k}}(\mathbf{r})$ is the non-equilibrium distribution function of excitations interacting with impurities, which satisfies the Boltzmann kinetic equation

$$\frac{\partial f_{\mathbf{k}}}{\partial t} + \frac{\partial E_{\mathbf{k}}}{\partial \mathbf{k}}\cdot\nabla f_{\mathbf{k}} - \frac{\partial f_{\mathbf{k}}}{\partial \mathbf{k}}\cdot\nabla E_{\mathbf{k}} = \left(\frac{\partial f_{\mathbf{k}}}{\partial t}\right)_{\text{imp}}, \tag{2.64}$$

where the right-hand side represents a collision integral due to impurities. In the case of a stationary thermal flow, and assuming that the distribution function $f_{\mathbf{k}}$ does not deviate much from its equilibrium value, the kinetic equation can be simplified by using the locally equilibrium distribution function $f^{(0)}_{\mathbf{k}}(\mathbf{r}) = \mathcal{F}(E_{\mathbf{k}}(\mathbf{r})/T(\mathbf{r}))$, where $\mathcal{F}$ is the Fermi function, such that

$$f^{(0)}_{\mathbf{k}}(\mathbf{r}) = \frac{1}{e^{E_{\mathbf{k}}(\mathbf{r})/T(\mathbf{r})}+1}. \tag{2.65}$$

The intermediate steps of this calculation will not be shown here, but more details can be found in Ref. [36]. In the approximation which is linear in the small difference between

the non-equilibrium and locally equilibrium distribution functions, one obtains for the two-dimensional thermal conductivity tensor,

$$\mathcal{K}_{\alpha\beta} = -\frac{2}{T}\int \frac{d^2k}{(2\pi)^2}\,\frac{\partial f_{\mathbf{k}}^{(0)}}{\partial E_{\mathbf{k}}}\,E_{\mathbf{k}}^2 v_{\mathbf{k}_\alpha} v_{\mathbf{k}_\beta}\tau_{\mathbf{k}}, \tag{2.66}$$

where $\tau_{\mathbf{k}}$ is the mean free time between two consecutive quasiparticle collisions,

$$\tau_{\mathbf{k}}^{-1} = 2\pi\mathcal{N}_{\text{imp}}u^2L^2\int \frac{d^2k'}{(2\pi)^2}\,C(\mathbf{k},\mathbf{k}')\,\delta(E_{\mathbf{k}} - E_{\mathbf{k}'}), \tag{2.67}$$

with the so-called coherence factor $C(\mathbf{k},\mathbf{k}')$ defined as

$$C(\mathbf{k},\mathbf{k}') = \frac{1}{2}\left(1 + \frac{\xi_{\mathbf{k}}\xi_{\mathbf{k}'} - \Delta_{\mathbf{k}}\Delta_{\mathbf{k}'}}{E_{\mathbf{k}}E_{\mathbf{k}'}}\right). \tag{2.68}$$

The parameter $\mathcal{N}_{\text{imp}}$ is the impurity concentration in the superconductor, while L^2 is the "volume" of the system. Finally, u is the quasiparticle scattering amplitude, assumed to be isotropic.

Adopting the same scaling scheme as before, one can write a dimensionless equation for the thermal conductivity tensor. In a system of units where $\hbar = k_B = 1$, both $\mathcal{K}_{\alpha\beta}$ and T have units of energy (and will be scaled with respect to $\epsilon_{F_{\max}}$), while the mean free time $\tau_{\mathbf{k}}$ has units of inverse energy (and will be scaled with respect to $\epsilon_{F_{\max}}^{-1}$). After evaluating the quasiparticle velocities $\mathbf{v}_{\mathbf{k}}$ and appropriately scaling the remaining variables, one obtains the following expression for the dimensionless thermal conductivity tensor (in terms of scaled quantities) in the limit of short range interactions ($k_0 \to \infty$),

$$\mathcal{K}_{\alpha\beta} = \frac{2}{\pi^2}\frac{1}{T^2}\int d^2k\,k_\alpha k_\beta\tau_{\mathbf{k}}\frac{e^{-E_{\mathbf{k}}/T}}{\left(e^{-E_{\mathbf{k}}/T}+1\right)^2}\left[k^2 - \mu + \left(\frac{\Delta_0}{k_1}\right)^2\Gamma(\mathbf{k})\cos(2\varphi)\right]^2. \tag{2.69}$$

However, the product $k_\alpha k_\beta$ causes the integral over all k-space to vanish for $\alpha \neq \beta$, such that the off-diagonal elements of $\mathcal{K}_{\alpha\beta}$ are zero ($\mathcal{K}_{xy} = \mathcal{K}_{yx} = 0$). Furthermore, assuming that $\tau_{\mathbf{k}}$ depends on the angle φ only via $\cos^2(2\varphi)$ (an assumption that will be justified later), one can also conclude that the diagonal elements of $\mathcal{K}_{\alpha\beta}$ are equal. Defining $\mathcal{K}(T) \equiv \mathcal{K}_{xx} = \mathcal{K}_{yy}$, one finally obtains

$$\mathcal{K}(T) = \frac{2}{\pi^2}\frac{1}{T^2}\int_0^{2\pi}d\varphi\int_0^{\infty}dk\,k^3\cos^2(\varphi)\tau_{\mathbf{k}}\frac{e^{-E_{\mathbf{k}}/T}}{\left(e^{-E_{\mathbf{k}}/T}+1\right)^2}\left[k^2 - \mu + \left(\frac{\Delta_0}{k_1}\right)^2\Gamma(\mathbf{k})\cos(2\varphi)\right]^2. \tag{2.70}$$

Among all the parameters in the equation for $\mathcal{K}(T)$, the only unknown is the lifetime $\tau_{\mathbf{k}}$ of the quasiparticles. In fact, most of the remaining of this section will be spent in the derivation of approximate equations for $\tau_{\mathbf{k}}$, the goal being to find expressions that do not involve an extra integration over $\mathbf{k}'$. Since the behavior of the integrand of Eq.(2.70) in the BCS regime is qualitatively different from its behavior in the BEC regime, the calculation of $\tau_{\mathbf{k}}$ in the cases of $\mu > 0$ and $\mu < 0$ will be performed separately.

Let us analyze the case of $\mu > 0$ first. The starting point to this calculation is the observation that the presence of $\partial f_{\mathbf{k}}^{(0)}/\partial E_{\mathbf{k}}$ in Eq.(2.70) causes the integrand to be negligible at regions of k-space where $E_{\mathbf{k}} \gg T$. This implies that, at low-T, the only relevant contribution to the integral will come from the vicinity of the Dirac points, which is where the excitation energy becomes low enough to be comparable to the temperature. This assumption will not only allow the integration to be restricted to a much smaller region of k-space, but will also lead to some other important approximations in the calculation of $\tau_{\mathbf{k}}$ for $\mu > 0$, which will be discussed in what follows.

The delta-function in Eq.(2.67) can be eliminated with the help of the following relation,

$$\delta(f(x)) = \sum_i \frac{\delta(x - x_i)}{\left|\frac{df}{dx}\right|_{x_i}}, \tag{2.71}$$

where the sum is over all roots x_i of $f(x)$. Using this in the equation for $\tau_{\mathbf{k}}^{-1}$ and performing the integration over k', one obtains

$$\tau_{\mathbf{k}}^{-1} = \frac{2}{\pi}\mathcal{N}_{\mathrm{imp}}u^2L^2\sum_{i=1}^{2}\int_0^{\pi/2} d\varphi\, k_i(\varphi)\, C(\mathbf{k}, k_i(\varphi))\left|\frac{\partial E_{\mathbf{k}}}{\partial k}\right|_{k_i(\varphi)}^{-1}, \tag{2.72}$$

where the function $k_i(\varphi)$ is defined by the condition $E_{k_i(\varphi)} = E_{\mathbf{k}}$ for a fixed value of $E_{\mathbf{k}}$. In other words, for a given angle φ, there will be two different vectors $\mathbf{k}'$, whose magnitudes are denoted $k_1(\varphi)$ and $k_2(\varphi)$, which are solutions of the equation $E_{\mathbf{k}'} = E_{\mathbf{k}}$. This situation is illustrated in Fig. 2.11-a, which shows the $\pi/4$ Dirac cone of a d-wave excitation spectrum and a plane of constant $E_{\mathbf{k}}$. The intersection between this plane and the excitation energy surface is a closed contour, whose projection onto the $k_x \times k_y$ plane is called "solution contour" in the figure. In fact, it is clear from the diagram that every vector $\mathbf{k}'$ whose tip

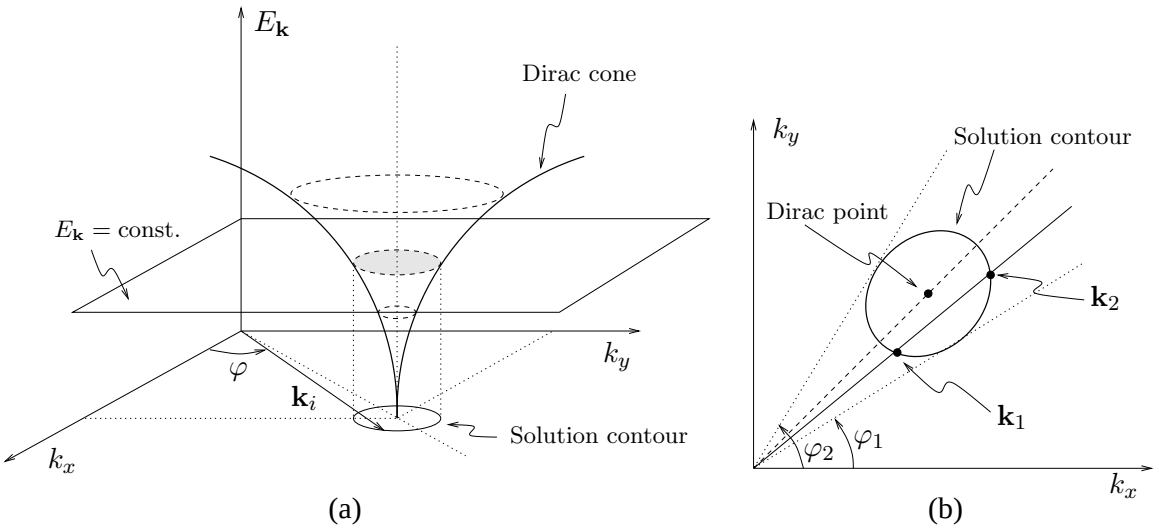

Figure 2.11: (a) Sketch of the $\pi/4$ Dirac cone in the excitation spectrum of a d-wave superconductor, intercepted by a plane of constant energy. The projection of this intersection onto the $k_x \times k_y$ plane constitutes the "solution contour" indicated in the figure. (b) Vicinity of the $\pi/4$ Dirac point on the $k_x \times k_y$ plane, showing the solution contour and the points $\mathbf{k}_1$ and $\mathbf{k}_2$ that satisfy $E_{\mathbf{k}_i} = E_{\mathbf{k}}$.

lies on this contour will satisfy $E_{\mathbf{k}'} = E_{\mathbf{k}}$. Furthermore, as shown in more detail in Fig. 2.11-b, there will be two of these vectors for any given angle φ in the interval $\varphi_1 < \varphi < \varphi_2$, since a line $\varphi = \text{const}$ on the $k_x \times k_y$ plane will intercept the solution contour at two points when $E_{\mathbf{k}}$ is small.

The evaluation of the integral in Eq.(2.72) over the polar angle φ requires the knowledge of an analytic expression for $k_i(\varphi)$, which can be easily obtained by imposing that $E_{k_i(\varphi)} = E_{\mathbf{k}}$, resulting in

$$k_i^2(\varphi) = \frac{\mu \pm \sqrt{E_{\mathbf{k}}^2 + (E_{\mathbf{k}}^2 - \mu^2)\frac{\Delta_0^2}{k_1^4}\cos^2(2\varphi)}}{1 + \frac{\Delta_0^2}{k_1^4}\cos^2(2\varphi)}, \tag{2.73}$$

where the plus sign provides $k_2(\varphi)$ and the minus sign provides $k_1(\varphi)$. Notice that the $\pi/4$-symmetry of the integrand in Eq.(2.72) was used to reduce the φ-integral to the first quadrant only, the final result being multiplied by 4. After evaluating $|\partial E_{\mathbf{k}}/\partial k|_{k_i(\varphi)}$ and using the condition $E_{k_i(\varphi)} = E_{\mathbf{k}}$ to simplify the expression for $C(\mathbf{k}, k_i(\varphi))$, Eq.(2.72) becomes

$$\tau_{\mathbf{k}}^{-1} = \frac{\mathcal{N}_{\text{imp}} u^2 L^2}{2\pi} \frac{1}{E_{\mathbf{k}}} \sum_{i=1}^{2} \int_{\varphi_1}^{\varphi_2} d\varphi \, \frac{E_{\mathbf{k}}^2 + \xi_{\mathbf{k}}\, \xi_{k_i(\varphi)} - \Delta_0^2\, \Gamma(\mathbf{k})\, \Gamma(k_i(\varphi))}{\left| k_i^2(\varphi) - \mu + \frac{\Delta_0^2}{k_1^4}\, k_i^2(\varphi)\, \cos^2(2\varphi) \right|}. \tag{2.74}$$

Observe that the integration over the first quadrant was further restricted to the interval

$\varphi_1 < \varphi < \varphi_2$, which is the only region where the equation $E_{k_i(\varphi)} = E_{\mathbf{k}}$ has solutions. This expression for $\tau_{\mathbf{k}}^{-1}$ can be immediately simplified by noticing (either from Fig. 2.11-b or from Eq.(2.73)) that the function $k_i(\varphi)$ is even with respect to $\varphi = \pi/4$. This implies that $\Gamma(k_i(\varphi)) \sim k_i^2(\varphi)\cos(2\varphi)$ will be an odd function with respect to $\varphi = \pi/4$ and, therefore, will vanish upon integration from φ_1 to φ_2. Furthermore, using the defining equation of $k_i(\varphi)$ to rewrite the denominator in the integrand of Eq.(2.74) as

$$\left| k_i^2(\varphi) - \mu + \frac{\Delta_0^2}{k_1^4}\, k_i^2(\varphi)\, \cos^2(2\varphi) \right| = \sqrt{E_{\mathbf{k}}^2 + (E_{\mathbf{k}}^2 - \mu^2)\, \frac{\Delta_0^2}{k_1^4}\, \cos^2(2\varphi)}, \tag{2.75}$$

the inverse mean free time $\tau_{\mathbf{k}}^{-1}$ becomes

$$\tau_{\mathbf{k}}^{-1} = \frac{\mathcal{N}_{\mathrm{imp}} u^2 L^2}{2\pi} \frac{1}{E_{\mathbf{k}}} \sum_{i=1}^{2} \int_{\varphi_1}^{\varphi_2} d\varphi\, \frac{E_{\mathbf{k}}^2 + \xi_{\mathbf{k}}\, \xi_{k_i(\varphi)}}{\sqrt{E_{\mathbf{k}}^2 + (E_{\mathbf{k}}^2 - \mu^2)\, \frac{\Delta_0^2}{k_1^4}\, \cos^2(2\varphi)}}. \tag{2.76}$$

Apart from the assumption of very short range interactions ($k_0 \to \infty$), all the calculations so far have been performed without any approximation, so that the equation above for $\tau_{\mathbf{k}}^{-1}$ is exact. However, since our final integral over $\mathbf{k}$ to find $\mathcal{K}(T)$ will be done numerically, it is convenient to have a closed analytic expression for $\tau_{\mathbf{k}}$ that does not involve any further integration. Therefore, in order to solve the integral over φ in Eq.(2.76), one can make use of the previously discussed fact that, at low temperatures, the only relevant contribution to the integral over $\mathbf{k}$ that determines $\mathcal{K}(T)$ will come from the vicinity of Dirac points. This implies that the two limiting angles φ_1 and φ_2 shown in Fig. 2.11-b will not deviate much from $\pi/4$, so that one will always have $\cos^2(2\varphi) \ll 1$. And since it is also true that $\Delta_0 \approx k_1^2$, the term $\frac{\Delta_0^2}{k_1^4}\cos^2(2\varphi)$ can be ignored in Eq.(2.73) for $k_i(\varphi)$, resulting in $k_i^2(\varphi) \approx \mu \pm E_{\mathbf{k}}$. Therefore,

$$\xi_{k_1(\varphi)} = k_1^2(\varphi) - \mu \approx E_{\mathbf{k}} \quad \text{and} \quad \xi_{k_2(\varphi)} = k_2^2(\varphi) - \mu \approx -E_{\mathbf{k}}.$$

Using this in Eq.(2.76) and performing the sum over the index i, one obtains

$$\tau_{\mathbf{k}}^{-1} = \frac{\mathcal{N}_{\mathrm{imp}} u^2 L^2}{\pi} E_{\mathbf{k}} \int_{\varphi_1}^{\varphi_2} \frac{d\varphi}{\sqrt{E_{\mathbf{k}}^2 + (E_{\mathbf{k}}^2 - \mu^2)\, \frac{\Delta_0^2}{k_1^4}\, \cos^2(2\varphi)}}. \tag{2.77}$$

This expression can be further simplified via the change of variables $\theta \equiv \varphi - \pi/4$, which

leads to

$$\tau_{\mathbf{k}}^{-1} = \frac{\mathcal{N}_{\rm imp} u^2 L^2}{\pi} E_{\mathbf{k}} \int_{-\theta_0}^{\theta_0} \frac{d\theta}{\sqrt{E_{\mathbf{k}}^2 + 4(E_{\mathbf{k}}^2 - \mu^2)\,\frac{\Delta_0^2}{k_1^4}\,\theta^2}}, \tag{2.78}$$

where the (small) angle $\theta_0 = \varphi_2 - \pi/4$ represents the maximum deviation of φ from $\pi/4$. An expression for θ_0 can be found from Eq.(2.73) by means of the condition $k_1(\theta_0) = k_2(\theta_0)$, which gives

$$\theta_0 = \frac{k_1^2}{\Delta_0} \frac{E_{\mathbf{k}}}{2\sqrt{\mu^2 - E_{\mathbf{k}}^2}}. \tag{2.79}$$

Finally, solving the θ-integral in the equation above for $\tau_{\mathbf{k}}^{-1}$ and using the expression for θ_0, one obtains the following result for the mean free time between quasiparticle collisions in the case of $\mu > 0$,

$$\tau_{\mathbf{k}} = \frac{2}{\mathcal{N}_{\rm imp} u^2 L^2} \frac{\Delta_0}{k_1^2} \frac{\sqrt{\mu^2 - E_{\mathbf{k}}^2}}{E_{\mathbf{k}}} \qquad (\mu > 0). \tag{2.80}$$

We now discuss the derivation of an expression for $\tau_{\mathbf{k}}$ valid for $\mu < 0$. The important difference in this case is the absence of nodes in the excitation spectrum, so that the quasiparticle energy surface in k-space assumes a different shape, as shown in Fig. 2.12-a. As a consequence, the solution contour (projection onto the $k_x \times k_y$ plane of the intersection between the $E_{\mathbf{k}} = \text{const}$ plane and the excitation energy surface) will not be a closed contour anymore. In other words, the line $\varphi = \text{const}$ will intercept the solution contour at only one point, as shown in Fig. 2.12-b, so that the equation $E_{k_i(\varphi)} = E_{\mathbf{k}}$ will have only one solution for a fixed value of $E_{\mathbf{k}}$. This solution, which will be denoted $k_2(\varphi)$ for consistency with the previous notation, can be obtained from Eq.(2.73) by retaining only the plus sign.

Starting with the definition of $\tau_{\mathbf{k}}^{-1}$ given by Eq.(2.67) and using the same technique of eliminating the delta-function by means of Eq.(2.71), one obtains in this case

$$\tau_{\mathbf{k}}^{-1} = \frac{2}{\pi} \mathcal{N}_{\rm imp} u^2 L^2 \int_0^{\pi/2} d\varphi\, k_2(\varphi)\, C(\mathbf{k}, k_2(\varphi)) \left| \frac{\partial E_{\mathbf{k}}}{\partial k} \right|_{k_2(\varphi)}^{-1}, \tag{2.81}$$

where the symmetry of the integrand was used to reduce the integral to the first quadrant. Evaluating the quantity $|\partial E_{\mathbf{k}}/\partial k|_{k_2(\varphi)}$, using the relation $E_{k_2(\varphi)} = E_{\mathbf{k}}$ to simplify the expression for $C(\mathbf{k}, k_2(\varphi))$, and again exploiting the fact that $k_2(\varphi)$ is an even function with

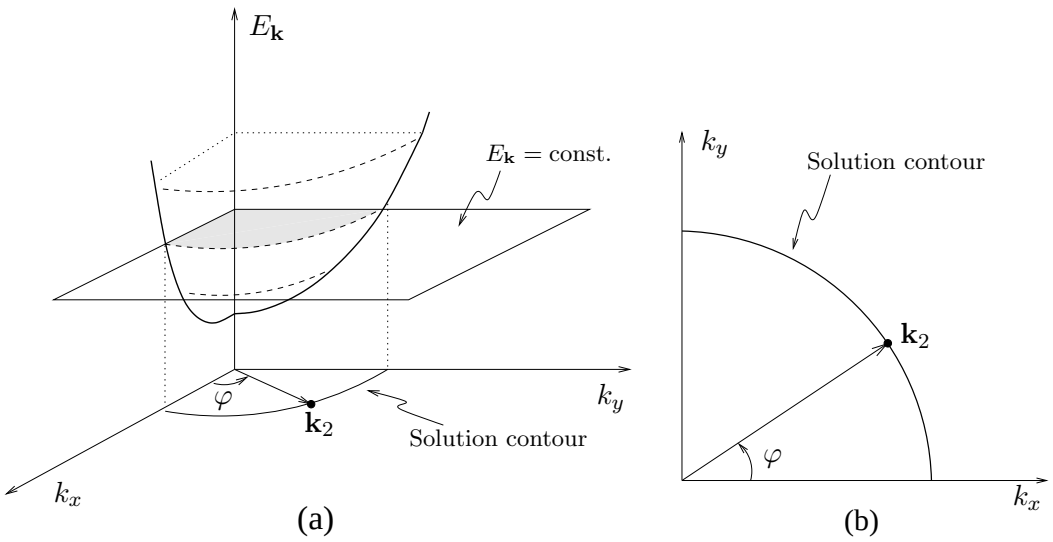

Figure 2.12: (a) Sketch of the quasiparticle excitation energy surface in k-space for a d-wave superconductor with $\mu < 0$, intercepted by a plane of constant energy. The projection of this intersection onto the $k_x \times k_y$ plane constitutes the "solution contour" indicated in the figure. (b) The solution contour shown in more detail, together with the only solution $\mathbf{k}_2$ of the equation $E_{\mathbf{k}_2} = E_{\mathbf{k}}$.

respect to $\pi/4$ (so that the term containing $\Gamma(k_2(\varphi))$ vanishes upon integration from $\varphi = 0$ to $\varphi = \pi/2$), one finds

$$\tau_{\mathbf{k}}^{-1} = \frac{\mathcal{N}_{\text{imp}} u^2 L^2}{2\pi} \frac{1}{E_{\mathbf{k}}} \int_0^{\pi/2} d\varphi \, \frac{E_{\mathbf{k}}^2 + \xi_{\mathbf{k}} \, \xi_{k_2(\varphi)}}{\sqrt{E_{\mathbf{k}}^2 + (E_{\mathbf{k}}^2 - \mu^2) \, \frac{\Delta_0^2}{k_1^4} \cos^2(2\varphi)}}. \tag{2.82}$$

Due to the absence of Dirac points in the spectrum of excitations, the quasiparticle energy $E_{\mathbf{k}}$ will assume finite values for all vectors $\mathbf{k}$ in this case, so that equally relevant contributions to the final integral that determines $\mathcal{K}(T)$ (Eq.(2.70)) will come from all directions in k-space. Therefore, the integration region cannot be restricted to the vicinity of $\varphi = \pi/4$, but must be extended to all angles, so that the approximation $\cos^2(2\varphi) \ll 1$ will not be valid here. Without this simplifying assumption, one would have to use the full expression for $k_2(\varphi)$ into the equation above for $\tau_{\mathbf{k}}^{-1}$, resulting in an integral that cannot be performed analytically.

In order to overcome this problem, one can make use of the fact that, although all directions in k-space have approximately equal weights, regions with small k values are still responsible for a greater contribution to the integral, since $E_{\mathbf{k}}$ has a minimum at $\mathbf{k} = 0$. Therefore, it is reasonable to limit the integral that determines $\mathcal{K}(T)$ to the vicinity of the

origin of k-space, where the excitation energy $E_{\mathbf{k}}$ does not deviate much from its minimum value $|\mu|$. Making the approximation $E_{\mathbf{k}} \approx |\mu| + \delta\omega$ in the expression for $k_2(\varphi)$ (with $\delta\omega \ll |\mu|$) and keeping only terms that are linear in $\delta\omega$, the equation above for $\tau_{\mathbf{k}}^{-1}$ becomes

$$\tau_{\mathbf{k}}^{-1} = \frac{\mathcal{N}_{\rm imp} u^2 L^2}{2\pi} \frac{1}{|\mu| + \delta\omega} \int_0^{\pi/2} d\varphi \, \frac{|\mu|^2 + 2|\mu|\delta\omega + \xi_{\mathbf{k}}(|\mu| + \delta\omega)}{|\mu| + \delta\omega \left(1 + \frac{\Delta_0^2}{k_1^4} \cos^2(2\varphi)\right)}. \tag{2.83}$$

Finally, performing the integral over φ and retaining only terms that are independent of $\delta\omega$, one obtains for the quasiparticle lifetime $\tau_{\mathbf{k}}$ in the case of $\mu < 0$,

$$\tau_{\mathbf{k}} = \frac{4}{\mathcal{N}_{\rm imp} u^2 L^2} \frac{|\mu|}{|\mu| + \xi_{\mathbf{k}}} \qquad (\mu < 0). \tag{2.84}$$

With the help of the (approximate) analytical expressions of $\tau_{\mathbf{k}}$ for $\mu > 0$ (Eq.(2.80)) and $\mu < 0$ (Eq.(2.84)), the electronic thermal conductivity $\mathcal{K}(T)$ can be obtained by numerically solving the integral over $\mathbf{k}$ given in Eq.(2.70). The results are shown in Fig. 2.13-a, where $\mathcal{K}(T)$ is plotted as a function of temperature for different values of the carrier density n. For $n > n_c = 1$, the low-temperature thermal conductivity is clearly linear in T, with a slope that depends on n. This result is in fact confirmed by our analytical calculations, which give $\mathcal{K}(T) \approx \mu T$ in the BCS limit. As in the case of the superfluid density, the linear dependence on T reflects the nodal structure of the d-wave symmetry in the gapless phase. For $n \leq n_c$, we found that $\mathcal{K}(T) \approx (1/\pi^2)(|\mu|^3/T)e^{-|\mu|/T}$, the exponential behavior being consistent with the appearance of a gap in the quasiparticle excitation spectrum in the BEC regime.

The zero-temperature slope of the thermal conductivity was also evaluated numerically, and is shown in Fig. 2.13-b as a function of density. One should notice that, although always continuous, this quantity develops a cusp at $n = n_c = 1$, which coincides with the rearrangement of the momentum distribution, the divergence of the electronic compressibility, and the appearance of a gap to the addition of quasiparticles. This further supports our hypothesis of a quantum phase transition in the BCS-to-BEC evolution of d-wave superconductors, confirming the previous claim that the physics of these systems is qualitatively different from the one in the case of isotropic (s-wave) symmetry.

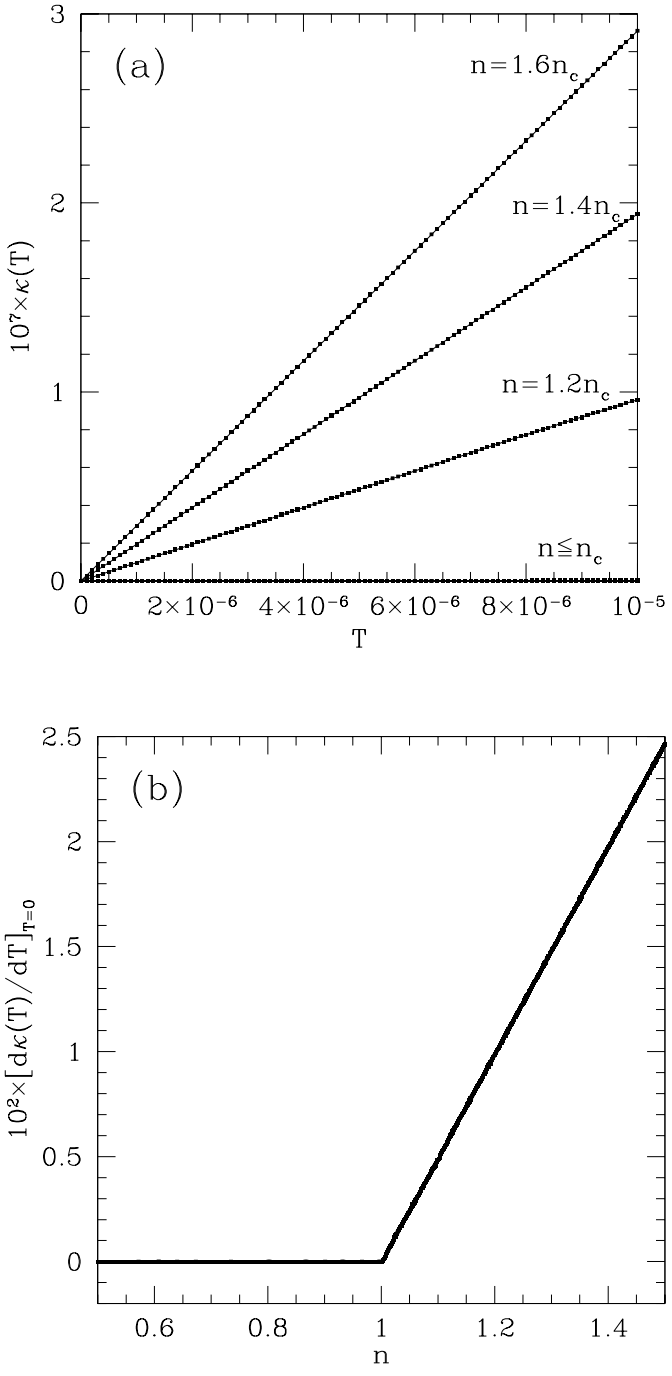

Figure 2.13: (a) Plot of the electronic thermal conductivity $\mathcal{K}(T)$ (in units of $\epsilon_{F_{\max}}$) as a function of temperature T (in units of $\epsilon_{F_{\max}}$) for several values of particle density in the case of d-wave symmetry. (b) Plot of the thermal conductivity zero-temperature slope $[d\mathcal{K}(T)/dT]_{T=0}$ (dimensionless) as a function of the particle density n (in units of $n_{\max}/2\pi$) for d-wave symmetry.

2.5 Summary

In this chapter, we have proposed the existence of a Lifshitz-like phase transition at $T = 0$ in clean d-wave superconductors. This transition takes place when the system is driven from the BCS regime of high density (or weak coupling) to the opposite BEC regime of low density (or strong coupling). Our analysis was based on a functional integral formulation of the problem of interacting fermions in two spatial dimensions, which led to the BCS order parameter and number equations at the saddle point (mean field) level of approximation.

We have shown that, as the chemical potential of the system reaches the bottom of tha band, a gap to the addition of quasiparticles opens up in the excitation spectrum, and the system goes from a gapless phase ($\mu > 0$) to a fully gapped phase ($\mu < 0$). This can be achieved either by varying the carrier density at constant interaction strength, or by changing the effective coupling at constant concentration. Either way, the appearance of the gap is accompanied by a massive rearrangement of the momentum distribution, which becomes discontinuous at the origin of k-space as μ crosses zero. As an immediate consequence, the electronic compressibility becomes non-analytic, diverging logarithmically at the critical density $n = n_c$ (which corresponds to $\mu = 0$). This is in clear contrast to the behavior of s-wave superconductors, in which case the compressibility was shown to be a smooth function of density throughout the BCS-to-BEC crossover, the system presenting a fully gapped excitation spectrum at both sides of the $\mu = 0$ point.

We also analyzed the behavior of the superfluid density tensor $\rho(T)$ in the case of d-wave symmetry, and showed that its temperature dependence exhibits a dramatic change at the critical point, going from power-law on the BCS side of the transition to exponential on the BEC side. Furthermore, the zero temperature slope of the superfluid density was shown to be a non-analytic function of the carrier density, presenting a discontinuity at $n = n_c$. Finally, we studied the evolution of the electronic thermal conductivity tensor $\mathcal{K}(T)$ across the BCS-to-BEC evolution, and concluded that it also shows a major change in behavior as the chemical potential reaches the bottom of the band. We found that its zero-temperature slope, despite being a continuous function of the density throughout the transition region, develops a cusp at the critical point $n = n_c$.

We conclude this chapter by suggesting that the search for this phase transition in d-wave superconductors may be possible by means of several different techniques. One possibility is the use of ferroelectric field-effect transistors (FFET), which were discussed earlier [25]. In these devices, some control over the particle density in cuprate superconductors may be achieved without chemical doping through the application of a polarizing electric field. Alternatively, the occurrence of this transition may be investigated by measuring the superfluid density as a function of doping [23], or through a direct measurement of the electronic compressibility as a function of particle density, as already done in the study of metal-insulator transitions [37].

Finally, it should be mentioned that the study of the BCS-to-BEC evolution has recently gained renewed interest in connection with cold fermionic atomic gases. In these systems, the scattering length (and, therefore, the effective interaction strength) can be tuned via Feshbach resonances for a given fixed density, which offers the possibility of coupling fermionic atoms into bosonic molecules in a highly controllable manner. The study of fermionic atomic systems will be deferred to Chapter IV of this thesis, where we will discuss the possibility of a quantum phase transition in ultra-cold spin-polarized Fermi gases which exhibit a p-wave Feshbach resonance. In the next chapter, however, we will give continuity to the functional integral analysis of the BCS-to-BEC evolution in d-wave superconductors, where the calculation of Gaussian fluctuations in the pairing field will lead to an expression for the collective mode contribution to the number of particles equation.

CHAPTER III

BEYOND THE SADDLE-POINT APPROXIMATION

3.1 Introduction

The formalism introduced in the last chapter allowed the BCS equations of superconductivity to be obtained as the saddle point solutions to the functional integral that determines the grand-canonical partition function of the system. That is, by calculating the effective action and imposing a stationarity condition, the finite temperature order parameter and number equations were derived at the mean field level of approximation.

However, as mentioned in the last chapter, one of the main advantages of this field-theoretical method is that it enables one to go beyond the saddle point results and calculate higher order corrections to the mean field solutions. In the present case, by considering fluctuations about the trivial uniform and static saddle point Δ_0, this approach allows one to gain considerable further insight into the BCS-to-BEC evolution problem.

Therefore, the analysis of fluctuation effects will be the main objective of this chapter, which is organized as follows. In Section 3.2, an expression for the Gaussian correction to the effective action due to fluctuations is derived. Then, in Section 3.3, the properties of the broken-symmetry state ($T < T_c$) are analyzed, and an expression for the fluctuation contribution to the particle number equation is obtained. The collective modes of the system are studied in Section 3.4, where the dispersion relation in the limit of small frequencies and momenta is derived. Finally, Section 3.5 discusses how quantum fluctuations affect the transition temperature in the framework of the Berezinskii-Kosterlitz-Thouless phase transition, and our concluding remarks are made in Section 3.6.

3.2 Gaussian Correction to the Effective Action

In order to obtain the first non-vanishing order correction to the effective action due to fluctuations, one can start by assuming that the pairing field $\phi_{\mathbf{k}}(\tau)$ consists not only of the

static and uniform saddle point $\Delta_0\delta_{\mathbf{k},0}$, but also of a small fluctuation field $\eta_{\mathbf{k}}(\tau)$, such that

$$\phi_{\mathbf{k}}(\tau) = \Delta_0\delta_{\mathbf{k},0} + \eta_{\mathbf{k}}(\tau). \tag{3.1}$$

Using this corrected pairing field in Eq.(2.31) for the effective action, Fourier transforming from imaginary time to Matsubara frequency, and using the notation $k \equiv (\mathbf{k}, i\omega_n)$, where $\omega_n = (2n+1)\pi/\beta$ is a fermionic Matsubara frequency, one obtains

$$S_{\text{eff}}[\eta,\eta^*] = \sum_k \left[\frac{1}{\lambda}\left|\Delta_0\delta_{\mathbf{k},0} + \eta(k)\right|^2 + \xi_{\mathbf{k}}\right] - \mathbf{Tr}\left[\ln\left(\mathbf{G}_0^{-1}(k,k') + \mathbf{W}(k,k')\right)\right], \tag{3.2}$$

where the matrix $\mathbf{G}_0^{-1}(k,k')$ is given by

$$\mathbf{G}_0^{-1}(k,k') = \mathbf{G}_0^{-1}(k)\delta_{k,k'}, \quad \text{with} \quad \mathbf{G}_0^{-1}(k) = \begin{pmatrix} i\omega_n - \xi_{\mathbf{k}} & \Delta_0\Gamma(\mathbf{k}) \\ \Delta_0\Gamma(\mathbf{k}) & i\omega_n + \xi_{\mathbf{k}} \end{pmatrix}, \tag{3.3}$$

while the correction matrix $\mathbf{W}(k,k')$ is defined as

$$\mathbf{W}(k,k') = \begin{pmatrix} 0 & \Gamma\left(\frac{\mathbf{k}+\mathbf{k}'}{2}\right)\eta(k-k') \\ \Gamma\left(\frac{\mathbf{k}+\mathbf{k}'}{2}\right)\eta^*(k'-k) & 0 \end{pmatrix}. \tag{3.4}$$

The next step consists in expanding the logarithm in the expression for the effective action up to second order in the fluctuation field $\eta(k)$. Recalling that the matrix elements of $\mathbf{W}(k,k')$ are small in comparison to the elements of $\mathbf{G}_0^{-1}(k,k')$, one obtains

$$\begin{aligned} \mathbf{Tr}\left[\ln\left(\mathbf{G}_0^{-1}(k,k') + \mathbf{W}(k,k')\right)\right] &= \mathbf{Tr}\left\{\ln\left[\mathbf{G}_0^{-1}(k,k')[\mathbf{1} + \mathbf{G}_0(k,k')\mathbf{W}(k,k')]\right]\right\} = \\ = \mathbf{Tr}\left(\ln\mathbf{G}_0^{-1}(k,k')\right) &+ \mathbf{Tr}\left[\mathbf{G}_0(k,k')\mathbf{W}(k,k') - \frac{1}{2}\left(\mathbf{G}_0(k,k')\mathbf{W}(k,k')\right)^2 + \dots\right], \end{aligned} \tag{3.5}$$

where $\mathbf{G}_0(k,k')$ is the inverse of $\mathbf{G}_0^{-1}(k,k')$, and can be shown to be given by

$$\mathbf{G}_0(k,k') = \mathbf{G}_0(k)\delta_{k,k'}, \quad \text{with} \quad \mathbf{G}_0(k) = \frac{1}{(i\omega_n)^2 - E_{\mathbf{k}}^2}\begin{pmatrix} i\omega_n + \xi_{\mathbf{k}} & -\Delta_0\Gamma(\mathbf{k}) \\ -\Delta_0\Gamma(\mathbf{k}) & i\omega_n - \xi_{\mathbf{k}} \end{pmatrix}. \tag{3.6}$$

One can then use these matrix expressions, together with the logarithm expansion, back in Eq.(3.2) for the corrected action. After collecting terms with equal powers of $\eta(k)$, one can easily conclude that the zeroeth order term will correspond to the saddle point

effective action $S_{\text{eff}}[\Delta_0]$, from which the BCS number and order parameter equations were derived in the last chapter. Furthermore, one can also show that the first order correction vanishes, as a consequence of the stationarity condition given by Eq.(2.32). Finally, the terms quadratic in $\eta(k)$ will correspond to the Gaussian correction to $S_{\text{eff}}[\Delta_0]$, so that the Gaussian approximation to the effective action becomes

$$S_{\text{Gauss}}[\eta,\eta^*] = S_{\text{eff}}[\Delta_0] + \sum_k \frac{|\eta(k)|^2}{\lambda} + \frac{1}{2}\,\mathbf{Tr}\left(\mathbf{G}_0(k,k')\mathbf{W}(k,k')\right)^2. \tag{3.7}$$

Recalling that the symbol **Tr** denotes not only a trace over Nambu indices, but also a sum over the momentum and Matsubara frequency variables $k = (\mathbf{k}, i\omega_n)$ and $k' = (\mathbf{k}', i\omega_n')$, one can rewrite the previous expression for the Gaussian action as

$$S_{\text{Gauss}}[\eta,\eta^*] = S_{\text{eff}}[\Delta_0] + \sum_k \frac{|\eta(k)|^2}{\lambda} + \frac{1}{2}\sum_{k,q} \text{tr}\left[\mathbf{G}_0(k)\mathbf{W}(k,k+q)\mathbf{G}_0(k+q)\mathbf{W}(k+q,k)\right], \tag{3.8}$$

where $q = (\mathbf{q}, i\nu_m)$, with $\nu_m = 2m\pi/\beta$ a bosonic Matsubara frequency. Finally, using the expressions for the matrices $\mathbf{G}_0$ and $\mathbf{W}$, evaluating the resulting matrix products, and performing the trace over Nambu indices, one obtains

$$S_{\text{Gauss}}[\eta,\eta^*] = S_{\text{eff}}[\Delta_0] + \frac{1}{2}\sum_q \underline{\eta}^\dagger(q)\mathbf{M}(q)\underline{\eta}(q), \tag{3.9}$$

where the vector $\underline{\eta}(q)$ is defined as

$$\underline{\eta}(q) = \begin{pmatrix} \eta(q) \\ \eta^*(-q) \end{pmatrix}, \tag{3.10}$$

and $\mathbf{M}(q)$ is a 2×2 matrix known as the inverse fluctuation propagator. Under the assumption that $\Gamma^2(-\mathbf{k}) = \Gamma^2(\mathbf{k})$, one can show (by inspection) that the matrix elements of $\mathbf{M}(q)$ are given by

$$M_{11}(-q) = M_{22}(q) = \frac{1}{\lambda} + \sum_k \frac{i\omega_n + \xi_{\mathbf{k}}}{(i\omega_n)^2 - E_{\mathbf{k}}^2}\,\frac{i\omega_n + i\nu_m - \xi_{\mathbf{k}+\mathbf{q}}}{(i\omega_n + i\nu_m)^2 - E_{\mathbf{k}+\mathbf{q}}^2}\,\Gamma^2(\mathbf{k}+\mathbf{q}/2) \tag{3.11}$$

and

$$M_{12}(q) = M_{21}(q) = \sum_k \frac{\Delta_0^2}{(i\omega_n)^2 - E_{\mathbf{k}}^2} \frac{1}{(i\omega_n + i\nu_m)^2 - E_{\mathbf{k}+\mathbf{q}}^2} \Gamma^2(\mathbf{k}+\mathbf{q}/2)\Gamma(\mathbf{k})\Gamma(\mathbf{k}+\mathbf{q}). \tag{3.12}$$

We next investigate the effects of Gaussian fluctuations to the behavior of the broken-symmetry state ($T < T_c$). In particular, we focus on the $T = 0$ limit of the formalism developed above, and study the collective mode contribution to the number equation, which will be a correction to the BCS number equation derived in the last chapter at the saddle point level of approximation.

3.3 The Broken-Symmetry State

The fluctuation correction to the effective action was shown in the last section to be given by

$$S_{\text{fluct}}[\eta, \eta^*] = \frac{1}{2} \sum_q \underline{\eta}^\dagger(q) \mathbf{M}(q) \underline{\eta}(q), \tag{3.13}$$

where the vector $\underline{\eta}(q)$ is such that $\underline{\eta}^\dagger(q) = [\eta^*(q), \eta(-q)]$, and the notation $q = (\mathbf{q}, i\nu_m)$ was used, where $\nu_m = 2m\pi/\beta$ is a bosonic Matsubara frequency. Therefore, the corresponding correction to the grand-canonical partition function of the system will be

$$\mathcal{Z}_{\text{fluct}} = \int \mathcal{D}[\eta, \eta^*] e^{-\frac{1}{2}\sum_q \underline{\eta}^\dagger(q)\mathbf{M}(q)\underline{\eta}(q)}, \tag{3.14}$$

which can be solved straightforwardly by means of a bosonic functional Gaussian integral, yielding simply

$$\mathcal{Z}_{\text{fluct}} = \frac{1}{\mathbf{Det}\, \mathbf{M}(q)}, \tag{3.15}$$

where the symbol **Det** denotes not only a product over Nambu indices, but also over momentum and Matsubara frequency. This immediately leads to an expression for the collective mode contribution to the thermodynamic potential, which can be written as

$$\Omega_{\text{fluct}} = -\frac{1}{\beta} \ln \mathcal{Z}_{\text{fluct}} = -\frac{1}{\beta} \ln[\mathbf{Det}\, \mathbf{M}(q)]^{-1} = \frac{1}{\beta} \mathbf{Tr}[\ln \mathbf{M}(q)] =$$

$$= \frac{1}{\beta} \sum_q \text{tr}[\ln \mathbf{M}(q)] = \frac{1}{\beta} \sum_{\mathbf{q}, i\nu_m} \ln[\det \mathbf{M}(q)]. \tag{3.16}$$

In this expression, the Matsubara sum over the frequencies ν_m cannot be performed directly, due to the branch cut of the logarithm. One way around this difficulty is to differentiate both sides of the above equation with respect to μ before summing, in order to eliminate the ln function, and then integrate back the resulting expression to recover $\Omega_{\rm fluct}$. One then obtains the following:

$$\frac{\partial}{\partial\mu}\Omega_{\rm fluct} = \frac{1}{\beta}\sum_{\mathbf{q},i\nu_m}\frac{\partial}{\partial\mu}\ln[\det\mathbf{M}(q)] = \frac{1}{\beta}\sum_{\mathbf{q},i\nu_m}\frac{1}{\det\mathbf{M}(q)}\frac{\partial}{\partial\mu}[\det\mathbf{M}(q)]. \tag{3.17}$$

In order to proceed further, one needs to make some assumptions about the singularity structure of $1/\det\mathbf{M}(q)$, which represents the two-particle excitation spectrum of the broken-symmetry state. These assumptions will be justified at the end of the calculation. Anticipating some of the results of the next section, the function $\det\mathbf{M}(q)$ will have only one zero located at $\omega = c_s|\mathbf{q}|$ for sufficiently small $|\mathbf{q}|$, where ω is the analytic continuation $i\nu_m \rightarrow \omega + i0^+$ and c_s is the speed of sound in the system.

One must now recognize that the function $\beta\, n_B(\omega)$, where $n_B(\omega) = (e^{\beta\omega}-1)^{-1}$ is the usual Bose function, has infinite poles $\tilde{\omega}_m = i2m\pi/\beta$ along the imaginary axis, with residue $+1$ at all the poles. Using this fact to rewrite the Matsubara sum in the previous equation as a sum of residues, and then applying Cauchy's Theorem to express the result as an integral along a closed path in the complex plane that encloses all the poles $\tilde{\omega}_m$ (see Ref. [38] for more details), one obtains

$$\begin{aligned}\frac{\partial}{\partial\mu}\Omega_{\rm fluct} &= \frac{1}{\beta}\sum_{\mathbf{q}}\sum_{m=-\infty}^{\infty}\frac{1}{\det\mathbf{M}(\mathbf{q},\tilde{\omega}_m)}\frac{\partial}{\partial\mu}[\det\mathbf{M}(\mathbf{q},\tilde{\omega}_m)]\,\mathrm{Res}[\beta\, n_B(\omega)]_{\tilde{\omega}_m} = \\ &= \frac{1}{\beta}\sum_{\mathbf{q}}\sum_{m=-\infty}^{\infty}\mathrm{Res}\left[\frac{1}{\det\mathbf{M}(\mathbf{q},\omega)}\frac{\partial}{\partial\mu}[\det\mathbf{M}(\mathbf{q},\omega)]\beta\, n_B(\omega)\right]_{\tilde{\omega}_m} = \\ &= \frac{1}{2\pi i}\sum_{\mathbf{q}}\oint_C dz\frac{1}{\det\mathbf{M}(\mathbf{q},z)}\frac{\partial}{\partial\mu}[\det\mathbf{M}(\mathbf{q},z)]\, n_B(z),\end{aligned} \tag{3.18}$$

where the contour C runs from $\epsilon - i\infty$ up to $\epsilon + i\infty$, and then back down from $-\epsilon + i\infty$ to $-\epsilon - i\infty$, as shown in Fig. 3.1-a, so that all the poles of the function $n_B(z)$ are enclosed.

Since the integrand has no branch cuts, the integration contour C can be continuously deformed to look like the one shown in Fig. 3.1-b, enclosing all of the complex plane but the

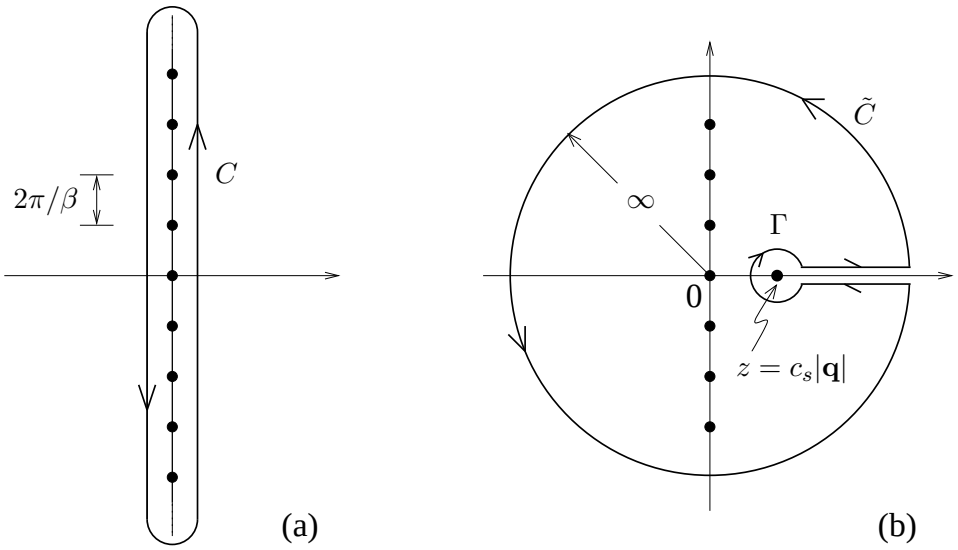

Figure 3.1: (a) The contour C encloses all the poles $\tilde{\omega}_m = i2m\pi/\beta$ of the Bose function $n_B(z) = 1/(e^{\beta z} - 1)$, where the integer m runs from $-\infty$ to $+\infty$. (b) Deformed integration contour $\tilde{C} + \Gamma$, which encloses all the poles of the integrand of Eq.(3.18) but the one at $z = c_s|\mathbf{q}|$.

point $z = c_s|\mathbf{q}|$, which is the only pole of the integrand not located on the imaginary axis. Therefore, the complex integral along the contour C in the previous equation is converted into an integral along the large arc $\tilde{C}$ and an integral along the small loop Γ around the $z = c_s|\mathbf{q}|$ pole. However, from Jordan's Lemma, the contribution from the arc $\tilde{C}$ vanishes as its radius approaches infinity, and one is left with the integral along Γ only. Finally, one can use Cauchy's Theorem to express this integral as $2\pi i$ times the residue of the integrand at $z = c_s|\mathbf{q}|$:

$$\frac{\partial}{\partial\mu}\Omega_{\rm fluct} = \frac{1}{2\pi i}\sum_{\mathbf{q}}\oint_{\Gamma} dz \frac{1}{\det \mathbf{M}(\mathbf{q},z)}\frac{\partial}{\partial\mu}[\det \mathbf{M}(\mathbf{q},z)]\, n_B(z) =$$

$$= -\sum_{\mathbf{q}} \mathrm{Res}\left[\frac{1}{\det \mathbf{M}(\mathbf{q},z)}\frac{\partial}{\partial\mu}[\det \mathbf{M}(\mathbf{q},z)]\, n_B(z)\right]_{z=c_s|\mathbf{q}|}, \tag{3.19}$$

where the minus sign reflects the clockwise orientation of Γ. In order to calculate this residue, one must again resort to results to be derived in the next section. In particular, one has to use the fact that, in the approximation of small $|\mathbf{q}|$ and ω, the determinant of the fluctuation matrix can be written as

$$\det \mathbf{M}(\mathbf{q},\omega) = A(\mu,\Delta_0)\left(\omega^2 - c_s^2|\mathbf{q}|^2\right), \tag{3.20}$$

where the function $A(\mu, \Delta_0)$ does not depend on $|\mathbf{q}|$ or ω. Recalling that the residue of a function $f(z)$ at a simple pole z_0 is given by $\lim_{z\to z_0}\left[f(z)(z-z_0)\right]$, one finally obtains for the collective mode contribution to the thermodynamic potential of the system,

$$\frac{\partial}{\partial\mu}\Omega_{\text{fluct}} = -\sum_{\mathbf{q}} \text{Res}\left\{ n_B(z)\left[\frac{\frac{\partial}{\partial\mu}A(\mu,\Delta_0)}{A(\mu,\Delta_0)} - \frac{2c_s\frac{\partial c_s}{\partial\mu}|\mathbf{q}|^2}{z^2-c_s^2|\mathbf{q}|^2}\right]\right\}_{z=c_s|\mathbf{q}|} =$$

$$= -\sum_{\mathbf{q}} n_B(c_s|\mathbf{q}|)\left[\frac{-2c_s\frac{\partial c_s}{\partial\mu}|\mathbf{q}|^2}{2c_s|\mathbf{q}|}\right] = \sum_{\mathbf{q}}\frac{|\mathbf{q}|}{e^{\beta c_s|\mathbf{q}|}-1}\frac{\partial c_s}{\partial\mu} = \frac{\partial}{\partial\mu}\left[\frac{1}{\beta}\sum_{\mathbf{q}}\ln\left(1-e^{-\beta c_s|\mathbf{q}|}\right)\right] \therefore$$

$$\therefore \quad \Omega_{\text{fluct}} = \frac{1}{\beta}\sum_{\mathbf{q}}\ln\left(1-e^{-\beta c_s|\mathbf{q}|}\right). \tag{3.21}$$

The corresponding fluctuation correction to the particle number equation can be obtained by applying the thermodynamic relation $N = -\partial\Omega/\partial\mu$ to the expression above for Ω_{fluct}. After transforming the sum over $\mathbf{q}$ into an integration, one obtains

$$N_{\text{fluct}} = -\frac{\partial\Omega_{\text{fluct}}}{\partial\mu} = -\sum_{\mathbf{q}}\frac{|\mathbf{q}|}{e^{\beta c_s|\mathbf{q}|}-1}\frac{\partial c_s}{\partial\mu} = -\frac{L^2}{(2\pi)^2}\int_0^{2\pi}d\varphi\int_0^{\infty}dq\,\frac{q^2}{e^{\beta c_s q}-1}\frac{\partial c_s}{\partial\mu}. \tag{3.22}$$

Finally, using the change of variables $x = \beta c_s q$, and recalling the definition of the Riemann zeta function,

$$\zeta(z) = \frac{1}{\Gamma(z)}\int_0^{\infty}dx\frac{x^{z-1}}{e^x-1}, \tag{3.23}$$

one finds

$$N_{\text{fluct}} = -\frac{L^2}{\pi}\frac{\zeta(3)}{c_s^3}\frac{\partial c_s}{\partial\mu}\,T^3, \tag{3.24}$$

which vanishes as T^3 in the limit of $T \to 0$. Therefore, one recovers the equivalent of Leggett's variational results [5, 9] at $T = 0$ for the saddle point order parameter and number equations in the context of ^{3}He. One can thus conclude that, for $T \ll T_c$, the corrections to the saddle point number equation due to collective modes are small for all couplings. In other words, although the BCS expression given by Eq.(2.44) does not take into account the contributions from pairing excitations, it does lead to a good description of the BCS-to-BEC transition region, as long as one is sufficiently far below the critical temperature. However, it is well known that the same is not true near T_c, where the effects of temporal fluctuations in the order parameter are essential to fully describe the BEC

regime [11]. This problem will be considered later in this chapter.

In the next section, the collective modes of the system will be analyzed, and an expression for the dispersion relation $\omega = \omega(\mathbf{q})$ will be obtained. Some results invoked during the calculations in this section will also be proved.

3.4 Collective Modes

The collective modes are determined by the poles of the propagator for the pair fluctuation fields, which describe the small deviations about the saddle point solution. The dispersion relation $\omega = \omega(\mathbf{q})$ can be obtained by solving

$$\det \mathbf{M}(\mathbf{q}, \omega) = 0, \tag{3.25}$$

with the usual analytic continuation $i\nu_m \to \omega + i0^+$. The first step towards this solution is to perform the Matsubara sums over $i\omega_n$ in Eqs.(3.11) and (3.12) for the matrix elements of $\mathbf{M}(q)$. One then obtains,

$$\begin{aligned} M_{11}(-q) = M_{22}(q) = \frac{1}{\lambda} + \\ + \sum_{\mathbf{k}} [n_F(E_{\mathbf{k}}) - n_F(E_{\mathbf{k+q}})] \left[\frac{u_{\mathbf{k}}^2 v_{\mathbf{k+q}}^2}{\omega + (E_{\mathbf{k}} - E_{\mathbf{k+q}})} - \frac{v_{\mathbf{k}}^2 u_{\mathbf{k+q}}^2}{\omega - (E_{\mathbf{k}} - E_{\mathbf{k+q}})} \right] \Gamma^2(\mathbf{k} + \mathbf{q}/2) + \\ + \sum_{\mathbf{k}} [1 - n_F(E_{\mathbf{k}}) - n_F(E_{\mathbf{k+q}})] \left[\frac{v_{\mathbf{k}}^2 v_{\mathbf{k+q}}^2}{\omega - (E_{\mathbf{k}} + E_{\mathbf{k+q}})} - \frac{u_{\mathbf{k}}^2 u_{\mathbf{k+q}}^2}{\omega + (E_{\mathbf{k}} + E_{\mathbf{k+q}})} \right] \Gamma^2(\mathbf{k} + \mathbf{q}/2), \end{aligned} \tag{3.26}$$

and

$$\begin{aligned} M_{12}(q) = M_{21}(q) = \\ + \sum_{\mathbf{k}} [n_F(E_{\mathbf{k}}) - n_F(E_{\mathbf{k+q}})] \left[\frac{u_{\mathbf{k}} v_{\mathbf{k}} u_{\mathbf{k+q}} v_{\mathbf{k+q}}}{\omega + (E_{\mathbf{k}} - E_{\mathbf{k+q}})} - \frac{u_{\mathbf{k}} v_{\mathbf{k}} u_{\mathbf{k+q}} v_{\mathbf{k+q}}}{\omega - (E_{\mathbf{k}} - E_{\mathbf{k+q}})} \right] \Gamma^2(\mathbf{k} + \mathbf{q}/2) + \\ + \sum_{\mathbf{k}} [1 - n_F(E_{\mathbf{k}}) - n_F(E_{\mathbf{k+q}})] \left[\frac{u_{\mathbf{k}} v_{\mathbf{k}} u_{\mathbf{k+q}} v_{\mathbf{k+q}}}{\omega - (E_{\mathbf{k}} + E_{\mathbf{k+q}})} - \frac{u_{\mathbf{k}} v_{\mathbf{k}} u_{\mathbf{k+q}} v_{\mathbf{k+q}}}{\omega + (E_{\mathbf{k}} + E_{\mathbf{k+q}})} \right] \Gamma^2(\mathbf{k} + \mathbf{q}/2). \end{aligned} \tag{3.27}$$

In these expressions, $n_F(x) = \left(e^{\beta x}+1\right)^{-1}$ is simply the Fermi function at temperature $T = \beta^{-1}$, while $u_{\mathbf{k}}$ and $v_{\mathbf{k}}$ are the well known coherence factors of BCS theory, defined as

$$u_{\mathbf{k}}^2 = \frac{1}{2}\left(1+\frac{\xi_{\mathbf{k}}}{E_{\mathbf{k}}}\right) \quad \text{and} \quad v_{\mathbf{k}}^2 = \frac{1}{2}\left(1-\frac{\xi_{\mathbf{k}}}{E_{\mathbf{k}}}\right). \tag{3.28}$$

It is important to observe that the terms containing the $[n_F(E_{\mathbf{k}}) - n_F(E_{\mathbf{k+q}})]$ prefactor have energy denominators that, in general, do not allow for a simple expansion in small ω, since $\min_{\mathbf{k}}\{E_{\mathbf{k}} - E_{\mathbf{k+q}}\} = 0$. Therefore, a small $|\mathbf{q}|$ and ω expansion will be possible only in two cases: (1) just below T_c, provided that $\Delta_0(T) \ll \omega$, and (2) at $T = 0$, where the terms containing the prefactor $[n_F(E_{\mathbf{k}}) - n_F(E_{\mathbf{k+q}})]$ vanish. We will focus on the latter case in this section.

At zero temperature, the Fermi function vanishes, and only the terms containing the $[1 - n_F(E_{\mathbf{k}}) - n_F(E_{\mathbf{k+q}})]$ prefactor remain. It is then convenient to write the matrix element $M_{11}(q)$ given in Eq.(3.26) as a sum of two contributions, namely,

$$M_{11}(q) = M_{11}^{(E)}(q) + M_{11}^{(O)}(q), \tag{3.29}$$

which are respectively even (E) and odd (O) in ω. Using the $T = 0$ order parameter equation to eliminate the explicit dependence on the interaction strength λ, together with the expressions for the coherence factors $u_{\mathbf{k}}$ and $v_{\mathbf{k}}$, the even term $M_{11}^{(E)}(q)$ can be shown to be given by

$$M_{11}^{(E)}(q) = \sum_{\mathbf{k}}\left[\frac{\Gamma^2(\mathbf{k})}{2E_{\mathbf{k}}} + \frac{E_{\mathbf{k}}E_{\mathbf{k+q}} + \xi_{\mathbf{k}}\xi_{\mathbf{k+q}}}{2E_{\mathbf{k}}E_{\mathbf{k+q}}}\,\frac{(E_{\mathbf{k}}+E_{\mathbf{k+q}})\,\Gamma^2(\mathbf{k}+\mathbf{q}/2)}{\omega^2-(E_{\mathbf{k}}+E_{\mathbf{k+q}})^2}\right], \tag{3.30}$$

while the odd contribution $M_{11}^{(O)}(q)$ becomes

$$M_{11}^{(O)}(q) = -\sum_{\mathbf{k}}\frac{\xi_{\mathbf{k+q}}E_{\mathbf{k}} + \xi_{\mathbf{k}}E_{\mathbf{k+q}}}{2E_{\mathbf{k}}E_{\mathbf{k+q}}}\,\frac{\Gamma^2(\mathbf{k}+\mathbf{q}/2)}{\omega^2-(E_{\mathbf{k}}+E_{\mathbf{k+q}})^2}\,\omega. \tag{3.31}$$

Finally, the matrix element $M_{21}(q)$ can be written, in the limit of $T \to 0$, as

$$M_{12}(q) = \sum_{\mathbf{k}}\frac{\Delta_0^2\,\Gamma(\mathbf{k})\Gamma(\mathbf{k}+\mathbf{q})}{2E_{\mathbf{k}}E_{\mathbf{k+q}}}\,\frac{(E_{\mathbf{k}}+E_{\mathbf{k+q}})\,\Gamma^2(\mathbf{k}+\mathbf{q}/2)}{\omega^2-(E_{\mathbf{k}}+E_{\mathbf{k+q}})^2}, \tag{3.32}$$

which is always even in ω.

Having obtained the matrix elements of $\mathbf{M}(q)$ in a more appropriate form, it is now

convenient to rotate the basis in which the fluctuation propagator is represented, in order to express it in the so-called amplitude-phase representation. For the small fluctuations relevant to the low temperature regime, we define

$$\eta(x) \equiv r(x)\, e^{i\phi(x)} \equiv \frac{1}{\sqrt{2}}(\lambda(x) + i\theta(x)), \tag{3.33}$$

where $\lambda(x)$ and $\theta(x)$ are real functions that can be identified with amplitude and phase fluctuations, respectively. The reality of $\lambda(x)$ and $\theta(x)$ implies that their Fourier transforms $\lambda(q)$ and $\theta(q)$ will be such that $\lambda(-q) = \lambda^*(q)$ and $\theta(-q) = \theta^*(q)$. Therefore, the vector $\underline{\eta}(q)$ defined in Eq.(3.10) can be rewritten in terms of amplitudes and phases as

$$\underline{\eta}(q) = \begin{pmatrix} \eta(q) \\ \eta^*(-q) \end{pmatrix} = \frac{1}{\sqrt{2}} \begin{pmatrix} \lambda(q) + i\theta(q) \\ \lambda(q) - i\theta(q) \end{pmatrix} = \frac{1}{\sqrt{2}} \begin{pmatrix} 1 & i \\ 1 & -i \end{pmatrix} \begin{pmatrix} \lambda(q) \\ \theta(q) \end{pmatrix}. \tag{3.34}$$

By means of this expression for $\underline{\eta}(q)$ (together with its Hermitian conjugate $\underline{\eta}^\dagger(q)$), and using the fact that $M_{12}(q) = M_{21}(q)$, the fluctuation correction to the effective action given in Eq.(3.13) will be written in terms of amplitudes and phases as

$$S_{\text{fluct}}[\lambda, \theta] = \frac{1}{2} \sum_q \begin{pmatrix} \lambda^*(q) & \theta^*(q) \end{pmatrix} \begin{pmatrix} M_{11}^{(E)}(q) + M_{12}(q) & iM_{11}^{(O)}(q) \\ -iM_{11}^{(O)}(q) & M_{11}^{(E)}(q) - M_{12}(q) \end{pmatrix} \begin{pmatrix} \lambda(q) \\ \theta(q) \end{pmatrix}, \tag{3.35}$$

where the matrix element $M_{11}(q)$ was expressed in terms of its even and odd contributions by means of the relations

$$\begin{cases} M_{11}(q) + M_{11}(-q) = 2M_{11}^{(E)}(q), \\ M_{11}(q) - M_{11}(-q) = 2M_{11}^{(O)}(q). \end{cases} \tag{3.36}$$

It is important to notice that, since $M_{11}^{(O)}(\mathbf{q}, \omega = 0) = 0$, the off-diagonal elements of the fluctuation matrix vanish in this representation in the limit of $\omega \to 0$, that is, the amplitude and phase fluctuations become completely decoupled at vanishingly small frequencies.

In the limit of small $|\mathbf{q}|$ and ω (more precisely, when $\omega, |\mathbf{q}|^2/m \ll \min_{\mathbf{k}}\{E_{\mathbf{k}}\}$), one can expand the matrix elements of $\mathbf{M}(q)$ in the amplitude-phase representation up to second

order in momentum and frequency, resulting in

$$S_{\rm fluct}[\lambda,\theta]=\frac{1}{2}\sum_{q}\begin{pmatrix}\lambda^*(q) & \theta^*(q)\end{pmatrix}\begin{pmatrix}C|\mathbf{q}|^2-D\omega^2 & iB\omega\\ -iB\omega & P+Q|\mathbf{q}|^2-R\omega^2\end{pmatrix}\begin{pmatrix}\lambda(q)\\ \theta(q)\end{pmatrix}+\ldots, \tag{3.37}$$

where the coefficients B, C, D, P, Q and R, which will be functions of μ and Δ_0 only, can be obtained from the expansions of $M_{11}^{(E)}(q)$, $M_{11}^{(O)}(q)$ and $M_{12}(q)$ around $|\mathbf{q}|=0$ and $\omega=0$. For arbitrary coupling, they can be shown to be given by $B=\sum_{\mathbf{k}}(\xi_{\mathbf{k}}/4E_{\mathbf{k}}^3)\Gamma^2(\mathbf{k})$, $D=\sum_{\mathbf{k}}(1/8E_{\mathbf{k}}^3)\Gamma^2(\mathbf{k})$, $P=\sum_{\mathbf{k}}(\Delta_0^2/2E_{\mathbf{k}}^3)\Gamma^4(\mathbf{k})$, $R=\sum_{\mathbf{k}}(\xi_{\mathbf{k}}^2/8E_{\mathbf{k}}^5)\Gamma^2(\mathbf{k})$, etc.

Finally, the collective mode dispersion relation $\omega=\omega(\mathbf{q})$ can be obtained by making use of the fact that the determinant is invariant under a similarity transformation (which is equivalent to a basis rotation). Therefore, $\det\mathbf{M}(q)$ will be, in the limit of small $|\mathbf{q}|$ and ω, equal to the determinant of the fluctuation matrix in the amplitude-phase representation given in Eq.(3.37). Keeping only terms up to quadratic order in $|\mathbf{q}|$ and ω, one obtains

$$\det\mathbf{M}(\mathbf{q},\omega)=CP|\mathbf{q}|^2-(DP+B^2)\omega^2\equiv A(\mu,\Delta_0)\left[\omega^2-c_s^2|\mathbf{q}|^2\right], \tag{3.38}$$

where $A(\mu,\Delta_0)=-(DP+B^2)$ does not depend on $|\mathbf{q}|$ or ω, as anticipated in the previous section. Furthermore, the speed of sound c_s is found to be

$$c_s=\sqrt{\frac{C}{D+B^2/P}}, \tag{3.39}$$

and the collective mode dispersion relation can be immediately obtained by equating the determinant of the fluctuation matrix to zero, yielding $\omega=c_s|\mathbf{q}|$. As discussed above, this collective mode appears as a pole in the two-particle excitation spectrum determined by the equation $\det\mathbf{M}(\mathbf{q},\omega)=0$, with $i\nu_m\to\omega+i0^+$. In fact, it can be shown [39] that, quite generally, this pole has the form $\omega=c_s|\mathbf{q}|-id|\mathbf{q}|^2$ for non-s-wave systems, where $c_s>0$ is the speed of sound and $d\geq 0$ is the damping coefficient. For $\mu<0$, d vanishes and the contribution from the collective mode pole $\omega=c_s|\mathbf{q}|$ dominates at sufficiently low temperatures, since the two-particle excitations are gapped. For $\mu>0$, d becomes positive, and the spectrum of two-particle excitations is gapless due to the presence of the Dirac points. Thus, unlike the s-wave case, Landau damping occurs even at $T=0$. However, for

small $|\mathbf{q}|$, the Goldstone mode is underdamped, i.e., the real part of the pole dominates. Therefore, for either $\mu > 0$ or $\mu < 0$, the fluctuation effects lead to the same correction to the number equation given by Eq.(3.24), which is negligible in the limit of $T \to 0$.

3.5 Finite Temperature Behavior

In this section, we justify the previous claim that the BCS-to-BEC transition region cannot be adequately described by the saddle point equations at temperatures close (or equal) to the transition temperature T_c. In fact, the mean field solution can be shown to miss the qualitative physics of the intermediate and strong coupling regimes when $T \approx T_c$. In this limit, the full frequency dependence of fluctuations about the saddle point has to be retained in order to account for the contribution of the bosonic degrees of freedom, which become increasingly important with growing attraction.

The first step will be to analyze how the fluctuations in the order parameter affect the superconducting transition temperature T_c. However, it is a well-known fact that there can be no Bose-Einstein condensation in strictly two-dimensional systems [40]. In fact, this is consequence of a more general result due to Mermin and Wagner [41, 42], who rigorously proved that, at any finite temperature, there can be no long-range order in one- or two-dimensional systems with finite-range interactions. Nevertheless, 2D systems can undergo another type of phase transition, known as Berezinskii-Kosterlitz-Thouless (BKT) transition [43, 44], which separates a high-temperature phase where the order parameter correlation function has an exponential decay, from a low-temperature (BKT) phase characterized by a power-law decay of the correlation function.

In order to calculate the BKT critical temperature T_{BKT} in the case of two-dimensional d-wave superconductors, it is convenient to establish a connection between this problem and a model system for which the BKT transition has already been extensively studied, namely, the XY model in two dimensions [45]. The classical two-dimensional XY model consists of a particular case of the n-vector model, in which planar rotors (2D classical spins $\mathbf{s}_i$) are

arranged on a two-dimensional square lattice, with the Hamiltonian given by

$$\mathcal{H}_{XY} = -J \sum_{\langle i,j \rangle} \mathbf{s}_i \cdot \mathbf{s}_j = -J \sum_{\langle i,j \rangle} \cos(\theta_i - \theta_j). \tag{3.40}$$

The notation $\langle i, j \rangle$ indicates all nearest neighbor sites in the lattice, J is a coupling constant, and θ_i denotes the angle between the rotor on site i and some arbitrary polar direction in the 2D space containing the rotors. If one assumes that the direction of the spins varies smoothly from site to site ($|\theta_i - \theta_j| \ll 1$), then one can approximate $\cos(\theta_i - \theta_j)$ by the first two terms $1 - \frac{1}{2}(\theta_i - \theta_j)^2$ of its Taylor expansion. Finally, approximating the sum over neighboring lattice sites by an integral, and absorbing any remaining constants into the definition of the ground state energy, the Hamiltonian can be expressed as

$$\mathcal{H}_{XY} \approx \frac{J}{2} \int d^2r \left[\nabla\theta(\mathbf{r})\right]^2 . \tag{3.41}$$

The critical temperature at which the dependence of the spin-spin correlation function on the separation between the two spins changes from exponential to power-law can be calculated exactly for this model [46], yielding

$$T_{\mathrm{BKT}} = \frac{\pi}{2} J. \tag{3.42}$$

Despite its extremely simple form, this result was derived using renormalization group techniques and, therefore, already includes corrections due to fluctuations of the field $\theta(\mathbf{r})$ to an order of approximation higher than Gaussian.

At this point, a direct connection to the original d-wave superconductivity problem can be made [47, 48]. The idea is to start with Eq.(3.35) for the fluctuation correction to the effective action written in terms of amplitudes $\lambda(q)$ and phases $\theta(q)$. Performing the necessary matrix operations and (functionally) integrating out the amplitudes, one is left with an expression for S_{fluct} only in terms of the phases. Finally, Fourier transforming back from momentum and frequency $(\mathbf{q}, \omega)$ to position and imaginary time $(\mathbf{r}, \tau)$, one can show [49] that the effective action will contain a term of the form $\frac{1}{2}\hbar^2 \int d^2r\, \rho(\mu, \Delta_0, T) \left[\nabla\theta(\mathbf{r})\right]^2$, where $\rho(\mu, \Delta_0, T)$ is the superfluid density at temperature T given by Eq.(2.59). Therefore, a direct comparison between this result and the Hamiltonian of the XY model given by

Eq.(3.41) provides the following expression for the BKT temperature of the superconductivity problem,

$$\frac{\pi}{2}\hbar^2\rho\left(\mu,\Delta_0,T_{\mathrm{BKT}}\right)=T_{\mathrm{BKT}}, \tag{3.43}$$

which is a self-consistent equation for T_{BKT}. With the help of the definition $\Delta\rho(T)=m\rho(T)-n$, together with the relation between particle density and Fermi energy in two dimensions, $n=(m/\pi\hbar^2)\epsilon_F$, this equation can be expressed in dimensionless form as

$$\frac{1}{4\pi}\left(\Delta\rho(T_{\mathrm{BKT}})+n\right)=T_{\mathrm{BKT}}, \tag{3.44}$$

where $\Delta\rho$ and n are written in units of $n_{\max}/2\pi$, while T_{BKT} is in units of $\epsilon_{F_{\max}}$.

Although the coupling constant J is assumed to have no dependence on temperature in the standard XY model, the superfluid density ρ does depend on T and, therefore, a self-consistent calculation of T_{BKT} as a function of density (or interaction strength) requires additional equations for μ and Δ_0. In the present case, these equations are precisely the finite-temperature order parameter and number BCS equations given by Eqs.(2.39) and (2.44) which, together with Eq.(3.44), form a complete set of equations to be solved self-consistently for μ, Δ_0 and T_{BKT} as functions of n or λ. Our numerical solution for the transition temperature T_{BKT} as a function of the interaction strength λ at fixed particle density ($n=1$) in the case of d-wave pairing symmetry is shown in Fig. 3.2. The curve labeled MF in the figure corresponds to the mean field (saddle point) solution for the transition temperature, which can be obtained by making $\Delta_0=0$ and solving the system of number and order parameter equations self-consistently for T_{MF} and μ. The figure still shows our results for T_{BKT} and T_{MF} as functions of density at fixed interaction strength (inset).

One should notice that the difference between the BKT and mean field solutions grows drastically with λ, showing that the strong coupling results become increasingly affected by the proper treatment of bound pairs. Therefore, although the saddle point description works well at low temperatures, it becomes completely inadequate at $T\approx T_c$, as can be concluded from the (unphysical) unbounded increase of T_{MF} with coupling shown in the figure, which is

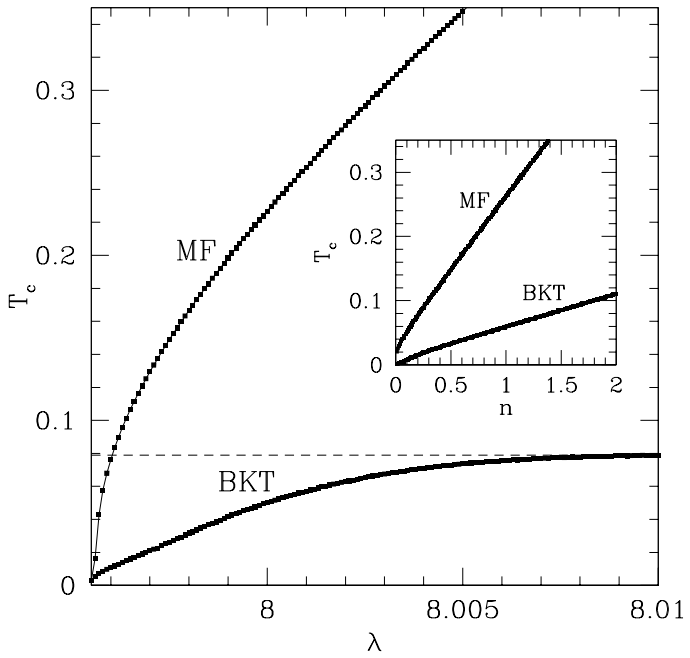

Figure 3.2: Berezinskii-Kosterlitz-Thouless (BKT) and mean field (MF) critical temperatures (in units of $\epsilon_{F_{\max}}$) as functions of the interaction strength λ (in units of g_{2D}^{-1}) at fixed particle density ($n = 1$) in the case of d-wave pairing. *Inset:* Same quantities as functions of the particle density n (in units of $n_{\max}/2\pi$) at fixed interaction strength.

clearly an artifact of the approximation. On the other hand, the BKT temperature converges asymptotically to a limiting value, which can be obtained from Eq.(3.44) by recalling that $\Delta\rho \to 0$ in the extreme strong coupling limit, yielding $T_{\rm BKT}^{(\max)} = 1/4\pi \approx 0.079$.

Finally, after solving the system of three coupled equations described above, one still obtains the chemical potential and order parameter amplitude at the critical temperature as byproducts of the calculation. These quantities are shown in Fig. 3.3 as functions of particle density at fixed interaction strength. One important point that should be noticed is the absence of cusps in $\mu(T_{\rm BKT})$ and $\Delta_0(T_{\rm BKT})$ at $n = 1$, contrary to what was found in the zero-temperature case (see Fig. 2.3). This indicates that the evolution from the BCS to the BEC limits at $T = T_c$ should be a smooth process, as opposed to the situation found at $T = 0$, in which case a quantum phase transition was shown to take place.

3.6 Summary

The goal of this chapter was basically two-fold. First, the correction to the saddle point effective action due to Gaussian fluctuations in the order parameter was calculated, and

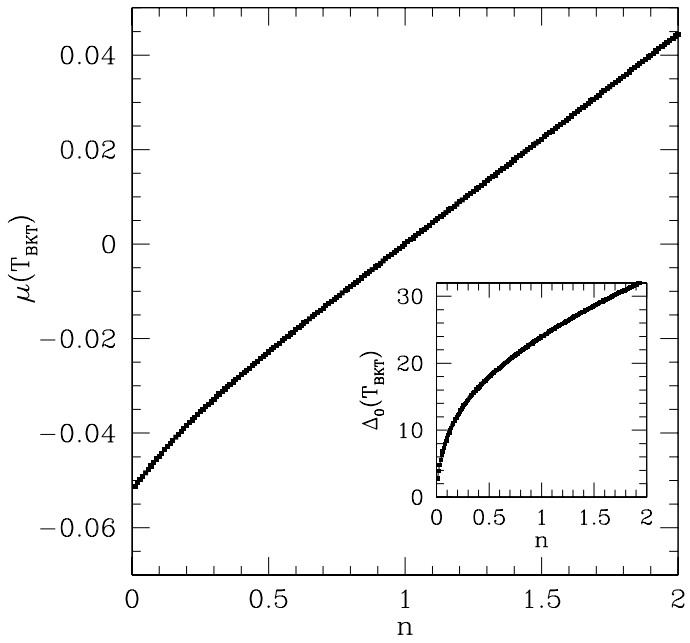

Figure 3.3: Chemical potential and order parameter amplitude (in units of $\epsilon_{F_{\max}}$) at the critical temperature as functions of the particle density n (in units of $n_{\max}/2\pi$) at fixed interaction strength in the case of d-wave pairing.

the effect of this correction on the BCS number equation was shown to vanish as T^3 and, therefore, to be negligible in the limit of small temperatures ($T \ll T_c$). As a requirement for this calculation, the collective mode dispersion relation was obtained in the limit of small $|\mathbf{q}|$ and ω. The second objective of this chapter was to show that the mean field approximation becomes progressively unreliable with increasing coupling. In fact, for $T \approx T_c$, the trivial saddle point solution cannot be used to describe the condensation of pairs (which dominates the strong coupling regime), and the bosonic degrees of freedom that come from two-body bound states can only be accounted for by going beyond the saddle point level of approximation.

CHAPTER IV

BCS-TO-BEC EVOLUTION IN P-WAVE ULTRACOLD GASES OF FERMIONIC ATOMS

4.1 Introduction

In the previous chapters, the possibility of a quantum phase transition in the BCS-to-BEC evolution of d-wave superconductors was analyzed. In particular, the feasibility of realizing such a transition in laboratory was discussed, and the use of *field effect transistors* (FETs) was pointed out as one of the most promising alternatives. In these systems, the application of an external electric field is used to create a thin charge accumulation or depletion layer, which can in principle be used to tune the carrier density of an oxide channel placed between a source and a drain contact [25]. In fact, the geometry of an FET is rather similar to that of a regular transistor, the main difference being the replacement of its semiconductor base by an oxide superconductor material. However, despite its conceptual simplicity, several technical challenges still impair the direct application of such systems to the electrostatic modulation of carrier densities in high-T_c materials. One of these issues is related to the fact that typical charge concentrations in oxide superconductors are in the range of 10^{19}-$10^{22}\,\mathrm{cm}^{-3}$, which is intermediate between those of normal metals and semiconductors. In order to control the carrier modulation at such high densities, extremely large electric fields must be applied, requiring the use of gate dielectrics with impractical breakdown field strengths for current standards. Other additional difficulties for organic FETs are the occurrence of leakage currents through the insulator, degradation of the oxide channel, design and fabrication of non-trivial drain and source contacts, etc.

Meanwhile, recent developments in a somewhat unrelated area of physics have provided scientists with an alternative way of investigating the behavior of highly degenerate quantum systems in a controlled environment. Ultracold atomic gases have emerged as a unique

testing ground for many theories of exotic matter in nature, allowing the creation of complex, but yet very accessible and well controlled many-body quantum systems. One of the most important breakthroughs in this field happened in 1995, when the theoretically predicted Bose-Einstein condensation [50, 51] was performed in laboratory for the first time using alkali atoms [52, 53, 54]. Since then, Bose-Einstein condensates (BECs) have been extensively studied, and atoms of eight chemical elements have already been condensed by several research groups all over the world [55].

The successfull condensation of dilute gases of bosonic atoms led to the investigation of the possibility of also cooling and trapping fermions to a state of high quantum degeneracy. One of the main goals of such experiments is the creation of molecular BECs, that is, pairs of fermionic atoms that behave like bosons and, theferore, can even undergo Bose-Einstein condensation. The most interesting feature of such experiments is the ability to explore the connection between the Fermi-Dirac and the Bose-Einstein statistics on the same physical system. The main idea is that, if one starts with a gas of bosonic atoms, only the bosonic degrees of freedom can be studied, since a pair of bosons is also a boson. On the other hand, when two fermions combine, they effectively behave as a single boson, as their half-integer spins add in such a way as to create a new entity with integer spin. Therefore, if one were able to create an effectively attractive interaction between the atoms in the gas, and directly control the strength of this interaction, it would be possible to continuously drive the system from a weak-coupling BCS-like regime of loosely correlated fermions in momentum space, to an opposite strong-coupling BEC-like regime of tightly bound atomic pairs that behave like bosons. This way, one would be able to experimentally explore the predicted BCS-to-BEC evolution in the context of atomic cold gases. Contrary to the case of d-wave superconductors described previously, in which the BCS-to-BEC evolution can (in principle) be studied as a function of carrier density, experiments with degenerate gases open the possibility of transitioning between the bosonic and fermionic behaviors by tuning the inter-atomic interaction strength at constant density.

Now the question remains of whether or not it is feasible to produce and control an attractive interaction between two fermionic atoms of an ultracold degenerate gas. As it

turns out, this can in fact be done by means of the so-called Feshbach resonances [56, 57], which occur when the energy of two colliding atoms becomes degenerate with the energy of a diatomic molecular bound state.

To better understand this idea, consider the sketch in Fig. 4.1, which shows a typical effective potential curve for a molecular state (closed channel), with one of its possible bound states highlighted. The atomic sample is prepared in the lower energy curve (open channel), and the total energy of a certain pair of atoms corresponds to the horizontal line denoted by E_{free} in the figure. Therefore, the bound state in the closed channel differs in energy by an amount ε from the open channel threshold. However, since the two channels generally have different spin configurations, they respond differently to externally applied magnetic fields. In particular, if the two channels have different total magnetic moments, one can tune their relative energies simply by varying the strength of an external magnetic field, which is the main concept behind the Feshbach resonance. In other words, the application of a magnetic field causes the two effective potential curves in the figure to be shifted with respect to each other, such that the energy distance to the closest molecular bound state varies as $\varepsilon = \Delta\mu(B - B_{\text{R}})$, where $\Delta\mu$ is the difference between the magnetic moments for the closed and open channels, and B_R is the resonance magnetic field.

In experiments with atomic gases, the mechanism described above has been extensively used to control the inter-particle interaction [58, 59, 60], which is a key ingredient to the production of condensates out of a Fermi gas of atoms. In fact, as the resonance magnetic field is approached, the emergence of a new bound state leads to the divergence of the s-wave scattering length a_s, which characterizes the strength of the interaction between two atoms. Furthermore, the quantity a_s undergoes a change of sign as the Feshbach resonance is crossed, going from positive on the lower magnetic field side of the resonance (BEC-like regime) to negative on the higher magnetic field side of the resonance (BCS-like regime), as shown in Fig. 4.2. In fact, the scattering length can be shown to depend on the magnetic field strength B according to [61]

$$a_s = a_{\text{nr}}\left(1 - \frac{w}{B - B_R}\right), \tag{4.1}$$

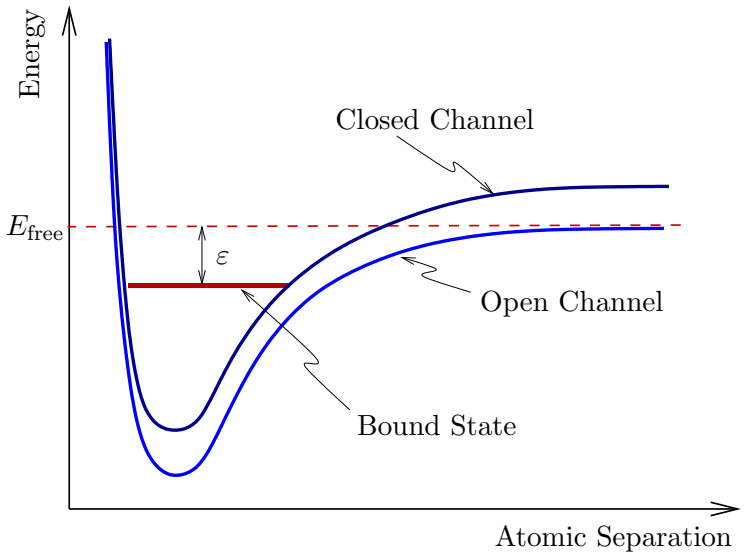

Figure 4.1: Sketch of the effective potential curves for the free atoms (open channel) and molecular bound state (closed channel) involved in a Feshbach resonance. The energy difference ε varies as a function of the detuning, $\varepsilon \sim B - B_R$, close to resonance.

where B_R is the resonance field, w measures the width of the resonance, and a_{nr} is the non-resonant, background contribution from distant bound states. This way, experimentalists have a powerful tool for tuning the intensity of the attraction between pairs of atoms in a degenerate Fermi gas. By changing the magnitude of an external magnetic field, it is possible to continuously vary the inter-particle interaction strength in a controlled and precise manner, enabling one to study the intermediate coupling regime that characterizes the BCS-to-BEC crossover region. The onset of a two-body bound state formation is associated with a divergence of the s-wave scattering length a_s, which changes sign as the resonance field $B = B_R$ is crossed.

The sketch in Fig. 4.2 also shows the behavior of the molecular binding energy E_b as a function of magnetic field. Close to resonance, this quantity is fundamentaly linked to the scattering length in three dimensions as $E_b = \hbar^2/ma_s^2$, where m is the atomic mass, and will play a very important role in the discussions that follow. In fact, the interaction strength λ (used in the context of superconductivity) will be eliminated from our calculations in favor of the two-body bound state energy E_b, in terms of which all our results will be expressed.

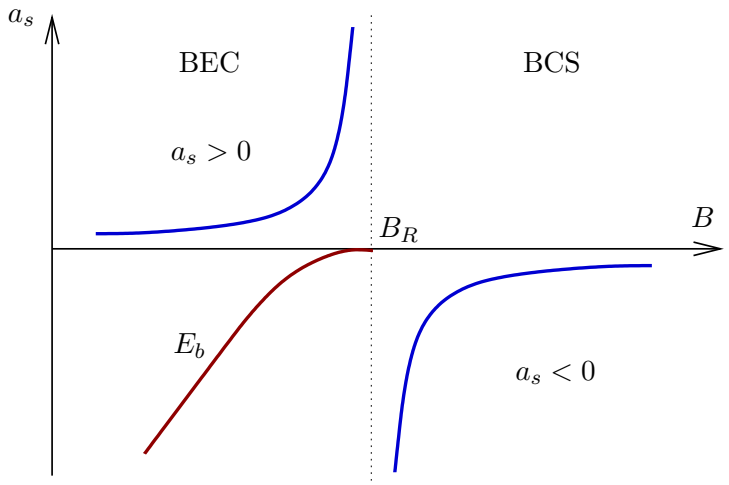

Figure 4.2: Plot of the s-wave scattering length a_s and of the molecular binding energy E_b as functions of the externally applied magnetic field B throughout the Feshbach resonance. Notice the divergence of a_s as the resonant field B_R is crossed.

The presence of strong interactions makes it difficult to understand the detailed properties of the macroscopic quantum state, and allows only a small fraction of the particles to occupy the lowest energy level. Therefore, in order to explore the behavior of a fermionic condensate, one has to work with very dilute, and hence weakly interacting, atomic gases. However, the condition for high quantum degeneracy can be expressed mathematicaly as $n\lambda_{\rm dB}^3 \gg 1$, where n is the number density and $\lambda_{\rm dB} = \sqrt{2\pi\hbar^2/k_B T m}$ is the thermal deBroglie wavelength at temperature T [40]. Thus, in order to fulfill this condition at low densities, one has to cool the atom gas to extraordinarily low temperatures near absolute zero. Furthermore, the fact that fermionic systems satisfy the Pauli exclusion principle (which forbids identical particles from occupying the same quantum state), implies that fermions cannot be directly evaporatively cooled, an essential ingredient in all BEC experiments.

Despite these stringent requirements, experimentalists are currently able to not only achieve such low temperatures, but they have also gained substantial control over the interatomic interaction strength by means of s-wave magnetic-field-induced Feshbach resonances. Several groups have now reached Fermi degeneracy by cooling atomic gases of ^{6}Li [62, 63, 64, 65, 66] and ^{40}K [67] down to about 0.1 to 0.2 of the Fermi temperature. Furthermore, by tuning the strength of an externally applied magnetic field, they have successfully driven the fermion gas from a BCS-like regime of large and weakly interacting atomic pairs (higher

magnetic fields) to a BEC-like regime of tightly bound and strongly interacting diatomic molecules (lower magnetic fields). Finally, it was recently reported [68, 69] that condensates of atomic fermion pairs have been observed on the BCS side of the crossover. In this regime, the two-body physics no longer supports the existence of bound molecular states, and the pairing between fermionic atoms can only be accounted for by cooperative many-body effects. Also, demonstrating the condensation of fermion pairs on the higher magnetic field side of the resonance presents some further challenges to the experimentalists, as standard time-of-flight expansion images do not work properly in this region, since the pairs depend on many-body effects and are not bound during the expansion of the gas. In fact, clear evidence of superfluidity on the BCS side has only been presented very recently [70], by means of an experiment in which vortices, a typical signature of superfluid behavior, were observed in an ultracold gas of ^{6}Li atoms.

In order to lower the temperature of the fermion gas to almost absolute zero, researchers typically use a combination of laser trapping followed by evaporative cooling in either a magnetic or optical trap. The group of Jin *et al*, for example, employed a technique in which two different Zeeman spin-states of ^{40}K, $|9/2, 9/2\rangle$ and $|9/2, 7/2\rangle$, are held in a magnetic trap and cooled by forced evaporation [71]. Because of the quantum statistics of fermions, such a mixture of two components is necessary to produce s-wave interactions between the atoms. The gas is then loaded into a resonance optical trap, which has the ability to hold atoms in any spin state, as well as any molecules created from these atoms. Finally, the spin mixture is further evaporatively cooled by lowering the optical potential depth [68].

An alternative approach, known as sympathetic cooling, was used by the group of Hulet *et al* to obtain a quantum degenerate Fermi gas of Lithium [72]. The idea consists in simultaneously cooling a gas of bosons (^{7}Li) and fermions (^{6}Li) using standard techniques of magnetic and optical trapping to confine both isotopes. After being loaded into a dual magneto-optical trap (MOT), bosons and fermions are optically pumped into the $|2, 2\rangle$ and $|3/2, 3/2\rangle$ states, respectively, and transfered to a purely magnetic trap. Degeneracy is then attained by microwave-induced evaporative cooling of ^{7}Li, the remaining ^{6}Li atoms being "sympathetically" cooled through their elastic collisions with the bosons that leave the trap.

A frequency-swept microwave pulse transfers the ^{6}Li atoms from the $|3/2, 3/2\rangle$ state to the $|1/2, 1/2\rangle$ state, and Feshbach resonances occur between the two lowest hyperfine levels, $|1/2, 1/2\rangle$ and $|1/2, -1/2\rangle$ [64].

Although there has been a great deal of activity in the area of quantum fermionic gases in the last several years, much of the experimental [62, 63, 64, 65, 66, 67] and theoretical [73, 74, 75, 76] efforts have concentrated on the study of the BCS-to-BEC crossover in s-wave systems. In this chapter, we present a functional integral analysis of the BCS-to-BEC evolution in p-wave fully spin-polarized Fermi gases, where p-wave Feshbach resonances have already been observed [59, 77, 78]. We show that a quantum phase transition takes place when the chemical potential crosses a critical value, instead of the usual smooth BCS-to-BEC crossover that occurs in s-wave superfluids. The atomic compressibility and the spin susceptibility of the Fermi gas are computed and are shown to be non-analytic functions of the molecular binding energy in the p-wave case, as a consequence of a major rearrangement in the momentum distribution as the critical point is approached. This non-analytic behavior suggests the occurrence of a quantum phase transition, which is further confirmed by a discontinuous change in the temperature dependence of the superfluid density of the gas at the transition point, which goes from power-law on the BCS side of the resonance to exponential on the BEC side of the resonance.

The physical system under investigation here will be considered quasi-two-dimensional. That is, the atomic gas will be assumed to be confined to a two-dimensional plane, the degress of freedom along the direction perpendicular to the plane being negligible with respect to the in-plane degrees of freedom. Such a geometry can in principle be prepared experimentally through the formation of a one-dimensional optical lattice [79, 80], where atom transfer between lattice sites is suppressed by a large trapping potential. The form of this potential can be chosen to be

$$V_{\rm trap} = -V_0 \exp\left[-2\left(\frac{x^2}{w_x^2} + \frac{y^2}{w_y^2}\right)\right] \cos^2(k_z z), \tag{4.2}$$

where $\lambda_z = 2\pi/k_z$ is the wavelength of the light used in the laser beam and $w_x \neq w_y$, so that the trap is asymmetric in the x and y directions. Is is also assumed that $w_x, w_y \gg \lambda_F$,

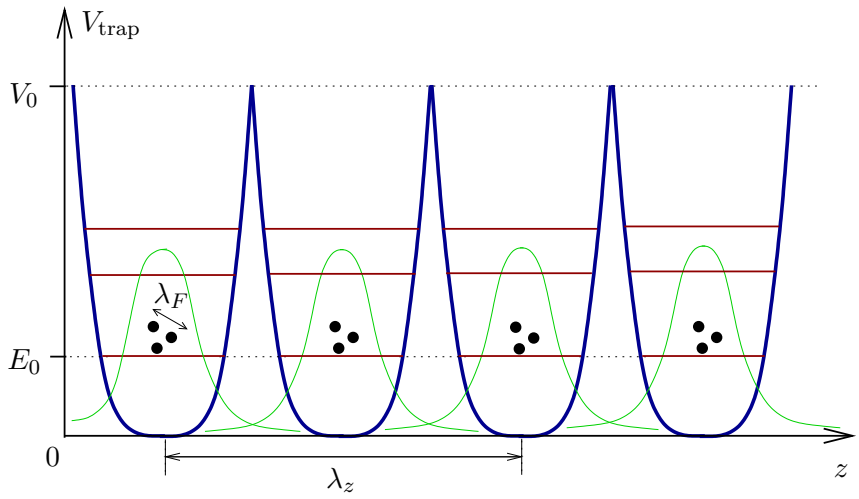

Figure 4.3: Sketch of a side view of the one-dimensional optical lattice used as the trapping potential for the fermionic atomic gas.

where $\lambda_F = 2\pi/k_F$ is proportional to the inter-particle spacing of a Fermi gas with Fermi wave-vector $\mathbf{k}_F$. This condition is important to ensure that the effects of the trapping potential can be neglected in the analysis of the problem, so that $V_{\rm trap}$ need not be explicitly included in the Hamiltonian in a first approximation. Finally, one must impose that $\epsilon_F \ll V_0 - E_0$, where $\epsilon_F = \hbar^2 k_F^2/2m$ is the Fermi energy in two dimensions and E_0 is the ground state of the Gaussian potential (with respect to its bottom), as shown in Fig. 4.3. This requirement is necessary to guarantee that the tunneling between two adjacent minima of the trapping potential is essentially suppressed, and the problem can be considered quasi-two-dimensional.

The remaining of this chapter is organized as follows. In the next section, symmetry arguments will be used to obtain an expression for the interaction potential energy between two fermionic atoms of the gas. In Section 4.3, the Hamiltonian of the system will be discussed, and the order parameter and number equations will be derived at the saddle point level of approximation by means of functional integral techniques. All the results of our numerical calculations will be shown in Section 4.4, and a discussion of fluctuation effects about the saddle point solution will be carried out in Section 4.5. Finally, the possibility of experimentally accessing some of our results are analyzed in Section 4.6, and our final remarks are summarized in Section 4.7.

4.2 Inter-atomic Interaction Potential

Although the exact mathematical form of the interaction between pairs of atoms in a Fermi gas is not known a priori, the choice of the inter-atomic potential is expected to play a central role in the analysis of the problem. Therefore, in the same spirit of what was done in Section 2.2, an expression for the k-space potential will be derived from first principles in this section, and a general equation valid for any angular momentum channel will be obtained. An analysis of both its long and short-wavelength limits will then be used to show that the expression obtained is physically reasonable. Although the derivation to be presented next follows very closely the one of Section 2.2, it will be repeated here not only for the sake of completeness, but mainly because there are some new issues that will be addressed in the context of cold gases that were not discussed in the case of superconductivity.

The matrix element $V_{\mathbf{k}\mathbf{k}'}$ of the interaction potential in k-space can be written in terms of the real space potential $V(r)$ as

$$V_{\mathbf{k}\mathbf{k}'} = \langle \mathbf{k}|V|\mathbf{k}'\rangle = \int d^2r \int d^2r' \langle \mathbf{k}|\mathbf{r}\rangle\langle \mathbf{r}|V|\mathbf{r}'\rangle\langle \mathbf{r}'|\mathbf{k}'\rangle = \int d^2r\, e^{-i\mathbf{k}\cdot\mathbf{r}} e^{i\mathbf{k}'\cdot\mathbf{r}}\, V(r), \tag{4.3}$$

where $V(r) = \langle \mathbf{r}|V|\mathbf{r}'\rangle$ is assumed to be a central potential and, therefore, to depend only on the radial coordinate r. Using the expansion of the exponential $e^{i\mathbf{k}\cdot\mathbf{r}}$ in terms of Bessel functions in polar coordinates,

$$e^{i\mathbf{k}\cdot\mathbf{r}} = \sum_{\ell=-\infty}^{\infty} i^\ell J_\ell(kr) e^{i\ell\phi}, \tag{4.4}$$

where $\phi = \arccos(\hat{\mathbf{k}}\cdot\hat{\mathbf{r}})$, the expression above for $V_{\mathbf{k}\mathbf{k}'}$ can be shown to become

$$V_{\mathbf{k}\mathbf{k}'} = \sum_{\ell=-\infty}^{\infty} e^{i\ell\phi_{\mathbf{k}\mathbf{k}'}}\, V_{kk'}^{(\ell)}, \tag{4.5}$$

where $\phi_{\mathbf{k}\mathbf{k}'} = \arccos(\hat{\mathbf{k}}\cdot\hat{\mathbf{k}}')$ is the angle between the vectors $\mathbf{k}$ and $\mathbf{k}'$, and the k-dependent coefficients $V_{kk'}^{(\ell)}$ are related to the real space potential $V(r)$ through the Fourier-Bessel transform,

$$V_{kk'}^{(\ell)} = 2\pi \int_0^\infty dr\, r\, J_\ell(kr) J_\ell(k'r) V(r). \tag{4.6}$$

In the long wavelength limit ($k \to 0$), one can show that the k and k' dependencies of

$V_{kk'}^{(\ell)}$ become exactly separable. In fact, for $kr \ll 1$ and $k'r \ll 1$, the asymptotic expression of the Bessel function for small arguments can be used in Eq.(4.6), giving $V_{kk'}^{(\ell)} = C_\ell k^\ell (k')^\ell$, with the coefficient C_ℓ dependent on the particular choice of the real space potential. In the opposite limit, $kr \gg 1$ and $k'r \gg 1$, the interaction is certainly not separable. However, one can show that, in this case, $V_{kk'}^{(\ell)}$ mixes different k and k' and shows an oscillatory behavior which is dependent on the exact form of $V(r)$, with a decaying envelope that is proportional to $k^{-1/2}(k')^{-1/2}$. Under these circumstances, in order to accomodate most of the features described above, the coefficients $V_{kk'}^{(\ell)}$ will be taken to be

$$V_{kk'}^{(\ell)} = -\lambda_\ell \, h_\ell(k) \, h_\ell(k'), \tag{4.7}$$

where $\lambda_\ell > 0$ is the interaction strength, and the function $h_\ell(k)$ is defined as

$$h_\ell(k) = \frac{(k/k_1)^\ell}{(1 + k/k_0)^{\ell+1/2}}, \tag{4.8}$$

where the constant k_0 plays the role of the inverse interaction range, and k_1 sets the scale at low momenta. This function indeed reduces to $h_\ell(k) \sim k^\ell$ for small k, and behaves as $h_\ell(k) \sim k^{-1/2}$ for large k, guaranteeing the correct behavior expected for $V_{kk'}^{(\ell)}$ according to the previous analysis in the long and short-wavelength limits.

In order to obtain an expression for the angular dependence of $V_{\mathbf{k}\mathbf{k}'}$, one reasonable strategy is to retain only a finite number of terms in the plane-wave expansion of Eq.(4.5). One possibility is to keep both the $+\ell$ and $-\ell$ terms in the expansion, which amounts physically to isolating only the contribution from the ℓ^{th} angular momentum channel to the scattering process responsible for the interaction between the fermionic atoms. Taking Eq.(4.7) into account, this results in

$$\begin{aligned} V_{\mathbf{k}\mathbf{k}'} &= -\lambda_\ell h_\ell(k) h_\ell(k') \cos\big(\ell(\varphi - \varphi')\big) = \\ &= -\lambda_\ell h_\ell(k) h_\ell(k') \left[\cos(\ell\varphi)\cos(\ell\varphi') + \sin(\ell\varphi)\sin(\ell\varphi')\right], \end{aligned} \tag{4.9}$$

where φ (φ') is the angle associated with the vector $\mathbf{k}$ ($\mathbf{k}'$) in momentum space. However, if one has either an anisotropic trap ($w_x \neq w_y$) or a weak perturbing asymmetric potential $V_{\text{add}} = -U_x \cos^2(k_x x) - U_y \cos^2(k_y y)$ on top of a symmetric trap, then the polar symmetry

in the xy-plane is broken, and the existence of an order parameter with nodes (in the BCS regime) becomes possible. This externally controlled symmetry breaking, which can in principle be accomplished by changing the focus, wavelength, or intensity of the trap laser beam, may lead to the existence of a spin-polarized superfluid state, in which pairing along one particular direction in k-space is favored. If, for instance, symmetry is broken in such a way that causes pairing in the x-direction to dominate, the sine functions in the expression above for $V_{\mathbf{k}\mathbf{k}'}$ can be neglected relative to the cosines, and one is left with a fully separable interaction potential in k-space, which can be written as

$$V_{\mathbf{k}\mathbf{k}'} = -\lambda_\ell \Gamma_\ell(\mathbf{k}) \Gamma^*_\ell(\mathbf{k}'), \tag{4.10}$$

where the (real) function $\Gamma_\ell(\mathbf{k})$ is defined as

$$\Gamma_\ell(\mathbf{k}) = h_\ell(k)\, \cos(\ell\varphi) = \frac{(k/k_1)^\ell}{(1+k/k_0)^{\ell+1/2}}\, \cos(\ell\varphi). \tag{4.11}$$

Symmetry requirements similar to the one employed above, in which lattice effects and anisotropy are used to justify the separation between angular momentum channels, have already been extensively used in the literature, most notably in the study of high-T_c superconductors [81]. In fact, this idea has also been used previously in the study of the BCS-to-BEC evolution of d-wave superconductors in 2D [14, 15], in which case a similar interaction potential was considered and symmetry arguments were used to select a $d_{x^2-y^2}$ order parameter over a d_{xy} order parameter.

Another equally plausible alternative for the angular dependence of the interaction potential can be obtained by keeping only the $+\ell$ term in the plane-wave expansion of Eq.(4.5), resulting in

$$V_{\mathbf{k}\mathbf{k}'} = -\lambda_\ell h_\ell(k) h_\ell(k') e^{i\ell(\varphi-\varphi')}. \tag{4.12}$$

Clearly, this expression can be written in exactly the same separable form as given in Eq.(4.10), with the (complex) symmetry function $\Gamma_\ell(\mathbf{k})$ now defined as

$$\Gamma_\ell(\mathbf{k}) = h_\ell(k)\, e^{i\ell\varphi} = \frac{(k/k_1)^\ell}{(1+k/k_0)^{\ell+1/2}}\, e^{i\ell\varphi}, \tag{4.13}$$

which will lead to a complex order parameter with an angle-independent energy gap. However, as it will be shown later, qualitatively equivalent results are obtained whether one uses the real (Eq.(4.11)) or the complex (Eq.(4.13)) symmetry function in the separable equation for the inter-atomic interaction potential.

In the particular case of p-wave symmetry, which will be the one analyzed in this chapter, the real and complex symmetry functions derived above reduce to $\Gamma(\mathbf{k}) = h(k)\cos(\varphi)$ (p_x-symmetry) and $\Gamma(\mathbf{k}) = h(k)e^{i\varphi}$ ($p_x + ip_y$-symmetry), respectively, with the function $h(k)$ given by

$$h(k) = \frac{k/k_1}{(1 + k/k_0)^{3/2}}. \tag{4.14}$$

Notice that the sub-index (ℓ) was dropped from all these expressions for the sake of notational simplicity, and this will continue to be done throughout what follows.

In the next section, the order parameter and particle number equations for the system will be derived as the saddle point solution to the functional integral representing the partition function. A relationship between the interaction strength λ and the molecular binding energy E_b will be obtained, allowing the former quantity to be eliminated from the order parameter equation in favor of the latter.

4.3 Hamiltonian and Saddle Point Equations

In this section, a uniform and homogeneous quasi-two-dimensional continuum model of fermionic atoms of mass m in the presence of an external magnetic field $\mathbf{h} = h_{\tilde{z}}\hat{\tilde{z}}$ will be considered. The system will be assumed to be spin-polarized (all atoms in the same hyperfine state), so that the density of the gas is $n = k_F^2/4\pi$. In a system of units where $\hbar = k_B = 1$, the Hamiltonian will be written as

$$\mathcal{H} = \sum_{\mathbf{k}} \xi_{\mathbf{k}} \psi^\dagger_{\mathbf{k}\uparrow} \psi_{\mathbf{k}\uparrow} + \frac{1}{2} \sum_{\mathbf{k},\mathbf{k}',\mathbf{q}} V_{\mathbf{k}\mathbf{k}'} b^\dagger_{\mathbf{k}\mathbf{q}} b_{\mathbf{k}'\mathbf{q}}, \tag{4.15}$$

where $b_{\mathbf{k}\mathbf{q}} = \psi_{-\mathbf{k}+\mathbf{q}/2\uparrow}\psi_{\mathbf{k}+\mathbf{q}/2\uparrow}$ is the pairing operator and $\xi_{\mathbf{k}} = \epsilon_{\mathbf{k}} - \mu$, with $\epsilon_{\mathbf{k}} = k^2/2m$. Furthermore, the Zeeman energy that arises from the application of the magnetic field $\mathbf{h}$ is already absorbed in the definition of the chemical potential, $\mu = \mu(h_{\tilde{z}} = 0) + g_{\tilde{z}\tilde{z}}\mu_B h_{\tilde{z}}$,

where $g_{\tilde{z}\tilde{z}}$ is the gyromagnetic ratio and μ_B is the Bohr magneton. The direction of the magnetic field $\mathbf{h}$, which was chosen to define the spin quantization axis $\tilde{z}$, need not coincide with the spatial direction z of the laser beam.

The grand-canonical partition function $\mathcal{Z}$ of the system at a temperature $T = \beta^{-1}$ will be written as a functional integral over the fermionic field $\psi_{\mathbf{k}\uparrow}(\tau)$ with action $S = \int_0^\beta d\tau \left[\sum_{\mathbf{k}} \psi^\dagger_{\mathbf{k}\uparrow}(\tau)\partial_\tau \psi_{\mathbf{k}\uparrow}(\tau) + \mathcal{H}\right]$. Analogously to what was done in Section 2.3, one can now introduce the Hubbard-Stratonovich field $\phi_{\mathbf{q}}(\tau)$, which will couple to $\psi^\dagger\psi^\dagger$ and render the action quadratic in the fermion fields. Since this calculation is very similiar to the one carried out in Section 2.3, it will not be repeated here, but only the main results will be outlined. After integrating out the fermionic degrees of freedom, the partition function becomes a functional integral over the bosonic field $\phi_{\mathbf{q}}(\tau)$,

$$\mathcal{Z} = \int \mathcal{D}\phi\mathcal{D}\phi^* \exp\left(-S_{\text{eff}}[\phi,\phi^*]\right), \tag{4.16}$$

with the effective action given by

$$S_{\text{eff}} = \int_0^\beta d\tau \sum_{\mathbf{k}} \left(\frac{|\phi_{\mathbf{k}}(\tau)|^2}{2\lambda} + \frac{\xi_{\mathbf{k}}}{2}\right) - \mathbf{Tr}\left(\ln \frac{1}{2}\mathbf{G}^{-1}_{\mathbf{k},\mathbf{k}'}(\tau)\right), \tag{4.17}$$

where the (inverse) Nambu matrix $\mathbf{G}^{-1}_{\mathbf{k},\mathbf{k}'}(\tau)$ is defined as

$$\mathbf{G}^{-1}_{\mathbf{k},\mathbf{k}'}(\tau) = \begin{pmatrix} -(\partial_\tau + \xi_{\mathbf{k}})\delta_{\mathbf{k}\mathbf{k}'} & \Gamma\left(\frac{\mathbf{k}+\mathbf{k}'}{2}\right)\phi_{\mathbf{k}-\mathbf{k}'}(\tau) \\ \Gamma\left(\frac{\mathbf{k}+\mathbf{k}'}{2}\right)\phi^*_{\mathbf{k}'-\mathbf{k}}(\tau) & -(\partial_\tau - \xi_{\mathbf{k}})\delta_{\mathbf{k}\mathbf{k}'} \end{pmatrix}. \tag{4.18}$$

As before, the symbol **Tr** indicates not only the trace over matrix elements, but also over momentum and time coordinates, that is, $\mathbf{Tr} \to \int_0^\beta d\tau \sum_{\mathbf{k},\mathbf{k}'} \text{tr}$.

4.3.1 Order Parameter Equation

Again, the derivation of the saddle point equations for the ultracold fermionic gas will proceed in a very similar fashion as in the case of d-wave superconductors carried out in full detail in Section 2.3. After Fourier transforming from time variables to Matsubara frequencies, $i\omega_n = i(2n+1)\pi/\beta$, and performing the frequency sum, the saddle point condition $\left[\delta S_{\text{eff}}/\delta\phi^*_{\mathbf{q}}(\tau')\right]_{\Delta_0} = 0$ can be cast in the form of the familiar order parameter

equation,

$$\frac{1}{\lambda} = \sum_{\mathbf{k}} \frac{|\Gamma(\mathbf{k})|^2}{2E_{\mathbf{k}}} \tanh\left(\frac{\beta E_{\mathbf{k}}}{2}\right), \tag{4.19}$$

where $E_{\mathbf{k}} = \left(\xi_{\mathbf{k}}^2 + |\Delta_{\mathbf{k}}|^2\right)^{1/2}$ is the quasiparticle excitation energy, and $\Delta_{\mathbf{k}} = \Delta_0\Gamma(\mathbf{k})$ plays the role of the order parameter function.

At this point, it is convenient to eliminate the interaction strength λ from the equation above in favor of the binding energy E_b, since the latter is a more experimentally accessible quantity. In fact, in three dimensions, there is a close relationship between E_b and the s-wave scattering length a_s, which is the quantity actually measured in the experiments [58]. A relation between λ and the two-body bound state energy $E_b(h_{\tilde{z}})$ in vacuum (and in the presence of a magnetic field) can be obtained by solving the Schroedinger equation for two fermions of mass m interacting via a central pairing potential $V(r)$. Assuming that the atoms are located at positions $\mathbf{x_1}$ and $\mathbf{x_2}$, the two-body Schroedinger equation will read

$$-\frac{1}{2m}\nabla_1^2\Psi(\mathbf{x_1},\mathbf{x_2}) - \frac{1}{2m}\nabla_2^2\Psi(\mathbf{x_1},\mathbf{x_2}) + V(|\mathbf{x_1}-\mathbf{x_2}|)\Psi(\mathbf{x_1},\mathbf{x_2}) = \left(E + 2g_{\tilde{z}\tilde{z}}\mu_B h_{\tilde{z}}\right)\Psi(\mathbf{x_1},\mathbf{x_2}). \tag{4.20}$$

Since the system is assumed to be translationally invariant and one neglects spin-dependent forces, the center-of-mass momentum $\mathbf{Q}$ of the pair and the total spin are constants of motion. The orbital wave-function of the pair can then be written as

$$\Psi(\mathbf{x_1},\mathbf{x_2}) = e^{i\mathbf{Q}\cdot\mathbf{R}}\,\Phi(\mathbf{r}), \tag{4.21}$$

where $\mathbf{r} = \mathbf{x_1} - \mathbf{x_2}$ and $\mathbf{R} = (\mathbf{x_1} + \mathbf{x_2})/2$ are the relative and center-of-mass coordinates, respectively. Using this wave-function in the Schroedinger equation above, and defining $M_r = m/2$ and $M_p = 2m$ as the reduced and pair masses, respectively, one obtains,

$$-\frac{1}{2M_r}\nabla_r^2\Phi(\mathbf{r}) + V(r)\Phi(\mathbf{r}) = E_b\,\Phi(\mathbf{r}), \tag{4.22}$$

where the eigenvalue E_b can be shown to be given by

$$E_b = E + 2g_{\tilde{z}\tilde{z}}\mu_B h_{\tilde{z}} - \frac{Q^2}{2M_p}. \tag{4.23}$$

The quantity E_b already has the interpretation of a two-body bound state energy, as it is

the eigenvalue of the Schroedinger equation for a pair of fermionic atoms in the presence of an external magnetic field $\mathbf{h} = h_{\tilde{z}}\hat{\tilde{z}}$. Fourier transforming $\Phi(\mathbf{r})$ and $V(r)$ from real to momentum space, one can convert Eq.(4.22) into a k-space Schroedinger equation for the pair wave-function $\Phi_{\mathbf{k}}$ in the center-of-mass frame,

$$2\epsilon_{\mathbf{k}}\Phi_{\mathbf{k}} + \sum_{\mathbf{q}} V_{\mathbf{kq}}\Phi_{\mathbf{q}} = E_b\,\Phi_{\mathbf{k}}. \tag{4.24}$$

Although this equation cannot be analytically solved in general, a solution for the wave-function $\Phi_{\mathbf{k}}$ becomes immediate if the interaction potential $V_{\mathbf{kq}}$ is assumed to be separable. In fact, using that $V_{\mathbf{kq}} = -\lambda\Gamma(\mathbf{k})\Gamma^*(\mathbf{q})$, one obtains

$$\Phi_{\mathbf{k}} = \frac{\lambda\, C\, \Gamma(\mathbf{k})}{2\epsilon_{\mathbf{k}} - E_b}, \tag{4.25}$$

where the constant C is defined as $C = \sum_{\mathbf{q}} \Gamma^*(\mathbf{q})\Phi_{\mathbf{q}}$. Finally, multiplying both sides of Eq.(4.25) by $\Gamma^*(\mathbf{k})$, and summing over all possible wave-vectors $\mathbf{k}$, one finds

$$\frac{1}{\lambda} = \sum_{\mathbf{k}} \frac{|\Gamma(\mathbf{k})|^2}{2\epsilon_{\mathbf{k}} - E_b}, \tag{4.26}$$

which is the mathematical relationship between the interaction strength λ and the two-body binding energy E_b in the presence of a magnetic field.

The dependence of λ on E_b in the case of p-wave interaction is shown in Fig. 4.4 for the symmetry functions $\Gamma(\mathbf{k}) = h(k)\cos(\varphi)$ (leading to a p_x-symmetry order parameter) and $\Gamma(\mathbf{k}) = h(k)e^{i\varphi}$ (leading to a $p_x + ip_y$-symmetry order parameter). Observe that λ remains positive for all values of $E_b < 0$, and does **not** change sign at the transition point $E_b^{(c)}$ (which corresponds to $\mu = 0$, as discussed later). This can be understood by noticing that λ is simply the amplitude of the interaction potential in k-space (see Eq.(4.10)) and, therefore, is not the only responsible for the sign of $V_{\mathbf{kk'}}$. It is important to emphasize that the expression of λ in terms of E_b is just a convenient way of describing the theory in terms of the molecular binding energy. We focus only on the case where E_b is negative, that is, when a two-body bound state appears, since this corresponds to the more physically interesting case, as shown below. By contrast, the corresponding situation in 3D s-wave systems is associated with a divergence and a change of sign of the scattering length a_s when

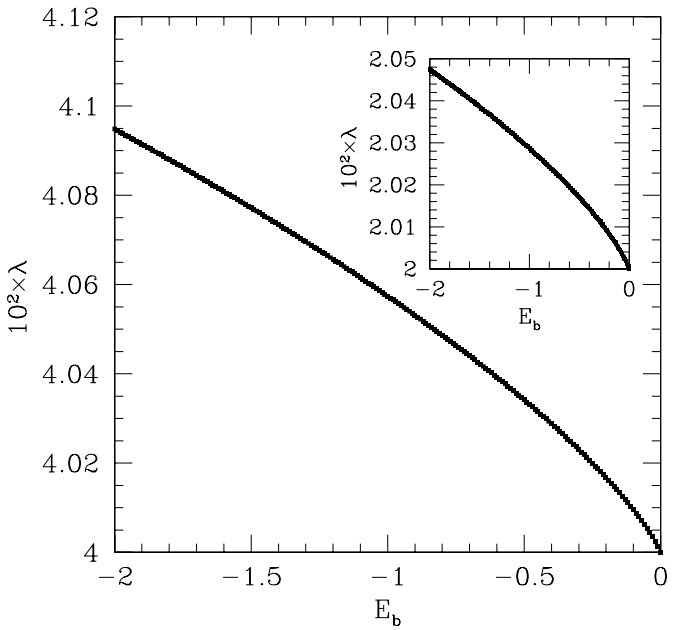

Figure 4.4: Plot of the inter-atomic interaction strength λ (in units of $g_{2\mathrm{D}}^{-1}$, where $g_{2\mathrm{D}}$ is the two-dimensional density of states) as a function of the binding energy E_b (in units of ϵ_F) for $k_0 = 10k_F$ and $k_1 = k_F$ in the case of $\Gamma(\mathbf{k}) = h(k)\cos(\varphi)$. *Inset:* The same quantities in the case of $\Gamma(\mathbf{k}) = h(k)e^{i\varphi}$.

a two-body bound state appears. In this case, it is common (although strictly incorrect) to refer to the inverse scattering length $1/a_s$ as the effective "interaction strength", which would then change sign when $a_s \to \pm\infty$. It is better to associate this change with the onset of a two-body bound state formation, which happens when the potential is sufficiently attractive. (See, for example, the zero-range s-wave system studied in Ref. [11].)

Finally, one can use the relation derived above between λ and E_b to rewrite the order parameter equation in terms of the two-body bound state energy. In fact, combining Eqs.(4.19) and (4.26), one obtains,

$$\sum_{\mathbf{k}} |\Gamma(\mathbf{k})|^2 \left[\frac{1}{2\epsilon_{\mathbf{k}} - E_b} - \frac{\tanh(\beta E_{\mathbf{k}}/2)}{2E_{\mathbf{k}}} \right] = 0. \tag{4.27}$$

4.3.2 Number Equation

The equation for the number of atoms in the gas can also be obtained from the effective action by means of the saddle point approximation for the thermodynamic potential,

$$\Omega_0 = -\frac{1}{\beta} \ln \mathcal{Z}_0 = \frac{S_{\mathrm{eff}}[\Delta_0]}{\beta}. \tag{4.28}$$

With the help of the thermodynamic relation $N = -\left(\partial\Omega/\partial\mu\right)_{T,V}$ for the number of particles in the grand-canonical ensemble, one can write the number equation as

$$N_0 = \sum_{\mathbf{k}} n_{\mathbf{k}}, \tag{4.29}$$

where the momentum distribution $n_{\mathbf{k}}$ is given by

$$n_{\mathbf{k}} = \frac{1}{2}\left[1 - \frac{\xi_{\mathbf{k}}}{E_{\mathbf{k}}}\tanh\left(\frac{\beta E_{\mathbf{k}}}{2}\right)\right]. \tag{4.30}$$

One should notice that the result obtained here for N_0 corresponds to one half of what was found in Section 2.3 (Eq.(2.44)) in the context of d-wave superconductors. This is due to the fact that the fermionic atoms analyzed here are assumed to be spin-polarized, which causes the total number of available states (and therefore the number of particles in the system) to be reduced by a factor of two.

In the following section, the zero-temperature saddle point equations will be numerically solved for the chemical potential μ and order parameter amplitude Δ_0 as functions of the molecular binding energy E_b at constant particle density. This will allow some other spectroscopic and thermodynamic properties of the system, such as the momentum distribution and the atomic compressibility, to be calculated for varying E_b in the case of p-wave symmetry. These quantities will then be shown to signal the occurrence of a quantum phase transition in the BCS-to-BEC evolution of p-wave Fermi gases.

4.4 Numerical Calculations

Before proceeding with the numerical results, it is instructive to briefly discuss how the physical quantities analyzed in this problem can be scaled, allowing the governing equations to be written in dimensionless form. Contrary to what was done in the context of superconductivity, where the energies were scaled with respect to the maximum Fermi energy $\epsilon_{F_{\max}}$, in the present case the Fermi energy ϵ_F itself will be used as the unit of energy. As it turns out, this scheme is more convenient to treat systems with fixed number of particles, since it allows the density $n = N_0/L^2$ to be eliminated from the number equation.

In fact, defining the dimensionless single-particle energy $\tilde{\epsilon}_{\mathbf{k}}$ as

$$\tilde{\epsilon}_{\mathbf{k}} = \frac{\epsilon_{\mathbf{k}}}{\epsilon_F}, \tag{4.31}$$

and the dimensionless wave-vector $\tilde{\mathbf{k}}$ as

$$\tilde{\mathbf{k}} = \frac{\mathbf{k}}{k_F}, \tag{4.32}$$

one can easily conclude that $\tilde{\epsilon}_{\tilde{\mathbf{k}}} = \tilde{k}^2$. Furthermore, the chemical potential and order parameter will be replaced by the scaled variables $\tilde{\mu} = \mu/\epsilon_F$ and $\tilde{\Delta}_{\mathbf{k}} = \Delta_{\mathbf{k}}/\epsilon_F$, respectively, such that the dimensionless excitation energy will be given by

$$\tilde{E}_{\tilde{\mathbf{k}}} = \frac{E_{\mathbf{k}}}{\epsilon_F} = \sqrt{(\tilde{k}^2 - \tilde{\mu})^2 + |\tilde{\Delta}_{\tilde{\mathbf{k}}}|^2}. \tag{4.33}$$

With the help of these conventions, and making use of the following prescription to convert the summations over $\mathbf{k}$ into two-dimensional integrals in polar coordinates (k, φ),

$$\sum_{\mathbf{k}} \to \frac{L^2}{(2\pi)^2} \int_0^{2\pi} d\varphi \int_0^{\infty} dk\, k, \tag{4.34}$$

where L^2 is the two-dimensional "volume" of the system, the zero-temperature order parameter equation can be written in terms of dimensionless quantities as

$$\int_0^{2\pi} d\varphi \int_0^{\infty} d\tilde{k}\, \tilde{k}\, |\Gamma(\tilde{\mathbf{k}})|^2 \left[\frac{1}{2\tilde{k}^2 - \tilde{E}_b} - \frac{1}{2\sqrt{(\tilde{k}^2 - \tilde{\mu})^2 + \tilde{\Delta}_0^2 |\Gamma(\tilde{\mathbf{k}})|^2}} \right] = 0, \tag{4.35}$$

where $\tilde{E}_b = E_b/\epsilon_F$. Furthermore, the number equation at zero-temperature can also be expressed in terms of scaled parameters as

$$1 = \frac{1}{2\pi} \int_0^{2\pi} d\varphi \int_0^{\infty} d\tilde{k}\, \tilde{k} \left[1 - \frac{\tilde{k}^2 - \tilde{\mu}}{\sqrt{(\tilde{k}^2 - \tilde{\mu})^2 + \tilde{\Delta}_0^2 |\Gamma(\tilde{\mathbf{k}})|^2}} \right]. \tag{4.36}$$

For the rest of this section, the tildes will be dropped for the sake of notational simplicity, but all the variables and parameters that will appear in what follows are to be understood as being already scaled. That is, all energies will be implicitly written in units of ϵ_F, all momenta in units of k_F, etc.

4.4.1 Chemical Potential and Order Parameter Amplitude

The saddle point equations derived above constitute a set of two coupled integral equations that depend on three independent parameters, namely, the order parameter amplitude Δ_0, the chemical potential μ, and the molecular binding energy E_b. In the spirit of the experiments with fermionic gases described in the beginning of this chapter, these equations will be simultaneously solved for μ and Δ_0 as functions of E_b, since the binding energy is the parameter that can be tuned experimentally by changing the strength of an externally applied magnetic field.

Our numerical results at $T = 0$ are shown in Fig. 4.5 for the case of $k_0 = 10$ and $k_1 = 1$. The two symmetry functions derived previously, corresponding to retaining either one or two terms in the plane-wave expansion of the interaction potential, are analyzed: $\Gamma(\mathbf{k}) = h(k)\cos(\varphi)$ (leading to a p_x-symmetry) and $\Gamma(\mathbf{k}) = h(k)e^{i\varphi}$ (leading to a $p_x + ip_y$-symmetry). The point $\mu = 0$, which will be shown next to have particular importance to this problem, is achieved for the critical binding energy $E_b^{(c)} = -1.088$ (corresponding to $\Delta_0 = 1.906$) in the case of p_x-symmetry, and for $E_b^{(c)} = -0.729$ (corresponding to $\Delta_0 = 1.277$) in the case of $p_x + ip_y$-symmetry. One should notice that qualitatively similar results are obtained regardless of whether the real or the complex symmetry function is used in the calculations. As it will be discussed in more detail later, this indicates that the existence of nodes (Dirac points) in the quasiparticle excitation spectrum $E_{\mathbf{k}}$ plays a rather unimportant role in determining the physical behavior of the system, which is instead dominated by the low-k dependence of the function $h(k)$.

4.4.2 Momentum Distribution

The momentum distribution defined in Eq.(4.30) is a relevant spectroscopic property that, as it turns out, has important consequences to the thermodynamic behavior of the system. In the limit of zero temperature, it reduces to

$$n_{\mathbf{k}} = \frac{1}{2}\left(1 - \frac{\xi_{\mathbf{k}}}{E_{\mathbf{k}}}\right) = \frac{1}{2}\left[1 - \frac{\epsilon_{\mathbf{k}} - \mu}{\sqrt{(\epsilon_{\mathbf{k}} - \mu)^2 + \Delta_0^2|\Gamma(\mathbf{k})|^2}}\right], \tag{4.37}$$

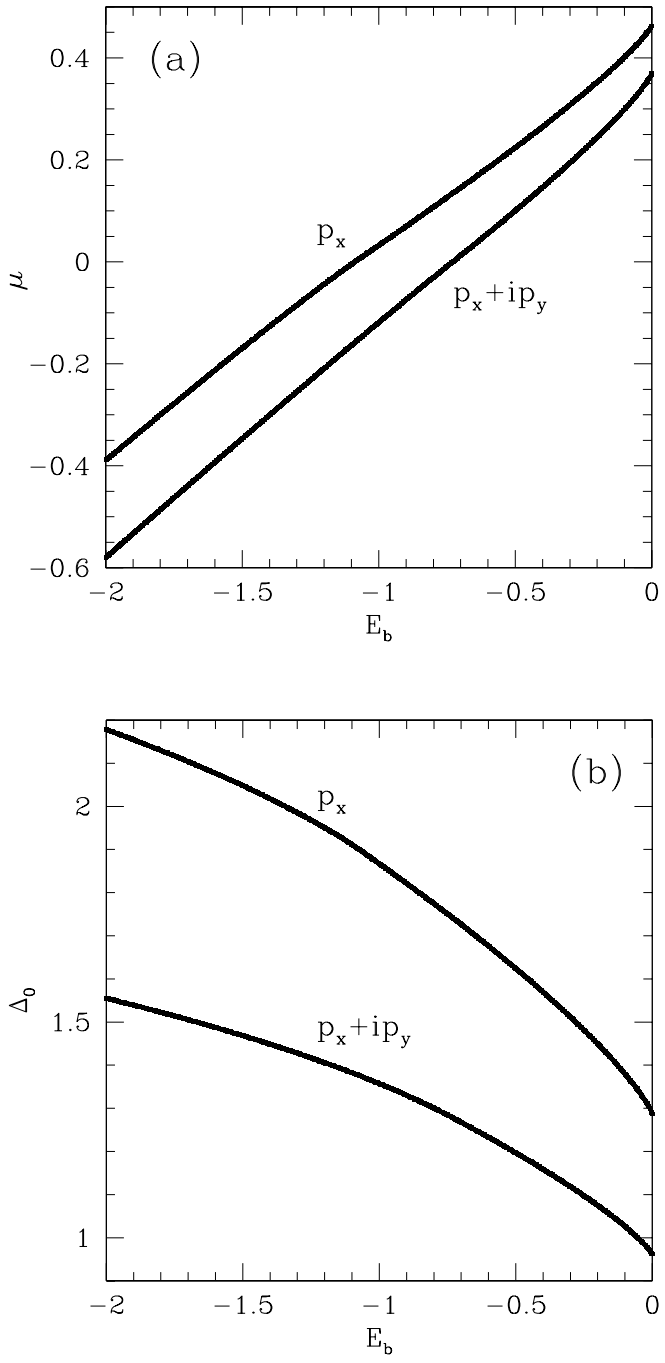

Figure 4.5: Universal plot (for any magnetic field $h_{\tilde{z}}$) of (a) the chemical potential $\mu = \mu(h_{\tilde{z}} = 0) + g_{\tilde{z}\tilde{z}}\mu_B h_{\tilde{z}}$ and (b) order parameter amplitude Δ_0 as functions of the binding energy $E_b = E_b(h_{\tilde{z}}=0) + 2g_{\tilde{z}\tilde{z}}\mu_B h_{\tilde{z}}$ (all quantities in units of ϵ_F) for $k_0 = 10k_F$ and $k_1 = k_F$ in the spin polarized p-wave case.

where $\epsilon_{\mathbf{k}} = k^2/2m$ is the single-particle energy. Plots of the momentum distribution in the case of p_x-symmetry are shown in Fig. 4.6 for three different values of the chemical potential: $\mu > 0$, $\mu = 0$ and $\mu < 0$. This corresponds to the situation where the quasiparticle excitation energy $E_{\mathbf{k}} = \left(\xi_{\mathbf{k}}^2 + \Delta_0^2 h^2(k)\cos^2(\varphi)\right)^{1/2}$ is gapless in the BCS regime and fully gapped in the BEC regime. Notice that $n_{\mathbf{k}}$ becomes discontinuous when μ crosses zero, which coincides with the collapse of the two Dirac points to a single point $\mathbf{k} = 0$ and the appearance of a full gap to the addition of quasiparticles as soon as μ becomes negative.

The use of the symmetry function $\Gamma(\mathbf{k}) = h(k)e^{i\varphi}$ results in an angle-independent quasiparticle excitation energy $E_{\mathbf{k}} = \left(\xi_{\mathbf{k}}^2 + \Delta_0^2 h^2(k)\right)^{1/2}$, which is gapped in both the BCS and BEC regimes. Consequently, the momentum distribution will have no Dirac points, but will possess polar symmetry in k-space, as shown in Fig. 4.7 for the same three values of the chemical potential. Notice, however, that the $\mu = 0$ momentum distribution develops a cusp at $\mathbf{k} = 0$ in this case, which is consequence of the vanishing of $E_{\mathbf{k}}$ at the origin of k-space when the chemical potential crosses the bottom of the band. This major rearrangement of $n_{\mathbf{k}}$ for both symmetry functions analyzed has a dramatic effect in the isothermal atomic compressibility κ of the gas, to be discussed next.

4.4.3 Atomic Compressibility and Spin Susceptibility

The isothermal compressibility κ is defined as

$$\kappa = -\frac{L^2}{N^2}\left(\frac{\partial^2\Omega}{\partial\mu^2}\right)_T = \frac{1}{n^2}\left(\frac{\partial n}{\partial\mu}\right)_T, \tag{4.38}$$

where $\Omega(T,\mu)$ is the thermodynamic potential of the system, and $n = N/L^2$ is the particle density. This quantity measures the resulting change in the density of atoms in the gas due to a variation of the chemical potential. As expected, this response will depend on the strength of the magnetic field that drives the system across the Feshbach resonance and, therefore, will be a function of the binding energy E_b.

One can easily show that the expression above for κ can be written in an alternative form in terms of $n_{\mathbf{k}}$ in the case of spin-polarized atoms as

$$n^2\kappa = \frac{2}{L^2}\sum_{\mathbf{k}}\frac{n_{\mathbf{k}}(1-n_{\mathbf{k}})}{E_{\mathbf{k}}}, \tag{4.39}$$

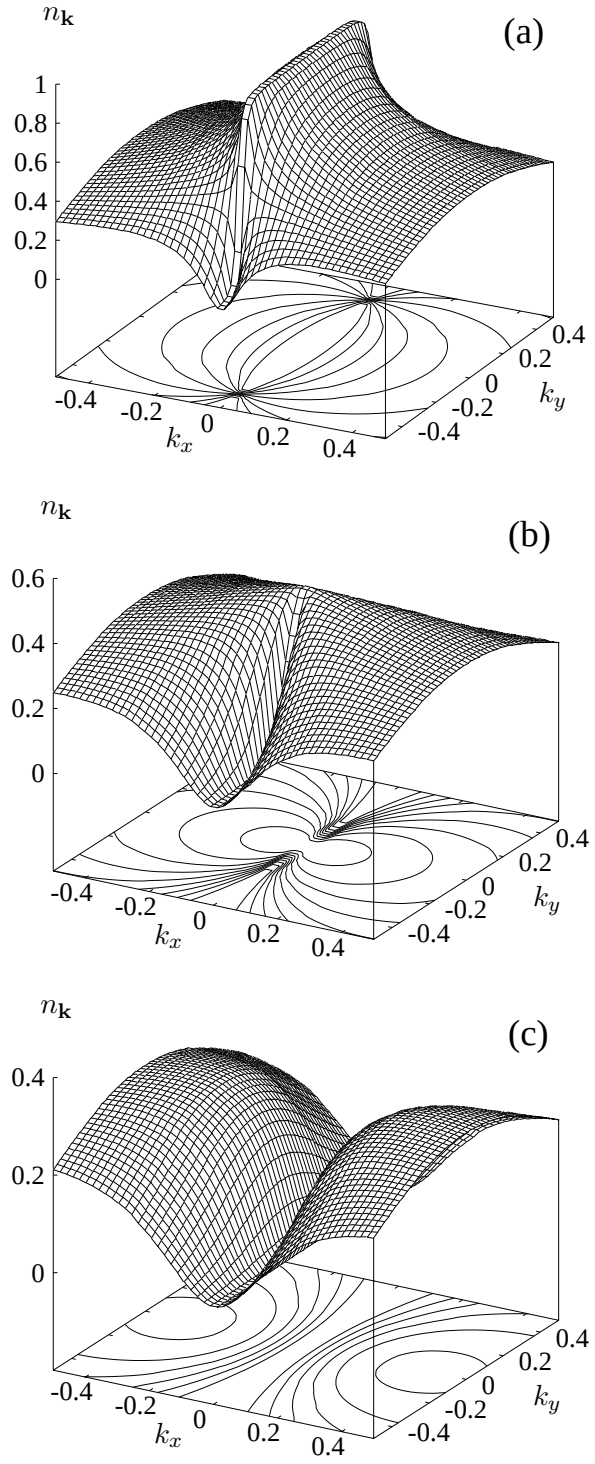

Figure 4.6: Plot of the momentum distribution $n_{\mathbf{k}}$ as a function of $\mathbf{k} = (k_x, k_y)$ (in units of k_F) in the spin-polarized p-wave case with $\Gamma(\mathbf{k}) = h(k)\cos(\varphi)$ (p_x-symmetry) for (a) $\mu = 0.15$, (b) $\mu = 0$ and (c) $\mu = -0.15$ (in units of ϵ_F). Notice the collapse of the two Dirac points when the chemical potential crosses zero.

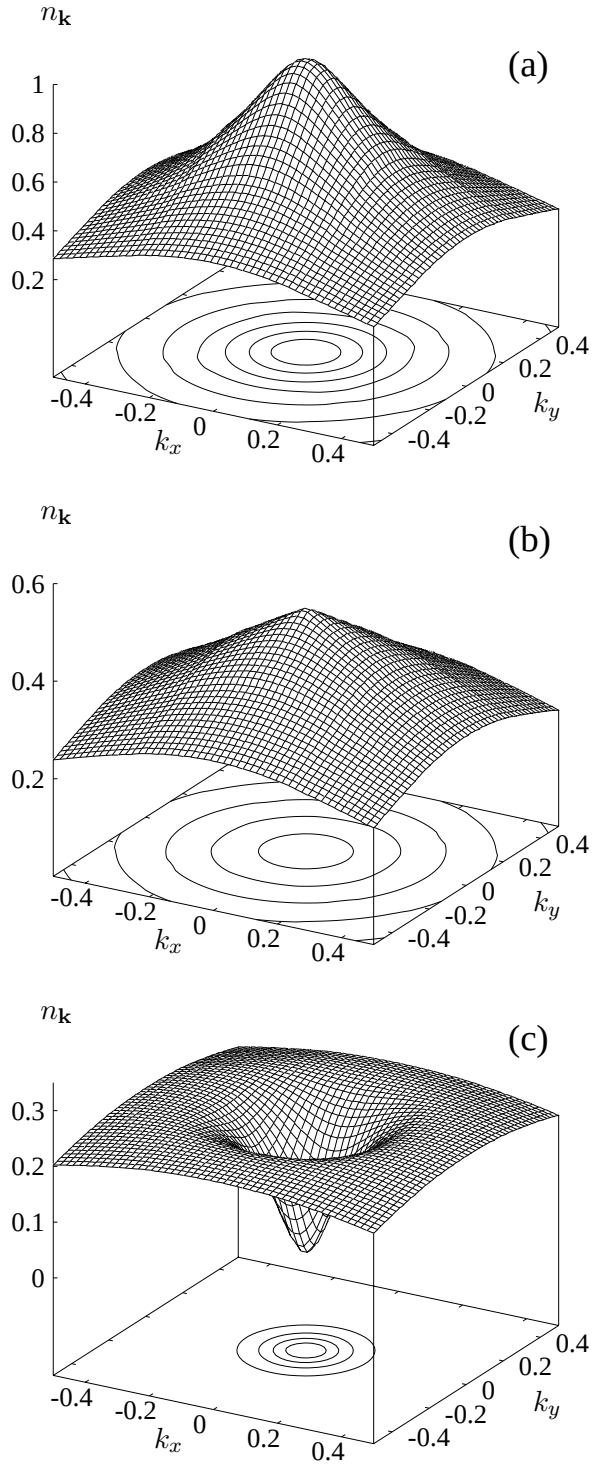

Figure 4.7: Plot of the momentum distribution $n_{\mathbf{k}}$ as a function of $\mathbf{k} = (k_x, k_y)$ (in units of k_F) in the spin-polarized p-wave case with $\Gamma(\mathbf{k}) = h(k)e^{i\varphi}$ ($p_x + ip_y$-symmetry) for (a) $\mu = 0.15$, (b) $\mu = 0$ and (c) $\mu = -0.15$ (in units of ϵ_F). Notice the appearance of a cusp in $n_{\mathbf{k}}$ when μ crosses zero.

which indicates a direct relationship between the atomic compressibility and the momentum distribution. Therefore, the singular behavior of $n_{\mathbf{k}}$ described in the last section for both symmetry functions analyzed should have some immediate effect on the compressibility of the gas as the binding energy (and therefore μ) is varied. The results of our calculations for $n^2\kappa$ as a function of E_b are shown in Fig. 4.8-a in the cases of p_x-symmetry and $p_x + ip_y$-symmetry.

As one can notice, the atomic compressibility develops a cusp when expressed in terms of E_b (or μ), the position of which coincides with the point where the chemical potential vanishes. Furthermore, the first derivative of κ with respect to E_b is discontinuous at the critical point $E_b^{(c)}$ (that corresponds to $\mu = 0$), as shown in Fig. 4.8-b. This is in clear contrast to the situation found in s-wave systems, in which case κ can be seen to be smooth for all values of E_b, as shown in the insets of Figs. 4.8-a and 4.8-b. This non-analyticity in the compressibility for both p-wave symmetry functions analyzed, combined with the momentum distribution rearrangement, suggests the existence of a quantum critical point at $\mu = 0$.

The non-analytic behavior of the atomic compressibility in the case of p_x-symmetry can be explained in terms of the collapse of the Dirac points toward $\mathbf{k} = 0$, together with the vanishing of $E_{\mathbf{k}}$ when μ crosses zero. On the other hand, the occurrence of a similar non-analyticity in κ for the $p_x + ip_y$-symmetry can be related to the appearence of a cusp on the $\mu = 0$ momentum distribution at $\mathbf{k} = 0$, and again to the vanishing of $E_{\mathbf{k}}$ when μ crosses zero. This leads to the conclusion that the existence of Dirac points in the quasiparticle excitation spectrum is not necessary to produce a non-analytic behavior in the atomic compressibility, which can still occur even in the case of an angle-independent order parameter, as long as $h(k)$ vanishes at $\mathbf{k} = 0$. In other words, the phase transition that we are proposing should happen even in the case of an angle-independent energy gap, since the anomalies in κ and $n_{\mathbf{k}}$ described above result from the vanishing of $E_{\mathbf{k}}$ at $\mathbf{k} = 0$ when μ reaches the bottom of the band, and not from the mere existence of Dirac points in the excitation spectrum.

The phase transition discussed above should also manifest itself in the spin susceptibility

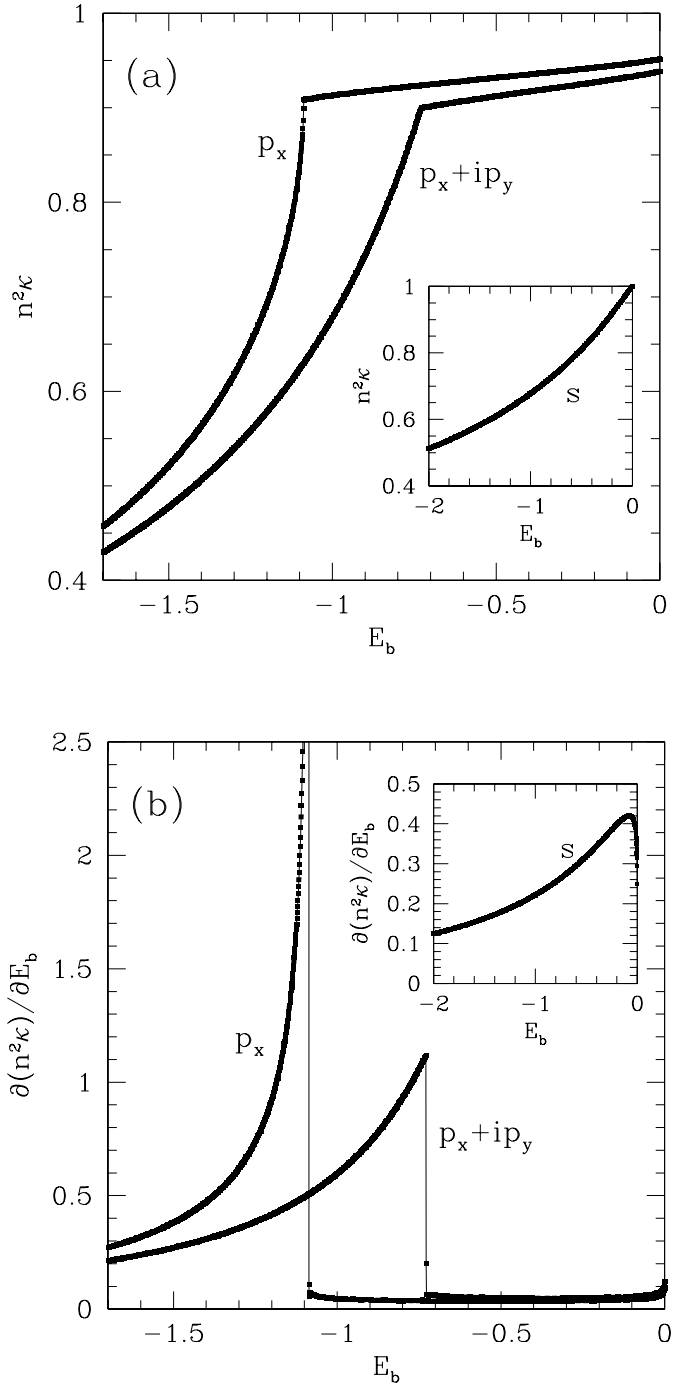

Figure 4.8: Universal plot (for any magnetic field $h_{\tilde{z}}$) of (a) $\partial n/\partial\mu$ (in units of $k_F^2/4\pi\epsilon_F$) and (b) its derivative with respect to E_b as functions of E_b (in units of ϵ_F) in the case of spin-polarized p-wave pairing and $k_0 = 10k_F$ and $k_1 = k_F$.

of the gas. The application of a small probe magnetic field $H_{\tilde{z}}$ along the same direction $\tilde{z}$ of the external field $\mathbf{h}$ generates the spin susceptibility response

$$\chi_{\tilde{z}\tilde{z}} = -\frac{1}{L^2}\left(\frac{\partial^2\Omega}{\partial H_{\tilde{z}}^2}\right)_T . \tag{4.40}$$

Recalling that the chemical potential μ depends on the external magnetic field $h_{\tilde{z}}$ as $\mu = \mu(h_{\tilde{z}} = 0) + g_{\tilde{z}\tilde{z}}\mu_B h_{\tilde{z}}$, the susceptibility can be rewritten in the case of spin-polarized atoms as

$$\chi_{\tilde{z}\tilde{z}} = -\frac{1}{L^2} g_{\tilde{z}\tilde{z}}^2 \mu_B^2 \left(\frac{\partial^2\Omega}{\partial\mu^2}\right)_T = g_{\tilde{z}\tilde{z}}^2 \mu_B^2 \left(\frac{\partial n}{\partial\mu}\right)_T . \tag{4.41}$$

Therefore, the graph in Fig. 4.8-a also represents a universal plot (for any magnetic field) of the quantity $\chi_{\tilde{z}\tilde{z}}/g_{\tilde{z}\tilde{z}}^2\mu_B^2$ as a function of E_b.

4.4.4 Superfluid Density

We now examine the behavior of the low temperature superfluid density tensor $\rho_{ij}(T, E_b)$ of the Fermi gas as the critical value of the binding energy $E_b^{(c)}$ is crossed. This tensor is associated with phase twists of the superconductor order parameter, and can be shown to be given by (see Section 2.4.4 of this thesis or Ref. [34] for more details)

$$\rho_{ij}(T) = \frac{1}{2L^2}\sum_{\mathbf{k}} \left[2n_{\mathbf{k}}\partial_i\partial_j\xi_{\mathbf{k}} - Y_{\mathbf{k}}\partial_i\xi_{\mathbf{k}}\partial_j\xi_{\mathbf{k}}\right], \tag{4.42}$$

where $n_{\mathbf{k}}$ is the momentum distribution, $Y_{\mathbf{k}} = (2T)^{-1}\mathrm{sech}^2(E_{\mathbf{k}}/2T)$ is the Yoshida distribution, and ∂_i denotes the partial derivative with respect to k_i. One can easily show that the ρ_{ij} tensor is diagonal, that is, $\rho_{xy} = \rho_{yx} = 0$. Furthermore, due to Galilean invariance of our continuum model, the zero-temperature superfluid density reduces to $\rho_{xx}(0) = \rho_{yy}(0) = n/m$, such that $\partial\rho_{ii}/\partial\mu = (1/m)\partial n/\partial\mu$ and $\partial\rho_{ii}/\partial H_{\tilde{z}} = (1/m)\partial n/\partial H_{\tilde{z}}$. However, contrary to what happens for d-wave symmetry, the two diagonal elements of the ρ_{ij} tensor are not equal to each other in the case of a p-wave order parameter. In fact, one can conclude that, if the symmetry function $\Gamma(\mathbf{k}) = h(k)\cos(\varphi)$ is used, $\rho_{xx}(T) \sim T^3$ and $\rho_{yy}(T) \sim T$ at low temperatures in the BCS regime. On the other hand, both the xx and the yy elements of the superfluid density tensor vanish exponentially with temperature on the BEC side of the transition.

Using our energy and momentum scales, we define the dimensionless quantity

$$\Delta\rho_i(T) \equiv \frac{m\rho_{ii}(T)}{n} - 1, \tag{4.43}$$

which emerges naturally from the calculations. Since $|\Delta\rho_x(T)| > |\Delta\rho_y(T)|$ for small T, we will focus here on the xx element of the superfluid density tensor, since this is the eigenvalue that will dominate the thermodynamic behavior of the system. Plots of $\Delta\rho_x(T)$ as a function of temperature (for $T \ll T_F$) at several fixed values of the binding energy E_b are shown in Fig. 4.9-a in the case of the symmetry function $\Gamma(\mathbf{k}) = h(k)\cos(\varphi)$. The linear behavior of $\Delta\rho_x(T)/T^2$ for values of E_b that correspond to $\mu > 0$ indicates a T^3 dependence of the superfluid density on temperature in the BCS regime. This confirms our theoretical prediction that, at low temperatures ($T \ll T_F$), $\Delta\rho_x(T) \sim CT^3$ in the BCS limit, with the coefficient C weakly dependent on E_b. This power-law behavior reflects the nodal (gapless) structure of the p-wave excitation spectrum. In the BEC limit, we obtained $\Delta\rho_x(T) \sim \exp(-|\mu|/T)$, the exponential behavior reflecting the appearence of a full gap to the addition of quasiparticles for $\mu < 0$.

The zero-temperature slope of $\Delta\rho_x(T)/T^2$ as a function of the binding energy E_b is shown in Fig. 4.9-b. This quantity is clearly discontinuous at the critical point $E_b^{(c)} = -1.088$ (which corresponds to $\mu = 0$), further confirming the existence of a quantum phase transition along the BCS-to-BEC evolution as a function of interaction strength (binding energy) in the case of p-wave spin-polarized atoms. It is important to point out that there is an additional contribution to $\rho_{xx}(T)$ due to Goldstone modes (underdamped for $\mu > 0$ due to Landau damping, but not dumped for $\mu < 0$ due to a full gap in the quasiparticle spectrum). In our formulation, this contribution comes as a next order correction, and has the form $\rho_{xx}^{(G)}(T) \sim -AT^3/c^4$ at low temperatures, where A is a function of E_b and c is the speed of sound. However, for $|\mu| \leq 0.4$ (which corresponds roughly to $-2 \leq E_b \leq 0$), A is essentially unchanged, and $\rho_{xx}^{(G)}(T)$ does not contribute to the discontinuity in the slope of $\Delta\rho_x(T)/T^2$ shown in Fig. 4.9-b.

In the case of the symmetry function $\Gamma(\mathbf{k}) = h(k)e^{i\varphi}$, it is clear that the superfluid density will have an exponential behavior on both sides of the transition line, vanishing as

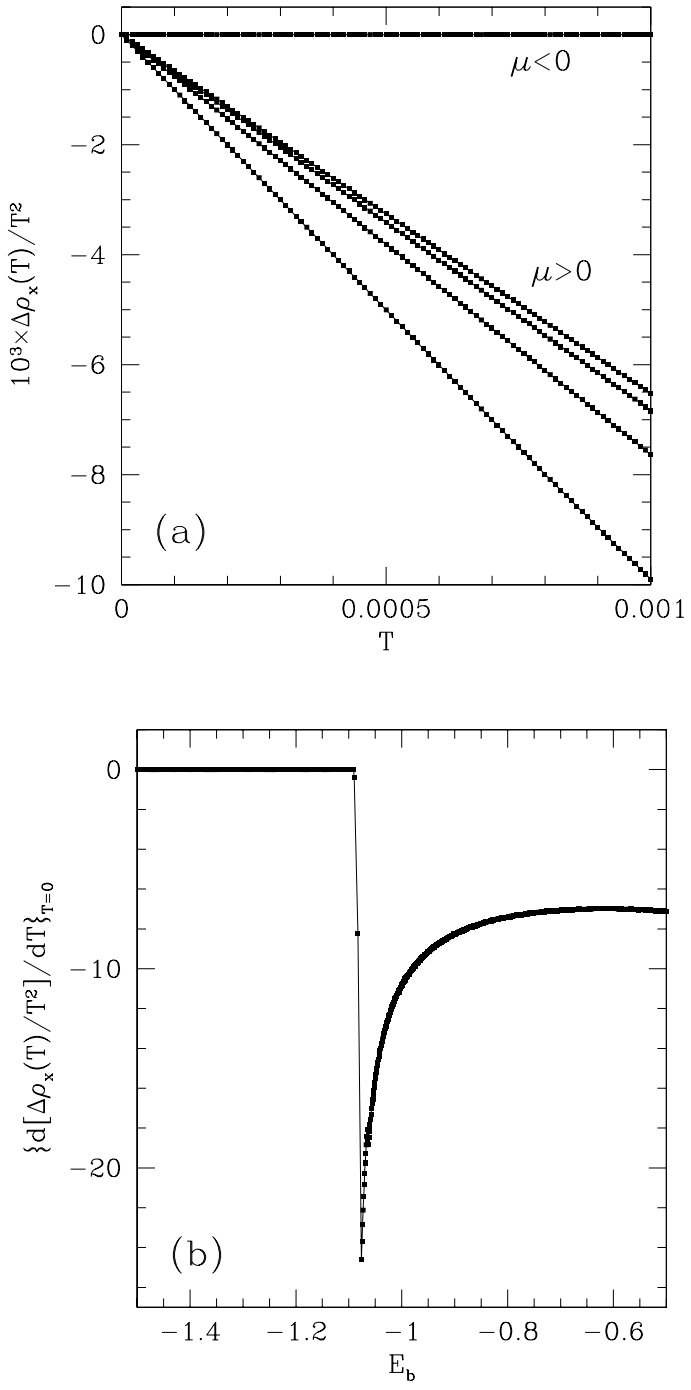

Figure 4.9: (a) Plot of $\Delta\rho_x(T)/T^2$ (in units of ϵ_F^{-2}) as a function of temperature (in units of ϵ_F) for various values of the binding energy E_b, in the case of the symmetry function $\Gamma(\mathbf{k}) = h(k)\cos(\varphi)$ with $k_0 = 10k_F$ and $k_1 = k_F$. (b) Zero temperature slope of $\Delta\rho_x(T)/T^2$ (in units of ϵ_F^{-3}) as a function of E_b (in units of ϵ_F).

$\Delta\rho_x(T) \sim B_1 \exp(-\Delta_{\mathbf{k}_F}/T)$ on the BCS side, and as $\Delta\rho_x(T) \sim B_2 \exp(-|\mu|/T)$ on the BEC side. This occurs because the quasiparticle excitation spectrum is gapped in both regimes. Therefore, the quantum phase transition that we discussed will not manifest itself explicitly in this case through the temperature dependence of the superfluid density. However, this fact does not preclude the pre-factors B_1 and B_2, which are functions of μ only, from having different behaviors for $\mu > 0$ and $\mu < 0$. In fact, this quantum phase transition will still be explicit in the $T = 0$ behavior of $\rho_{ii}(0) = n/m$, since $\partial\rho_{ii}/\partial\mu = (1/m)\partial n/\partial\mu$ is directly proportional to the atomic compressibility κ.

4.5 Fluctuation Effects

We now turn our attention to the investigation of the effects of Gaussian fluctuations in the pairing field $\phi_{\mathbf{q}}(\tau)$ about the static saddle point value Δ_0. Since this calculation is very similar to the one performed in the context of d-wave superconductivity, only the main results will be highlighted (the reader should refer to Sections 3.2 and 3.3 for more details). Assuming $\phi_{\mathbf{q}}(\tau) = \Delta_0\delta_{\mathbf{q},0} + \eta_{\mathbf{q}}(\tau)$ and performing an expansion in S_{eff} to quadratic order in η, one obtains

$$S_{\text{Gauss}}[\eta, \eta^*] = S_{\text{eff}}[\Delta_0] + \frac{1}{2}\sum_q \underline{\eta}^\dagger(q)\mathbf{M}(q)\underline{\eta}(q), \tag{4.44}$$

where $S_{\text{eff}}[\Delta_0]$ is the saddle point action, the vector $\underline{\eta}(q)$ is such that $\underline{\eta}^\dagger(q) = [\eta^*(q), \eta(-q)]$, and $q \equiv (\mathbf{q}, i\nu_m)$, where $\nu_m = 2m\pi/\beta$ is a bosonic Matsubara frequency. The 2×2 matrix $\mathbf{M}(q)$ is the inverse fluctuation propagator.

The Gaussian fluctuation term in the effective action leads to a correction to the thermodynamic potential, which can be rewritten as $\Omega_{\text{Gauss}} = \Omega_0 + \Omega_{\text{fluct}}$, with $\Omega_{\text{fluct}} = \beta^{-1}\sum_q \ln[\det \mathbf{M}(q)]$. Therefore, using the thermodynamic relation $N = -\partial\Omega/\partial\mu$, one can write the corrected number equation as $N_{\text{Gauss}} = N_0 + N_{\text{fluct}}$, where N_0 is the saddle point number of particles given in Eq.(4.29), and

$$N_{\text{fluct}} = -\frac{\partial\Omega_{\text{fluct}}}{\partial\mu} = -T\sum_{\mathbf{q}}\sum_{i\nu_m}\left[\frac{\partial(\det \mathbf{M})/\partial\mu}{\det \mathbf{M}(\mathbf{q}, i\nu_m)}\right]. \tag{4.45}$$

At low T, the Goldstone mode $\omega = c_s|\mathbf{q}|$ dominates the contribution to $N_{\rm fluct}$, leading to

$$N_{\rm fluct} \sim -\frac{L^2}{2\pi}\zeta(3)\frac{1}{c_s^3}\frac{\partial c_s}{\partial \mu}T^3, \tag{4.46}$$

which vanishes in the limit of $T \to 0$. Therefore, analogously to the three-dimensional s-wave case [31], the saddle point equations provide a very accurate description of the broken-symmetry state near and at $T = 0$.

The next step will be to show that the same is not true near T_c, where the effects of temporal fluctuations in the order parameter, which are related to the appearence of bosonic (two-body) degrees of freedom, become essential to describe the BEC regime. This can be accomplished by means of the same technique employed in the case of two-dimensional superconductors, that is, by calculating the Berezinskii-Kosterlitz-Thouless (BKT) transition temperature of the system[1]. Following the same procedure outlined in Section 3.5, one can show that the real-space effective action, when expressed in terms of the phase fluctuations $\theta(\mathbf{r})$, will contain a term of the form $\frac{1}{2}\hbar^2 \int d^2r\, \rho_{xx}(\mu, \Delta_0, T)\left[\partial_x\theta(\mathbf{r})\right]^2$, where $\rho_{xx}(\mu, \Delta_0, T)$ is the xx element of the superfluid density tensor given in Eq.(4.42). Clearly, a term involving $[\partial_y\theta(\mathbf{r})]^2$ will also be present in the action, but its contribution to the transition temperature will be irrelevant (for reasons discussed above), and only the ρ_{xx} term will be taken into account. From a direct comparison to the Hamiltonian of the XY model in two dimensions, one obtains the following expression for the BKT temperature,

$$\frac{\pi}{2}\hbar^2\rho_{xx}(\mu, \Delta_0, T_{\rm BKT}) = T_{\rm BKT}, \tag{4.47}$$

which is a self-consistent equation for $T_{\rm BKT}$. In the present case, the dimensionless quantity $\Delta\rho_x(T)$ is defined as $\Delta\rho_x(T) = m\rho_{xx}(T)/n - 1$, where m is the mass of the atom and n is the particle density. When combined with Eq.(4.47), and using the relation between number density and Fermi energy for spin-polarized particles in 2D, $n = (m/2\pi\hbar^2)\epsilon_F$, this definition yields

$$\frac{1}{4}\left(\Delta\rho_x(T_{\rm BKT}) + 1\right) = T_{\rm BKT}, \tag{4.48}$$

[1]This carries the implicit assumption that the fermionic gas can be confined to quasi-two-dimensional "sheets" located on the sites of a one-dimensional optical lattice.

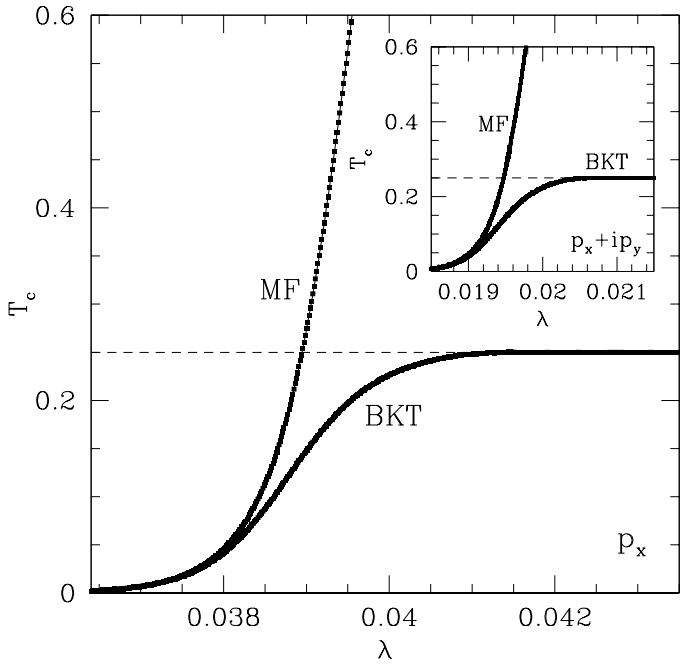

Figure 4.10: Berezinskii-Kosterlitz-Thouless (BKT) and mean field (MF) transition temperatures (in units of ϵ_F) as functions of the interaction strength λ (in units of g_{2D}^{-1}) in the case of p_x symmetry. *Inset:* Same quantities in the case of $p_x + ip_y$ symmetry.

where $T_{\rm BKT}$ is written in units of ϵ_F. This equation, together with the finite-temperature BCS order parameter and number equations given in (4.27) and (4.29), respectively, constitute a complete set of equations to be solved self-consistently for μ, Δ_0 and $T_{\rm BKT}$.

Our numerical solution for the BKT transition temperature of spin-polarized fermionic atoms is shown in Fig. 4.10 in the cases of p_x (main figure) and $p_x + ip_y$ (inset) pairing symmetries. As it turns out, it is more convenient to plot $T_{\rm BKT}$ as a function of the interparticle interaction strength λ, simply because some important features are not as apparent when $T_{\rm BKT}$ is expressed in terms of E_b. The mean field solution, which can be obtained by solving the BCS number and order parameter equations with $\Delta_0 = 0$ for μ and $T_{\rm MF}$, is also shown in the figure. The main conclusion is that the mean field description works fairly well in the weak coupling region, but $T_{\rm MF}$ and $T_{\rm BKT}$ start to depart from each other as intermediate values of λ are reached, and the difference between them becomes increasingly large as one approaches the strong coupling regime. This shows that the bosonic degrees of freedom arising from the condensation of atomic pairs, which are not included in the saddle point calculation, become essential to describe the strong coupling behavior. In the

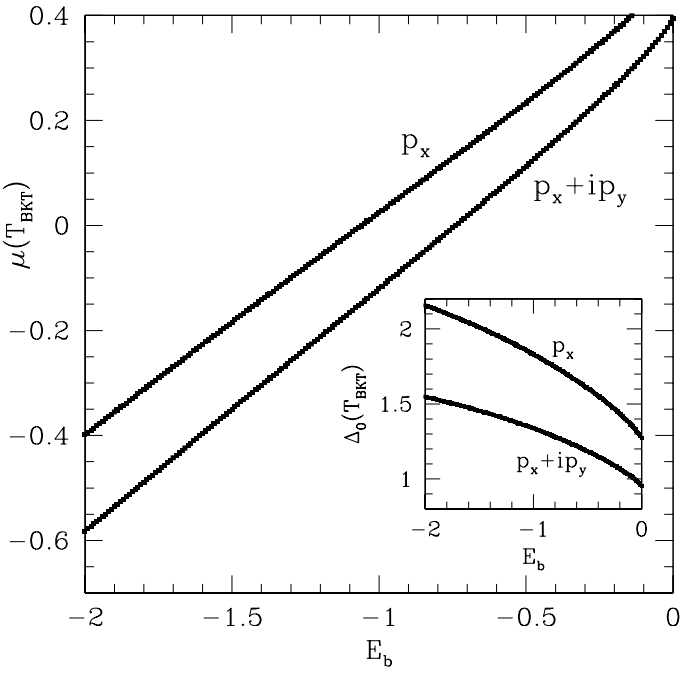

Figure 4.11: Chemical potential μ and order parameter amplitude Δ_0 (inset) evaluated at $T = T_{\rm BKT}$ as functions of the binding energy E_b (all quantities in units of ϵ_F) for both p_x and $p_x + ip_y$ pairing symmetries.

extreme strong coupling limit, one can show that $\Delta\rho_x \to 0$, which, according to Eq.(4.48), explains the limiting value $T_{\rm BKT}(\lambda \to \infty) = 1/4$ observed in the figure. Finally, one should notice that the results for p_x and $p_x + ip_y$ symmetries are qualitatively the same, the only difference being the scale of λ.

When solving the self-consistent system of equations that determines $T_{\rm BKT}$, one automatically obtains, as byproducts of the calculation, the chemical potential and order parameter amplitude evaluated at the transition temperature, which are shown in Fig. 4.11 as functions of the binding energy E_b. One should notice that these quantitites behave very similarly to their zero-temperature counterparts (see Fig. 4.5). It is only by looking at the evolution of $\partial n/\partial\mu$ that it becomes clear that there is no phase transition at $T = T_{\rm BKT}$. In fact, as shown in Fig. 4.12, $\partial n/\partial\mu$ varies smoothly with E_b at $T = T_{\rm BKT}$ for both symmetry functions analyzed (the $T = 0$ results are also shown for comparison purposes).

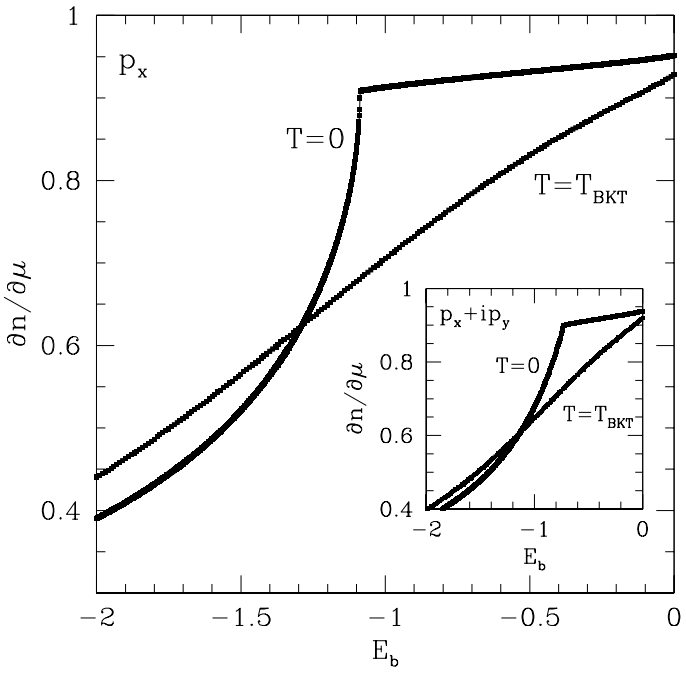

Figure 4.12: Plots of $\partial n/\partial\mu$ (in units of $k_F^2/4\pi\epsilon_F$) at $T = 0$ and $T = T_{\rm BKT}$ as function of the binding energy E_b (in units of ϵ_F) in the case of p_x symmetry. *Inset:* Same quantities in the case of $p_x + ip_y$ symmetry.

4.6 Experimental Realization

In this section, we suggest a possible experiment to measure the atomic compressibility of ultra-cold fermionic gases. It is well known from thermodynamics that the isothermal compressibility κ is given by

$$\kappa = -\frac{1}{V}\left(\frac{\partial V}{\partial P}\right)_{T,N}, \tag{4.49}$$

where V is the volume and P is the pressure of the system. Using the thermodynamic relation $Vdp = Nd\mu + SdT$, the compressibility can also be expressed as in Eq.(4.38), where one can consider some fixed sub-volume that is allowed to exchange energy and particles through its imaginary walls. Theoretically, it is easier to compute κ using variations of n with respect to μ, but experimentally it is easier to measure κ through variations of P with respect to V.

In order to discuss the feasibility of measurements of κ in ultra-cold Fermi gases, we assume first the simpler situation of one single spherically symmetric cloud, which is allowed to expand isothermally (at constant temperature) as the gas is released from the trap. In

order to estimate κ from a typical measurement of the cold atom cloud, we assume that the initial radius of the cloud is R, and that the average pressure P on the surface area S of the cloud is given by $P = F/S$, where F is the total average force exerted along the direction normal to the cloud surface (the *radial* force in the case of spherical symmetry). To estimate F, we write $F = N_S ma$, where N_S is the number of atoms *hitting* the surface of the cloud, m is the mass of each atom, and a is the average acceleration of the atoms normal to the surface of the cloud (*radial* acceleration in the spherically symmetric case). N_S may be estimated from two photos of the cloud taken at instants of time t_0 and t_1, with the time interval $\tau = t_1 - t_0$ corresponding to a small change in volume $\Delta V_{10} = V_1 - V_0 \ll V_0$. In this case, $N_S(R_0) = n(R_0)\Delta V_{10}$, where $n(R_0)$ is the density of the cloud at R_0.

To estimate the pressure, we also need to determine the acceleration a of the atoms crossing the surface area bounding the cloud. This can be achieved by taking a third photo of the cloud expansion at time t_2, such that $t_2 - t_1 = \tau$. From the first pair of photos at (t_1, t_0), we can get the radial velocity $v_{10} = (R_1 - R_0)/\tau$; and from the second pair of photos at (t_2, t_1), we can get the radial velocity $v_{21} = (R_2 - R_1)/\tau$. The average acceleration at $t = t_0$ is then given by $a_0 = (v_{21} - v_{10})/\tau$, which can also be expressed in terms of the cloud radii as $a_0 = (R_2 - 2R_1 + R_0)/\tau^2$.

These three photos are then necessary and sufficient to estimate the pressure P_0 at t_0, but are not sufficient to estimate the change in pressure $\Delta P_{10} = P_1 - P_0$, which is essential for the measurement of the compressibility. Thus, taking a fourth photo at time t_3, with the same time interval $t_3 - t_2 = \tau$, allows one to find $a_1 = (R_3 - 2R_2 + R_1)/\tau^2$, which together with $N_S(R_1) = n(R_1)\Delta V_{21}$, with $\Delta V_{21} = V_2 - V_1 \ll V_1$, provides the estimate of the pressure P_1 at $t = t_1$. The sequence of photos obtained during the cloud expansion is sketched in Fig. 4.13, which shows the density profile of the atomic cloud in the trap as a function of time. Finally, the ratio $\Delta V_{10}/\Delta P_{10}$ can be evaluated, and the experimental compressibility can be extracted from the four photos of the cloud expansion by means of the relation

$$\kappa_{\rm exp} = -\frac{1}{V_0}\frac{\Delta V_{10}}{\Delta P_{10}}. \tag{4.50}$$

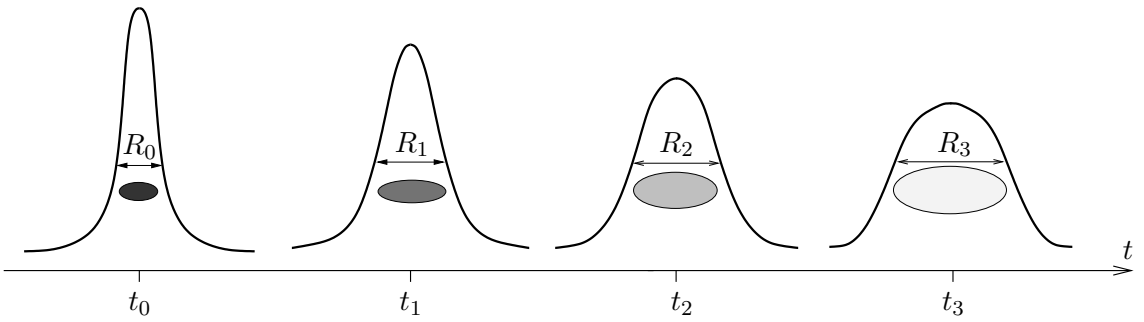

Figure 4.13: Sketch of the density profile of the atomic cloud in the trap as a function of time. Four photos taken during the cloud expansion are necessary to determine the isothermal compressibility $\kappa_{\rm exp}$ of the Fermi gas.

It is important to emphasize that, if the assumption of constant temperature during the cloud expansion does not hold, one can still use the procedure described above to measure the atomic compressibility. In fact, if the gas is released from the trap so quickly that the atoms do not have enough time to exchange heat with the external medium, the cloud expansion will constitute an adiabatic process, rather than an isothermal one. If this is the case, the quantity calculated in Eq.(4.50) will be the adiabatic compressibility κ_S, which can be related [82] to the isothermal compressibility κ through the equation

$$\kappa_S = \frac{c_V}{c_P}\kappa, \tag{4.51}$$

where c_V and c_P are the specific heat of the gas at constant volume and pressure, respectively. Clearly, this would require two more thermodynamic properties of the system to be measured via independent experiments. Nevertheless, the procedure outlined above constitutes a possible experiment that, in principle, could be used to test our theoretical predictions by means of standard techniques that are currently used in the study of ultra-cold fermionic gases.

In order to perform a direct measurement of the spin susceptibility, one idea is to devise an experimental setup in which the atomic cloud could be moved relative to a set of Helmholtz coils (pick-up coils) in a direction parallel to the magnetic moment of the atoms. The induced voltage resulting from the change in magnetic flux through the coils could then be used to estimate the paramagnetic response of the gas, allowing the determination of its spin susceptibility.

However, based on a simple model for the interaction between one magnetic dipole and a circular coil, we estimated the induced voltage that would be obtained in such an experiment. Considering a coil of radius 1 mm and assuming that the cloud can move as fast as 10 m/s relative to the coil, the induced voltage that would be produced by 10^6 atoms is still of the order of 10^{-21} Volts. Therefore, even if a "solenoid" of tightly packed coils could be used, this effect would still be negligible. The reason why such a technique can be successful in a condensed matter system is that, in this situation, a number of atoms of the order of 10^{23} will be contributing to the induced voltage. On the other hand, one is limited to a much smaller number of atoms ($\sim 10^6$) in the case of an optical trap, making this experiment unfeasible for Fermi gases. Based on this result, we stress the importance of the relation given by Eq.(4.41) between spin susceptibility and atomic compressibility. Since a direct measurement of $\chi_{\tilde{z}\tilde{z}}$ does not seem feasible, one would have to resort to compressibility measurements, as for example the one described above, in order to estimate the susceptibility.

4.7 Summary

The main goal of this chapter was to propose the existence of a quantum phase transition in the BCS-to-BEC evolution of fully spin-polarized p-wave Fermi gases in two dimensions as a function of the two-body bound state energy. Two different types of order parameter symmetries were analyzed: p_x and $p_x + ip_y$. In both cases, we have shown that the momentum distribution undergoes a major rearrangement in k-space at a critical value of the binding energy, which leads to a non-analytic behavior of the atomic compressibility and spin susceptibility of the gas. Furthermore, in the case of p_x-symmetry, the low temperature superfluid density of the system was shown to change dramatically as the critical point is crossed, with a zero-temperature slope that is discontinuous at the critical binding energy. It is important to note that we used a homogeneous model to describe the fermionic gas, in the sense that the trapping potential was not taken directly into account in the calculations (not included in the Hamiltonian of the system). This can be justified if one assumes that the typical size of the atom cloud is small compared with the laser wavelength, such that

the interaction between the atoms and the trap is negligible relative to the inter-particle attraction, and the trap effects can be safely ignored in a first approximation.

Up to now, experiments on cold Fermi gases have focused only on the formation of atomic pairs in s-wave channels, and it has been established that a smooth crossover takes place in this case between the BCS and BEC limits as the binding energy (controlled by an external magnetic field via Feshbach resonance) is varied, a result fully supported by theoretical calculations [73, 74, 75, 76]. Although p-wave Feshbach resonances have already been found in cold atom systems [59, 77, 78], p-wave atomic pairs have never been directly observed. One of the main reasons why s-wave pairing is more easily achieved is the fact that p-wave resonances are much narrower and, therefore, require a more precise tunning of magnetic fields. Furthermore, in order to experimentally realize the phase transition predicted by our results, one must not only be able to drive the fermionic gas through a p-wave Feshbach resonance, but also to measure certain properties that could signal the occurrence of a non-analytic behavior. Although we have suggested one possible experimental procedure by means of which this could be done, the measurement of quantities as the atomic compressibility and the superfluid density in gaseous systems still remains a challenge for experimentalists.

APPENDIX A

SECOND QUANTIZATION FORMALISM

In this appendix, the formalism of second quantization, which is extremely useful to the description of quantum many-particle systems, will be reviewed. The symmetry (or anti-symmetry) properties of bosonic and fermionic state vectors will be discussed, the many-body creation and annihilation operators will be introduced, and the commutation (or anti-commutation) relations among them will be derived.

A.1 Many-Particle States

Let $\{|\psi_1\rangle, \ldots, |\psi_N\rangle\}$ be a complete set of one-particle states belonging to a single-particle Hilbert space $\mathcal{H}_1$. A many-particle state describing a system of N independent and distinguishable (classical) particles will then be obtained from the tensor product of these N single-particle states,

$$|\psi_1, \psi_2, \ldots, \psi_N\rangle = |\psi_1\rangle|\psi_2\rangle \ldots |\psi_N\rangle, \tag{A.1}$$

and will belong to an N-particle Hilbert space $\mathcal{H}_N$, which can be constructed from the N^{th} tensor product of single-particle Hilbert spaces,

$$\mathcal{H}_N = \mathcal{H}_1 \otimes \mathcal{H}_2 \otimes \cdots \otimes \mathcal{H}_N. \tag{A.2}$$

The inner product (overlap) of two of these state vectors is defined as

$$\langle \Phi|\Psi\rangle = (\langle\phi_1|\langle\phi_2| \ldots \langle\phi_N|)(|\psi_1\rangle|\psi_2\rangle \ldots |\psi_N\rangle) \equiv \langle\phi_1|\psi_1\rangle\langle\phi_2|\psi_2\rangle \ldots \langle\phi_N|\psi_N\rangle. \tag{A.3}$$

If the system under consideration is composed of indistinguishable particles, the corresponding state vector has to satisfy certain symmetry conditions. These conditions, which are ultimately founded on experiment, imply corresponding restrictions on the underlying Hilbert spaces of the N-particle systems. Particles obeying Bose-Einstein statistics (bosons) must have state vectors which are symmetric under the permutation of any two

particles, while particles obeying Fermi-Dirac statistics (fermions) must be described by anti-symmetric state vectors. Therefore, the appropriately symmetrized many-particle state vector describing a system of N independent and indistinguishable particles is defined as

$$\boxed{|\psi_1, \psi_2, \ldots, \psi_N\rangle \equiv |\psi_1\rangle \otimes |\psi_2\rangle \otimes \cdots \otimes |\psi_N\rangle = \frac{1}{\sqrt{N!}} \sum_P \zeta^P |\psi_{P(1)}\rangle |\psi_{P(2)}\rangle \ldots |\psi_{P(N)}\rangle}, \tag{A.4}$$

where P runs through all possible permutations of N objects, and the index ζ distinguishes between bosons and fermions,

$$\zeta = \begin{cases} +1 & \text{for bosons;} \\ -1 & \text{for fermions.} \end{cases} \tag{A.5}$$

It is important to notice that the state vectors defined by Eq.(A.4), although symmetrized, are not necessarily normalized, but can be shown to have norm $\sqrt{n_1! n_2! \ldots n_N!}$, where n_i is the number of particles in the system occupying the state i. Since there can be at most one fermion at each quantum state, the fermionic state vectors will be automatically normalized as given by Eq.(A.4), but the bosonic ones must be divided by $\sqrt{n_1! n_2! \ldots n_N!}$. However, in order to simplify the notation, the state vectors in this appendix will be kept unnormalized, unless stated otherwise.

From the definition Eq.(A.3) of the overlap between two (non-symmetrized) vectors, the inner product of two symmetrized state vectors can be shown to be (a proof is given, for example, in Ref. [83])

$$\langle \Psi | \Phi \rangle = \langle \psi_1, \psi_2, \ldots, \psi_N | \phi_1, \phi_2, \ldots, \phi_N \rangle = \begin{vmatrix} \langle \psi_1 | \phi_1 \rangle & \cdots & \langle \psi_1 | \phi_N \rangle \\ \vdots & & \vdots \\ \langle \psi_N | \phi_1 \rangle & \cdots & \langle \psi_N | \phi_N \rangle \end{vmatrix}_\zeta , \tag{A.6}$$

where $|\mathbf{M}|_\zeta$ denotes the determinant of the matrix $\mathbf{M}$ for fermions ($\zeta = -1$) and the *permanent* of $\mathbf{M}$ for bosons ($\zeta = +1$). The permanent of a matrix is defined in the same way as the determinant, but with all negative signs replaced by positive signs. As an application, the inner product can be used to find the many-body wave function describing a system of N independent and indistinguishable particles, which is simply the collapse of

the state vector of the system onto the state $|x_1, x_2, \ldots, x_N\rangle$:

$$\Psi(x_1, \ldots, x_N) = \langle x_1, \ldots, x_N | \psi_1, \ldots, \psi_N \rangle = \begin{vmatrix} \psi_1(x_1) & \cdots & \psi_N(x_1) \\ \vdots & & \vdots \\ \psi_1(x_N) & \cdots & \psi_N(x_N) \end{vmatrix}_\zeta , \tag{A.7}$$

where $\psi_i(x_j) = \langle x_j | \psi_i \rangle$ is the one-body wave function describing particle i at position x_j. For example, the (non-normalized) wave function of a system of three independent bosons would be given by

$$\begin{aligned} \Psi_B(x_1, x_2, x_3) = {} & \psi_1(x_1)\psi_2(x_2)\psi_3(x_3) + \psi_1(x_2)\psi_2(x_3)\psi_3(x_1) + \psi_2(x_1)\psi_3(x_2)\psi_1(x_3) + \\ & + \psi_3(x_1)\psi_2(x_2)\psi_1(x_3) + \psi_2(x_1)\psi_1(x_2)\psi_3(x_3) + \psi_3(x_2)\psi_2(x_3)\psi_1(x_1), \end{aligned}$$

while a system of three independent fermions would be described by

$$\begin{aligned} \Psi_F(x_1, x_2, x_3) = {} & \psi_1(x_1)\psi_2(x_2)\psi_3(x_3) + \psi_1(x_2)\psi_2(x_3)\psi_3(x_1) + \psi_2(x_1)\psi_3(x_2)\psi_1(x_3) + \\ & - \psi_3(x_1)\psi_2(x_2)\psi_1(x_3) - \psi_2(x_1)\psi_1(x_2)\psi_3(x_3) - \psi_3(x_2)\psi_2(x_3)\psi_1(x_1). \end{aligned}$$

A.2 Creation and Annihilation Operators

The creation operator $a_\phi^\dagger$ is defined to be the linear operator that adds one particle at state $|\phi\rangle$ to an N-particle state, converting it into an $(N+1)$-particle state:

$$\boxed{a_\phi^\dagger |\psi_1, \ldots, \psi_N\rangle = |\phi, \psi_1, \ldots, \psi_N\rangle}. \tag{A.8}$$

When acting on a system with no particles, the creation operator produces a single-particle state, $|\phi\rangle = a_\phi^\dagger |0\rangle$, where $|0\rangle$ represents the vacuum (absence of particles), not to be confused with the zero of the Hilbert space.

The adjoint a_ϕ of the creation operator, known as the destruction (or annihilation) operator, has the opposite effect of producing an $(N-1)$-particle state out of an N-particle state. To find the state vector resulting from applying a_ϕ to $|\psi_1, \ldots, \psi_N\rangle$, one can calculate

its inner product with an $(N-1)$-particle state $|\chi_1,\ldots,\chi_{N-1}\rangle$:

$$\langle\chi_1,\ldots,\chi_{N-1}|a_\phi|\psi_1,\ldots,\psi_N\rangle = \langle\psi_1,\ldots,\psi_N|a_\phi^\dagger|\chi_1,\ldots,\chi_{N-1}\rangle^* =$$

$$= \langle\psi_1,\ldots,\psi_N|\phi,\chi_1,\ldots,\chi_{N-1}\rangle^* = \begin{vmatrix} \langle\psi_1|\phi\rangle & \langle\psi_1|\chi_1\rangle & \cdots & \langle\psi_1|\chi_{N-1}\rangle \\ \langle\psi_2|\phi\rangle & \langle\psi_2|\chi_1\rangle & \cdots & \langle\psi_2|\chi_{N-1}\rangle \\ \vdots & \vdots & & \vdots \\ \langle\psi_N|\phi\rangle & \langle\psi_N|\chi_1\rangle & \cdots & \langle\psi_N|\chi_{N-1}\rangle \end{vmatrix}_\zeta^* .$$

Expanding the determinant (permanent) by minors along the first column, one has:

$$\langle\chi_1,\ldots,\chi_{N-1}|a_\phi|\psi_1,\ldots,\psi_N\rangle = \sum_{i=1}^{N}\zeta^{i-1}\langle\psi_i|\phi\rangle^* \begin{vmatrix} \langle\psi_1|\chi_1\rangle & \cdots & \langle\psi_1|\chi_{N-1}\rangle \\ \vdots & (\text{no } \psi_i) & \vdots \\ \langle\psi_N|\chi_1\rangle & \cdots & \langle\psi_N|\chi_{N-1}\rangle \end{vmatrix}_\zeta^* =$$

$$= \sum_{i=1}^{N}\zeta^{i-1}\langle\psi_i|\phi\rangle^*\langle\psi_1,\ldots,(\text{no } \psi_i),\ldots,\psi_N|\chi_1,\ldots,\chi_{N-1}\rangle^* =$$

$$= \sum_{i=1}^{N}\zeta^{i-1}\langle\phi|\psi_i\rangle\langle\chi_1,\ldots,\chi_{N-1}|\psi_1,\ldots,(\text{no } \psi_i),\ldots,\psi_N\rangle.$$

And since this is valid for any vector $|\chi_1,\ldots,\chi_{N-1}\rangle$, one can finally conclude that

$$\boxed{a_\phi|\psi_1,\ldots,\psi_N\rangle = \sum_{i=1}^{N}\zeta^{i-1}\langle\phi|\psi_i\rangle|\psi_1,\ldots,(\text{no } \psi_i),\ldots,\psi_N\rangle}. \tag{A.9}$$

The symmetry or anti-symmetry properties of the many-particle states impose certain commutation or anti-commutation relations between the creation operators. Since a bosonic (fermionic) state vector is symmetric (anti-symmetric) with respect to the permutation of any two particles, one will have

$$a_{\phi_1}^\dagger a_{\phi_2}^\dagger|\psi_1,\ldots,\psi_N\rangle = a_{\phi_1}^\dagger|\phi_2,\psi_1,\ldots,\psi_N\rangle = |\phi_1,\phi_2,\psi_1,\ldots,\psi_N\rangle = \zeta|\phi_2,\phi_1,\psi_1,\ldots,\psi_N\rangle =$$

$$= \zeta a_{\phi_2}^\dagger|\phi_1,\psi_1,\ldots,\psi_N\rangle = \zeta a_{\phi_2}^\dagger a_{\phi_1}^\dagger|\psi_1,\ldots,\psi_N\rangle \quad \therefore \quad a_{\phi_1}^\dagger a_{\phi_2}^\dagger = \zeta a_{\phi_2}^\dagger a_{\phi_1}^\dagger \quad \therefore$$

$$\therefore \quad \boxed{[a_{\phi_1}^\dagger, a_{\phi_2}^\dagger]_{-\zeta} = 0}, \tag{A.10}$$

where the notation $[A,B]_{-\zeta} = AB - \zeta BA$ was used. And from the Hermitian adjoint of Eq.(A.10), one obtains:

$$\boxed{[a_{\phi_1}, a_{\phi_2}]_{-\zeta} = 0}. \tag{A.11}$$

To find the commutation relation between a creation and an annihilation operator, one can start by applying $a_{\phi_1} a^\dagger_{\phi_2}$ to the state vector of the system:

$$a_{\phi_1} a^\dagger_{\phi_2} |\psi_1, \ldots, \psi_N\rangle = a_{\phi_1} |\phi_2, \psi_1, \ldots, \psi_N\rangle =$$

$$= \langle\phi_1|\phi_2\rangle |\psi_1, \ldots, \psi_N\rangle + \sum_{i=1}^{N} \zeta^i \langle\phi_1|\psi_i\rangle |\phi_2, \psi_1, \ldots, (\text{no } \psi_i), \ldots, \psi_N\rangle. \tag{A.12}$$

On the other hand:

$$a^\dagger_{\phi_2} a_{\phi_1} |\psi_1, \ldots, \psi_N\rangle = a^\dagger_{\phi_2} \left[\sum_{i=1}^{N} \zeta^{i-1} \langle\phi_1|\psi_i\rangle |\psi_1, \ldots, (\text{no } \psi_i), \ldots, \psi_N\rangle \right] =$$

$$= \sum_{i=1}^{N} \zeta^{i-1} \langle\phi_1|\psi_i\rangle a^\dagger_{\phi_2} |\psi_1, \ldots, (\text{no } \psi_i), \ldots, \psi_N\rangle =$$

$$= \sum_{i=1}^{N} \zeta^{i-1} \langle\phi_1|\psi_i\rangle |\phi_2, \psi_1, \ldots, (\text{no } \psi_i), \ldots, \psi_N\rangle. \tag{A.13}$$

Multiplying Eq.(A.13) by ζ and subtracting from Eq.(A.12), one obtains:

$$\left(a_{\phi_1} a^\dagger_{\phi_2} - \zeta a^\dagger_{\phi_2} a_{\phi_1} \right) |\psi_1, \ldots, \psi_N\rangle = \langle\phi_1|\phi_2\rangle |\psi_1, \ldots, \psi_N\rangle \quad \therefore \tag{A.14}$$

$$\therefore \quad a_{\phi_1} a^\dagger_{\phi_2} - \zeta a^\dagger_{\phi_2} a_{\phi_1} = \langle\phi_1|\phi_2\rangle \quad \therefore$$

$$\boxed{[a_{\phi_1}, a^\dagger_{\phi_2}]_{-\zeta} = \langle\phi_1|\phi_2\rangle}. \tag{A.15}$$

In general, for an orthonormal basis $\{|\phi_i\rangle\}$ of single-particle state vectors, the commutation relations between many-particle creation and annihilation operators can be written as:

$$\begin{cases} [a_{\phi_i}, a_{\phi_j}]_{-\zeta} = [a^\dagger_{\phi_i}, a^\dagger_{\phi_j}]_{-\zeta} = 0; \\ \\ [a_{\phi_i}, a^\dagger_{\phi_j}]_{-\zeta} = \delta_{ij}. \end{cases} \tag{A.16}$$

A.3 Occupation Number Representation

For many applications (specially to bosonic systems), it may be more convenient to express the many-particle state vectors in the so-called *occupation number* representation, in which the vectors are indexed by the numbers of particles occupying each of the available single-particle states of the system. That is, the vector

$$|n_1, n_2, \ldots, n_i, \ldots\rangle = \frac{1}{\sqrt{n_1! n_2! \ldots n_i! \ldots}} |\overbrace{\psi_1 \ldots \psi_1}^{n_1 \text{ times}}, \overbrace{\psi_2 \ldots \psi_2}^{n_2 \text{ times}}, \ldots, \overbrace{\psi_i \ldots \psi_i}^{n_i \text{ times}}, \ldots\rangle \tag{A.17}$$

represents a system with n_1 particles at the single-particle state ψ_1, n_2 particles at state ψ_2, etc., and is properly normalized. The total number of particles in the system will be given by $N = \sum_i n_i$, where the index i runs through all possible single-particle states.

To find the vector resulting from the action of the creation operator a_{ψ_i} on an N-particle bosonic state expressed in occupation number representation, one must notice that

$$a^\dagger_{\psi_i}|n_1, \ldots, n_i, \ldots\rangle = \frac{a^\dagger_{\psi_i}|\ldots, \overbrace{\psi_i \ldots \psi_i}^{n_i \text{ times}}, \ldots\rangle}{\sqrt{n_1! \ldots n_i! \ldots}} = \frac{|\ldots, \overbrace{\psi_i \ldots \psi_i}^{(n_i+1) \text{ times}}, \ldots\rangle}{\sqrt{n_1! \ldots n_i! \ldots}}. \tag{A.18}$$

On the other hand, one also has that

$$|n_1, \ldots, (n_i + 1), \ldots\rangle = \frac{|\ldots, \overbrace{\psi_i \ldots \psi_i}^{(n_i+1) \text{ times}}, \ldots\rangle}{\sqrt{n_1! \ldots (n_i + 1)! \ldots}}. \tag{A.19}$$

Combining Eqs. (A.18) and (A.19), one obtains

$$\boxed{a^\dagger_{\psi_i}|n_1, n_2, \ldots, n_i, \ldots\rangle = \sqrt{n_i + 1}\,|n_1, n_2, \ldots, (n_i + 1), \ldots\rangle} \text{ (bosons).} \tag{A.20}$$

And since there can be at most one fermion at any given single-particle state, the action of $a^\dagger_{\psi_i}$ on a fermionic many-particle vector takes the simpler form

$$\boxed{a^\dagger_{\psi_i}|n_1, n_2, \ldots, n_i, \ldots\rangle = \delta_{n_i,0}\,|n_1, n_2, \ldots, 1_i, \ldots,\rangle} \text{ (fermions),} \tag{A.21}$$

where the occupation numbers n_j can be only zero or one. To find the action of the

annihilation operator on a bosonic many-particle state, one can follow the same procedure:

$$a_{\psi_i}|n_1,\ldots,n_i,\ldots\rangle = \frac{1}{\sqrt{n_1!\ldots n_i!\ldots}}\sum_j \langle\psi_i|\psi_j\rangle|\ldots,\ \overbrace{\psi_i\ldots\psi_i}^{(n_i-1)\text{ times}},\ldots\rangle =$$

$$= \frac{1}{\sqrt{n_1!\ldots n_i!\ldots}}\, n_i\,|\ldots,\ \overbrace{\psi_i\ldots\psi_i}^{(n_i-1)\text{ times}},\ldots\rangle. \quad \text{(A.22)}$$

But on the other hand:

$$|n_1,\ldots,(n_i-1),\ldots\rangle = \frac{|\ldots,\ \overbrace{\psi_i\ldots\psi_i}^{(n_i-1)\text{ times}},\ldots\rangle}{\sqrt{n_1!\ldots(n_i-1)!\ldots}}. \quad \text{(A.23)}$$

Combining Eqs. (A.22) and (A.23), one obtains

$$\boxed{a_{\psi_i}|n_1,n_2,\ldots,n_i,\ldots\rangle = \sqrt{n_i}\,|n_1,n_2,\ldots,(n_i-1),\ldots\rangle} \text{ (bosons)}, \quad \text{(A.24)}$$

which in the case of fermionic systems simplifies to

$$\boxed{a_{\psi_i}|n_1,n_2,\ldots,n_i,\ldots\rangle = \delta_{n_i,1}\,|n_1,n_2,\ldots,0_i,\ldots,\rangle} \text{ (fermions)}. \quad \text{(A.25)}$$

A.4 Change of Basis

In order to obtain the creation and annihilation operators in different representations, consider the expansion of a single-particle state $|\alpha\rangle$ in terms of a complete set of single-particle states $\{|\beta\rangle\}$,

$$|\alpha\rangle = \sum_\beta |\beta\rangle\langle\beta|\alpha\rangle = \sum_\beta \langle\beta|\alpha\rangle|\beta\rangle. \quad \text{(A.26)}$$

Using that $|\alpha\rangle = a_\alpha^\dagger|0\rangle$ and $|\beta\rangle = a_\beta^\dagger|0\rangle$, one obtains:

$$a_\alpha^\dagger|0\rangle = \sum_\beta \langle\beta|\alpha\rangle a_\beta^\dagger|0\rangle \quad \therefore \quad \boxed{a_\alpha^\dagger = \sum_\beta \langle\beta|\alpha\rangle\, a_\beta^\dagger}, \quad \text{(A.27)}$$

and the adjoint transformation equation is

$$\boxed{a_\alpha = \sum_\beta \langle\alpha|\beta\rangle\, a_\beta}. \quad \text{(A.28)}$$

Of particular importance is the position eigenstates representation, in which case the creation and annihilation operators are called *field operators*. Making $|\alpha\rangle = |x\rangle$ in Eqs. (A.27)

and (A.28), one obtains

$$\begin{cases} a^\dagger(x) = \sum_\beta \langle \beta|x\rangle a^\dagger_\beta = \sum_\beta u^*_\beta(x) a^\dagger_\beta; \\ a(x) = \sum_\beta \langle x|\beta\rangle a_\beta = \sum_\beta u_\beta(x) a_\beta, \end{cases} \tag{A.29}$$

where $u_\beta(x) = \langle x|\beta\rangle$ is the coordinate representation wave function of the state $|\beta\rangle$.

A.5 Many-body Operators

One of the most important properties of the creation and annihilation operators is that they provide a basis for all operators in Fock space, that is, any many-body operator can be expressed as a linear combination of products of a_α and $a^\dagger_\alpha$. One can obtain an expression for a many-particle operator $\mathbf{A}$ in second quantized form by imposing that its action on a symmetrized N-particle state $|\psi_1, \ldots, \psi_N\rangle$ be such that

$$\mathbf{A}|\psi_1, \ldots, \psi_N\rangle = (\mathbf{A}_1|\psi_1\rangle) \otimes \cdots \otimes |\psi_N\rangle + \cdots + |\psi_1\rangle \otimes \cdots \otimes (\mathbf{A}_1|\psi_N\rangle), \tag{A.30}$$

where $\mathbf{A}_1$ is the corresponding one-particle operator. Therefore, in the simplest case where $\mathbf{A}_1 = |\alpha\rangle\langle\beta|$, one obtains:

$$\begin{aligned} \mathbf{A}|\psi_1, \ldots, \psi_N\rangle &= \langle\beta|\psi_1\rangle|\alpha\rangle \otimes \cdots \otimes |\psi_N\rangle + \cdots + \langle\beta|\psi_N\rangle|\psi_1\rangle \otimes \cdots \otimes |\alpha\rangle = \\ &= \langle\beta|\psi_1\rangle|\alpha, \ldots, \psi_N\rangle + \cdots + \langle\beta|\psi_N\rangle|\psi_1, \ldots, \alpha\rangle = \\ &= \sum_{i=1}^{N} \langle\beta|\psi_i\rangle|\psi_1, \ldots, \psi_{i-1}, \alpha, \psi_{i+1}, \ldots, \psi_N\rangle. \end{aligned} \tag{A.31}$$

However, due to the symmetry properties of the state vectors, one has

$$|\psi_1, \psi_2, \ldots, \psi_{i-1}, \alpha, \psi_{i+1}, \ldots, \psi_N\rangle = \zeta^{i-1}|\alpha, \psi_1, \psi_2, \ldots, \psi_N\rangle. \tag{A.32}$$

Therefore:

$$\begin{aligned} \mathbf{A}|\psi_1, \ldots, \psi_N\rangle &= \sum_{i=1}^{N} \zeta^{i-1}\langle\beta|\psi_i\rangle|\alpha, \psi_1, \ldots (\text{no } \psi_i) \ldots, \psi_N\rangle = \\ &= a^\dagger_\alpha \left[\sum_{i=1}^{N} \zeta^{i-1}\langle\beta|\psi_i\rangle|\psi_1, \ldots (\text{no } \psi_i) \ldots, \psi_N\rangle\right] = a^\dagger_\alpha a_\beta|\psi_1, \ldots, \psi_N\rangle. \end{aligned} \tag{A.33}$$

This shows that the second quantization representation of the N-particle operator $\mathbf{A}$ whose corresponding single-particle operator is $\mathbf{A}_1 = |\alpha\rangle\langle\beta|$ can be written as $\mathbf{A} = a^\dagger_\alpha a_\beta$. However, any linear one-particle operator can be represented with respect to a particular set of basis vectors in the form

$$\mathbf{A}_1 = \left[\sum_\alpha |\alpha\rangle\langle\alpha|\right] \mathbf{A}_1 \left[\sum_\beta |\beta\rangle\langle\beta|\right] = \sum_{\alpha,\beta} \langle\alpha|\mathbf{A}_1|\beta\rangle |\alpha\rangle\langle\beta| = \sum_{\alpha,\beta} \mathrm{A}^{(1)}_{\alpha\beta} |\alpha\rangle\langle\beta|, \tag{A.34}$$

where $\mathrm{A}^{(1)}_{\alpha\beta} = \langle\alpha|\mathbf{A}_1|\beta\rangle$ are the matrix elements of $\mathbf{A}_1$ in this base. Therefore, the second quantized representation of the many-particle operator $\mathbf{A}$ with respect to the one-particle basis vectors $\{|\alpha\rangle\}$ will be given by

$$\boxed{\mathbf{A} = \sum_{\alpha,\beta} \mathrm{A}^{(1)}_{\alpha\beta}\, a^\dagger_\alpha\, a_\beta}. \tag{A.35}$$

As an example, consider the important problem of writing in second quantized form the Hamiltonian of a system of N independet particles (no mutual interaction) in three dimensions, which are acted upon by an external potential $V(\mathbf{x})$. If the corresponding one-particle Hamiltonian is given by

$$\mathcal{H}_1 = \frac{\mathbf{p}^2}{2m} + V(\mathbf{x}), \tag{A.36}$$

then, using a basis of position eigenstates and applying Eq.(A.35), the N-particle Hamiltonian can be written as

$$\mathcal{H} = \int d^3x \int d^3x' \langle\mathbf{x}|\mathcal{H}_1|\mathbf{x}'\rangle a^\dagger(\mathbf{x}) a(\mathbf{x}'). \tag{A.37}$$

However, the matrix elements of $\mathcal{H}_1$ in this basis are given by

$$\langle\mathbf{x}|\mathcal{H}_1|\mathbf{x}'\rangle = \frac{1}{2m}\langle\mathbf{x}|\mathbf{p}^2|\mathbf{x}'\rangle + \langle\mathbf{x}|V(\mathbf{x})|\mathbf{x}'\rangle = -\frac{\hbar^2}{2m}\nabla^2\delta(\mathbf{x}-\mathbf{x}') + V(\mathbf{x})\delta(\mathbf{x}-\mathbf{x}'). \tag{A.38}$$

Finally, using this back into Eq.(A.37) and integrating the kinetic term by parts, one obtains

$$\boxed{\mathcal{H} = \int d^3x\; a^\dagger(\mathbf{x}) \left[-\frac{\hbar^2}{2m}\nabla^2 + V(\mathbf{x})\right] a(\mathbf{x})}. \tag{A.39}$$

In many applications, however, it may be more convenient to write the many-particle Hamiltonian in terms of momentum eigenstates. This can be obtained by calculating the

matrix elements of $\mathcal{H}_1$ with respect to a basis of momentum states. However, an alternative approach is to Fourier transform the second quantized Hamiltonian from coordinate to momentum representation. The formulas relating the creation and annihilation operators in both basis can be obtained by making $|\beta\rangle = |\mathbf{p}\rangle$ in Eq.(A.29), and using that $\langle \mathbf{x}|\mathbf{p}\rangle = (2\pi\hbar)^{-3/2}\exp(\frac{i}{\hbar}\mathbf{p}\cdot\mathbf{x})$ in three dimensions. This results in

$$\begin{cases} a^\dagger(\mathbf{x}) = \dfrac{1}{(2\pi\hbar)^{3/2}}\displaystyle\int d^3p\; e^{-\frac{i}{\hbar}\mathbf{p}\cdot\mathbf{x}}a^\dagger(\mathbf{p}); \\ a(\mathbf{x}) = \dfrac{1}{(2\pi\hbar)^{3/2}}\displaystyle\int d^3p\; e^{\frac{i}{\hbar}\mathbf{p}\cdot\mathbf{x}}a(\mathbf{p}). \end{cases} \tag{A.40}$$

Substituting these expressions in Eq.(A.39), defining the Fourier transform $\tilde{V}(\mathbf{q})$ of the external potential such that

$$V(\mathbf{x}) = \int d^3q\; e^{\frac{i}{\hbar}\mathbf{q}\cdot\mathbf{x}}\,\tilde{V}(\mathbf{q}), \tag{A.41}$$

and using the integral representation of the delta-function in three dimensions,

$$\delta(\mathbf{x}-\mathbf{x}') = \frac{1}{(2\pi)^3}\int d^3y\; e^{-i(\mathbf{x}-\mathbf{x}')\cdot\mathbf{y}}, \tag{A.42}$$

one obtains for the second quantized many-particle Hamiltonian in momentum representation:

$$\boxed{\mathcal{H} = \int d^3p\; a^\dagger(\mathbf{p})\frac{p^2}{2m}a(\mathbf{p}) + \int d^3p\int d^3q\; a^\dagger(\mathbf{p}+\mathbf{q})\tilde{V}(\mathbf{q})a(\mathbf{p})}. \tag{A.43}$$

As already mentioned, this description applies only to *independent* particles, that is, it neglects interparticle interactions and considers only the possible effect of an external potential on each particle individually. If two particles at positions $\mathbf{x}_1$ and $\mathbf{x}_2$ are allowed to interact via a potential $V_2(\mathbf{x}_1,\mathbf{x}_2)$, then one can show (see, for example, Ref. [83]) that the second quantized expression for the interparticle interaction potential will be

$$V_2 = \frac{1}{2}\int d^3x\int d^3y\, a^\dagger(\mathbf{x})a^\dagger(\mathbf{y})V_2(\mathbf{x},\mathbf{y})a(\mathbf{y})a(\mathbf{x}). \tag{A.44}$$

Analogously to the independent particle case, it may be more convenient to express the two-body interaction potential in momentum representation. Assuming that the system

has translational invariance, such that

$$V_2(\mathbf{x}_1, \mathbf{x}_2) = V_2(\mathbf{x}_2, \mathbf{x}_1), \tag{A.45}$$

the interparticle potential can be written in terms of its Fourier transform as

$$V_2(\mathbf{x}_1, \mathbf{x}_2) = \int d^3q \, e^{\frac{i}{\hbar}\mathbf{q}\cdot(\mathbf{x}_1 - \mathbf{x}_2)} \, \tilde{V}_2(\mathbf{q}). \tag{A.46}$$

Writing the creation and annihilation operators in momentum space with the help of Eq.(A.40), and using the representation of the delta-function given by Eq.(A.42), one obtains for the second quantized expression of the two-particle interaction potential:

$$V_2 = \frac{1}{2} \int d^3p \int d^3p' \int d^3q \, a^\dagger(\mathbf{p} + \mathbf{q}) a^\dagger(\mathbf{p}' - \mathbf{q}) \tilde{V}_2(\mathbf{q}) a(\mathbf{p}') a(\mathbf{p}). \tag{A.47}$$

This concludes this summary of the most important properties and applications of the algebra of creation and annihilation many-particle operators, which is known as second quantization formalism.

APPENDIX B

FEYNMAN PATH INTEGRAL

B.1 Quantum Mechanical Propagator

Let a one-dimensional quantum mechanical system be described at time t by a state vector $|\psi(t)\rangle$, which can be related to the state vector $|\psi(t_0)\rangle$ at some previous time $t_0 < t$ through the time-evolution operation

$$|\psi(t)\rangle = \mathcal{U}(t, t_0)\,|\psi(t_0)\rangle = e^{-\frac{i}{\hbar}\mathcal{H}(t-t_0)}\,|\psi(t_0)\rangle, \tag{B.1}$$

where $\mathcal{H}$ is the Hamiltonian of the system. Projecting both sides onto $|x\rangle$ and inserting the identity operator written in terms of position eigenkets $|x'\rangle$, one obtains:

$$\psi(x,t) = \langle x|\psi(t)\rangle = \langle x|e^{-\frac{i}{\hbar}\mathcal{H}(t-t_0)}|\psi(t_0)\rangle = \int dx'\,\langle x|e^{-\frac{i}{\hbar}\mathcal{H}(t-t_0)}|x'\rangle\langle x'|\psi(t_0)\rangle. \tag{B.2}$$

Defining the *propagator* $G(x,t;x',t_0)$ as

$$G(x,t;x',t_0) \equiv \langle x|e^{-\frac{i}{\hbar}\mathcal{H}(t-t_0)}|x'\rangle, \tag{B.3}$$

the previous expression can be written as:

$$\psi(x,t) = \int dx'\,G(x,t;x',t_0)\,\psi(x',t_0). \tag{B.4}$$

This means that, if the wave function is known at time t_0, the knowledge of the propagator $G(x,t;x',t_0)$ allows one to obtain the wave function $\psi(x,t)$ at any future time $t > t_0$.

We now consider the development of a path integral formulation of the quantum mechanical propagator. The idea is to break the finite time interval $(t - t_0)$ into infinitesimal steps, evaluate the evolution operator for each step, and then add the matrix elements together to obtain the result for the finite interval. If there are N equal steps of size ϵ,

$$\epsilon = \frac{t - t_0}{N}, \tag{B.5}$$

then, using the composition property of the time-evolution operator, Eq.(B.3) can be written as:

$$G(x,t;x',t_0) = \langle x_N|e^{-\frac{i}{\hbar}\mathcal{H}(t_N-t_{N-1})}\, e^{-\frac{i}{\hbar}\mathcal{H}(t_{N-1}-t_{N-2})} \ldots e^{-\frac{i}{\hbar}\mathcal{H}(t_2-t_1)}\, e^{-\frac{i}{\hbar}\mathcal{H}(t_1-t_0)}|x_0\rangle, \quad \text{(B.6)}$$

where the following notation was used: $x_N = x$, $x_0 = x'$, and $t_N = t$. Inserting the identity operator in terms of position eigenkets $N-1$ times between successive exponentials, one obtains:

$$G(x,t;x',t_0) = \left[\int \prod_{k=1}^{N-1} dx_k\right] \langle x_N|e^{-\frac{i}{\hbar}\epsilon\mathcal{H}}|x_{N-1}\rangle \ldots \langle x_k|e^{-\frac{i}{\hbar}\epsilon\mathcal{H}}|x_{k-1}\rangle \ldots \langle x_1|e^{-\frac{i}{\hbar}\epsilon\mathcal{H}}|x_0\rangle =$$

$$= \left[\int \prod_{k=1}^{N-1} dx_k\right] \prod_{k=1}^{N} \langle x_k|e^{-\frac{i}{\hbar}\epsilon\mathcal{H}}|x_{k-1}\rangle. \quad \text{(B.7)}$$

Using the Baker-Campbell-Hausdorff formula,

$$e^{\mathbb{A}}\, e^{\mathbb{B}} = e^{\mathbb{A}+\mathbb{B}+\frac{1}{2}[\mathbb{A},\mathbb{B}]+\cdots}, \quad \text{(B.8)}$$

one can write the previous exponentials as:

$$e^{-\frac{i}{\hbar}\epsilon\mathcal{H}} = e^{-\frac{i}{\hbar}\epsilon(\mathbb{T}+\mathbb{V})} = e^{-\frac{i}{\hbar}\epsilon\mathbb{T}}\, e^{-\frac{i}{\hbar}\epsilon\mathbb{V}}\, e^{-\frac{i}{\hbar^2}\epsilon^2\mathbb{X}}, \quad \text{(B.9)}$$

where $\mathbb{T}$ and $\mathbb{V}$ are the kinetic and potential energy operators, respectively, and the operator $\mathbb{X}$ contains multiple commutators of $\mathbb{T}$ and $\mathbb{V}$. The argument of the third exponential on the right-hand side of Eq.(B.9) is proportional to ϵ^2 and, therefore, becomes negligible for $\epsilon \to 0$. That is, in the limit of an infinite number N of subintervals, the approximation

$$e^{-\frac{i}{\hbar}\epsilon(\mathbb{T}+\mathbb{V})} \approx e^{-\frac{i}{\hbar}\epsilon\mathbb{T}}\, e^{-\frac{i}{\hbar}\epsilon\mathbb{V}} \quad \text{(B.10)}$$

becomes exact, and the matrix elements in Eq.(B.7) can be written as:

$$\langle x_k|e^{-\frac{i}{\hbar}\epsilon\mathcal{H}}|x_{k-1}\rangle = \lim_{N\to\infty} \langle x_k|e^{-\frac{i}{\hbar}\epsilon\mathbb{T}}\, e^{-\frac{i}{\hbar}\epsilon\mathbb{V}}|x_{k-1}\rangle =$$

$$= \lim_{N\to\infty} \int dp_k \langle x_k|e^{-\frac{i}{\hbar}\frac{\epsilon}{2m}p_k^2}|p_k\rangle\, \langle p_k|e^{-\frac{i}{\hbar}\epsilon V(x_{k-1})}|x_{k-1}\rangle =$$

$$= \lim_{N\to\infty} \left\{ e^{-\frac{i}{\hbar}\epsilon V(x_{k-1})} \int dp_k\, e^{-\frac{i\epsilon}{2m\hbar}p_k^2}\, \langle x_k|p_k\rangle\langle p_k|x_{k-1}\rangle \right\}, \quad \text{(B.11)}$$

where an identity operator in terms of momentum eigenstates was introduced and the kinetic energy operator was written as $\mathbb{T} = \frac{\mathbb{P}^2}{2m}$. Using that

$$\langle x_k|p_k\rangle = \frac{1}{(2\pi\hbar)^{1/2}} e^{\frac{i}{\hbar}p_k x_k}, \tag{B.12}$$

one has:

$$\langle x_k|e^{-\frac{i}{\hbar}\epsilon\mathcal{H}}|x_{k-1}\rangle = \lim_{N\to\infty}\left\{\frac{1}{2\pi\hbar}\, e^{-\frac{i}{\hbar}\epsilon V(x_{k-1})}\int_{-\infty}^{\infty} dp_k\, e^{-\frac{i\epsilon}{2m\hbar}p_k^2}\, e^{\frac{i}{\hbar}p_k(x_k-x_{k-1})}\right\}. \tag{B.13}$$

The integral over p_k can be evaluated with the help of the following Gaussian integral,

$$\int_{-\infty}^{\infty} dx\, e^{ax^2+bx} = i\sqrt{\frac{\pi}{a}}\, e^{-b^2/4a}, \tag{B.14}$$

leading to

$$\langle x_k|e^{-\frac{i}{\hbar}\epsilon\mathcal{H}}|x_{k-1}\rangle = \lim_{N\to\infty}\left\{\sqrt{\frac{m}{2\pi\hbar i\epsilon}}\, e^{-\frac{i}{\hbar}\epsilon V(x_{k-1})}\, \exp\left(\frac{im}{2\hbar\epsilon}\delta x_k^2\right)\right\}, \tag{B.15}$$

where the notation $\delta x_k \equiv x_k - x_{k-1}$ was used. Substituting this result back into Eq.(B.7), the propagator will be written as:

$$G(x,t;x',t_0) = \lim_{N\to\infty}\left[\int\prod_{k=1}^{N-1} dx_k\right]\left\{\prod_{k=1}^{N}\sqrt{\frac{m}{2\pi\hbar i\epsilon}}\, \exp\left[-\frac{i}{\hbar}\epsilon V(x_{k-1}) + \frac{im}{2\hbar\epsilon}\delta x_k^2\right]\right\} =$$

$$= \lim_{N\to\infty}\sqrt{\frac{m}{2\pi\hbar i\epsilon}}\left[\int\prod_{k=1}^{N-1} dx_k\sqrt{\frac{m}{2\pi\hbar i\epsilon}}\right]\, \exp\left[\frac{i}{\hbar}\sum_{k=1}^{N}\epsilon\left(\frac{m}{2}\left(\frac{\delta x_k}{\epsilon}\right)^2 - V(x_{k-1})\right)\right]. \tag{B.16}$$

The set of points $\{x_0, x_1, \ldots, x_N\}$ defines a trajectory in space-time. In the limit of $N\to\infty$, it is convenient to denote this trajectory by $x(t)$, with starting point $x(t_0) = x_0$ and endpoint $x(t_N) = x_N$. However, it is important to note that this notation does not imply continuity or differentiability. Rather, the trajectory should always be thought of as a set of N points $x(t_k)$ indexed by the discrete times t_k. With this notation, Eq.(B.16) can be written as

$$G(x,t;x',t_0) = \lim_{N\to\infty}\sqrt{\frac{m}{2\pi\hbar i\epsilon}}\left[\int\prod_{k=1}^{N-1} dx_k\sqrt{\frac{m}{2\pi\hbar i\epsilon}}\right]\, \exp\left[\frac{i}{\hbar}\int_{t_0}^{t} dt'\left(\frac{m}{2}\dot{x}^2(t') - V(x(t'))\right)\right]. \tag{B.17}$$

Finally, denoting the *integration measure* by

$$\int\mathcal{D}[x(t)] \equiv \lim_{N\to\infty}\sqrt{\frac{m}{2\pi\hbar i\epsilon}}\left[\int\prod_{k=1}^{N-1} dx_k\sqrt{\frac{m}{2\pi\hbar i\epsilon}}\right], \tag{B.18}$$

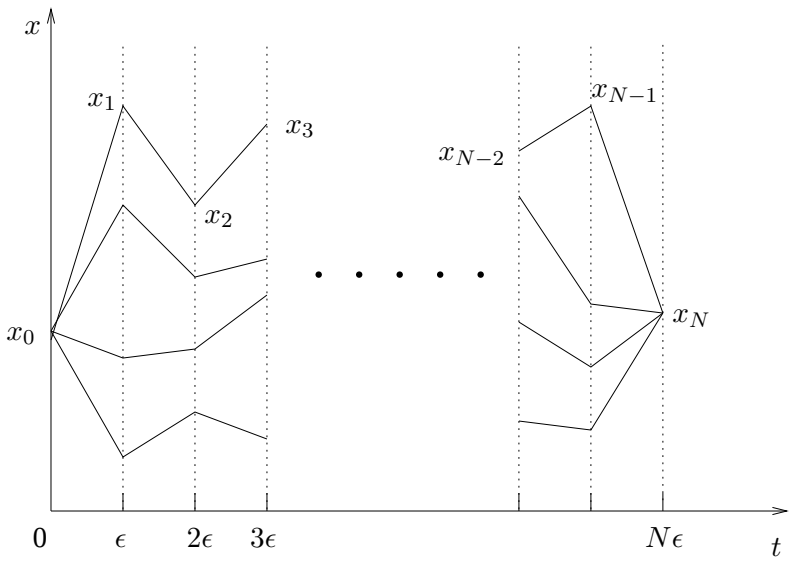

Figure B.1: Typical N-step trajectories in space-time that contribute to the path integral.

and recalling that the classical action $\mathcal{S}[x(t)]$ is given by

$$\mathcal{S}[x(t)] = \int_{t_0}^{t} dt'\, L[x(t')], \tag{B.19}$$

where $L[x(t)]$ is the Lagrangian,

$$L[x(t)] = \frac{1}{2}\, m\dot{x}^2(t) - V(x(t)), \tag{B.20}$$

the path integral expression for the quantum mechanical propagator becomes

$$\boxed{G(x,t;x',t_0) = \int \mathcal{D}[x(t)]\, e^{\frac{i}{\hbar}\,\mathcal{S}[x(t)]}}. \tag{B.21}$$

The matrix element of the evolution operator between states $|x_0\rangle$ and $|x_N\rangle$ is thus the sum of exponentials of $\frac{i}{\hbar}$ times the action along different trajectories beginning at x_0 at time t_0 and ending at x_N at time t, some of which are sketched in Fig. B.1.

B.2 Canonical Partition Function

Let a system described by a time independent Hamiltonian $\mathcal{H}$ be in contact with a thermal reservoir at fixed temperature T. The partition function of the system will be

$$Z = \mathrm{tr}\left(e^{-\beta\mathcal{H}}\right). \tag{B.22}$$

Since the trace is invariant under a change of basis vectors, it can be evaluated using, for instance, a complete set of position eigenvectors $|x\rangle$:

$$Z = \mathrm{tr}\left(e^{-\beta\mathcal{H}}\right) = \int dx\, \langle x|e^{-\beta\mathcal{H}}|x\rangle. \tag{B.23}$$

This expression for the partition function can be written in terms of path integrals. One starts defining a new quantity $\tau \equiv \beta\hbar$, which can be seen to have dimension of time. Then, Eq.(B.23) becomes:

$$Z = \int dx\, \langle x|e^{-\frac{1}{\hbar}\tau\mathcal{H}}|x\rangle. \tag{B.24}$$

Now one can use the same idea of dividing the "time" interval τ into N subintervals of equal size $\epsilon = \tau/N$, and inserting the identity operator in terms of position eigenkets $N-1$ times:

$$Z = \int dx\, \langle x|e^{-\frac{1}{\hbar}\tau\mathcal{H}}|x\rangle = \int dx_N\, \langle x_N| \left(e^{-\frac{1}{\hbar}\epsilon\mathcal{H}}\right)^N |x_0\rangle =$$

$$= \int dx_N \left[\int \prod_{k=1}^{N-1} dx_k\right] \langle x_N|e^{-\frac{\epsilon}{\hbar}\mathcal{H}}|x_{N-1}\rangle \ldots \langle x_2|e^{-\frac{\epsilon}{\hbar}\mathcal{H}}|x_1\rangle \langle x_1|e^{-\frac{\epsilon}{\hbar}\mathcal{H}}|x_0\rangle =$$

$$= \left[\int \prod_{k=1}^{N} dx_k\right] \prod_{k=1}^{N} \langle x_k|e^{-\frac{\epsilon}{\hbar}\mathcal{H}}|x_{k-1}\rangle, \tag{B.25}$$

where the convention $x = x_N = x_0$ was used. It is important to note that, in this case, there are N integrations over position variables due to the extra integral over the final position $x_N = x_0$, which represents the quantum mechanical trace.

The matrix elements in this expression can be evaluated using the same approximation (which becomes exact in the limit of $N \to \infty$) of neglecting terms of order ϵ^2 and higher, assuming that the "time" τ is divided into intervals small enough to make the terms containing commutators of the kinetic and potential energy operators negligible:

$$\langle x_k|e^{-\frac{\epsilon}{\hbar}\mathcal{H}}|x_{k-1}\rangle = \lim_{N\to\infty} \langle x_k|e^{-\frac{\epsilon}{\hbar}\frac{\mathbb{p}^2}{2m}}\, e^{-\frac{\epsilon}{\hbar}\mathbb{V}(x)}|x_{k-1}\rangle. \tag{B.26}$$

Inserting the identity operator in terms of momentum eigenkets, and using Eq.(B.12) for

the overlap between position and momentum eigenvectors, one obtains:

$$\langle x_k|e^{-\frac{\epsilon}{\hbar}\mathcal{H}}|x_{k-1}\rangle = \lim_{N\to\infty}\int dp_k\,\langle x_k|e^{-\frac{\epsilon}{\hbar}\frac{\mathbb{P}^2}{2m}}|p_k\rangle\,\langle p_k|e^{-\frac{\epsilon}{\hbar}\mathbb{V}(x)}|x_{k-1}\rangle =$$

$$= \lim_{N\to\infty} e^{-\frac{\epsilon}{\hbar}V(x_{k-1})}\int dp_k\, e^{-\frac{\epsilon}{\hbar}\frac{p_k^2}{2m}}\,\langle x_k|p_k\rangle\,\langle p_k|x_{k-1}\rangle =$$

$$= \lim_{N\to\infty}\left\{\frac{1}{2\pi\hbar}\, e^{-\frac{\epsilon}{\hbar}V(x_{k-1})}\int_{-\infty}^{\infty} dp_k\, e^{-\frac{\epsilon}{\hbar}\frac{p_k^2}{2m}}\, e^{\frac{i}{\hbar}p_k(x_k-x_{k-1})}\right\}. \tag{B.27}$$

Again, the Gaussian integral given by Eq.(B.14) can be used to evaluate the integral over p_k, yielding

$$\langle x_k|e^{-\frac{\epsilon}{\hbar}\mathcal{H}}|x_{k-1}\rangle = \lim_{N\to\infty}\left\{\sqrt{\frac{m}{2\pi\hbar\epsilon}}\,\exp\left\{-\frac{\epsilon}{\hbar}\left[\frac{m}{2}\left(\frac{x_k-x_{k-1}}{\epsilon}\right)^2 + V(x_{k-1})\right]\right\}\right\}. \tag{B.28}$$

Substituting this back into Eq.(B.25), the partition function becomes:

$$Z = \lim_{N\to\infty}\left[\int\prod_{k=1}^{N} dx_k\right]\left\{\prod_{k=1}^{N}\sqrt{\frac{m}{2\pi\hbar\epsilon}}\,\exp\left\{-\frac{\epsilon}{\hbar}\left[\frac{m}{2}\left(\frac{\delta x_k}{\epsilon}\right)^2 + V(x_{k-1})\right]\right\}\right\} =$$

$$= \lim_{N\to\infty}\left[\int\prod_{k=1}^{N} dx_k\sqrt{\frac{m}{2\pi\hbar\epsilon}}\right]\,\exp\left\{-\frac{1}{\hbar}\sum_{k=1}^{N}\epsilon\left[\frac{m}{2}\left(\frac{\delta x_k}{\epsilon}\right)^2 + V(x_{k-1})\right]\right\}. \tag{B.29}$$

Finally, using the trajectory notation introduced in the last section, one obtains:

$$\boxed{Z = \oint_{x(\beta\hbar)=x(0)}\mathcal{D}[x(\tau)] = e^{-\frac{1}{\hbar}\mathcal{S}_e[x(\tau)]}}, \tag{B.30}$$

where the *Euclidian action* $\mathcal{S}_e$ is defined as

$$\mathcal{S}_e[x(\tau)] = \int_0^{\beta\hbar} d\tau\,\left(\frac{1}{2}m\dot{x}^2(\tau) + V(x(\tau))\right), \tag{B.31}$$

and the integration measure is

$$\oint_{x(\beta\hbar)=x(0)}\mathcal{D}[x(\tau)] = \lim_{N\to\infty}\left[\int\prod_{k=1}^{N} dx_k\sqrt{\frac{m}{2\pi\hbar\epsilon}}\right]. \tag{B.32}$$

The partition function is thus a sum over all periodic trajectories of period $\beta\hbar$, and the symbol

$$\oint_{x(\beta\hbar)=x(0)}$$

indicates that the integral over the "endpoint" variable x_N satisfies the periodic boundary condition $x(\beta\hbar) = x(0)$.

APPENDIX C

COHERENT STATES AND FUNCTIONAL INTEGRALS

When the operators that represent physical observables are expressed in terms of creation and annihilation operators, in which case they are said to be written in *second quantization* form, a natural representation for the quantum mechanics of many-particle systems is defined in terms of *coherent states*. In this section, bosonic and fermionic coherent states will be treated separately, and their most important properties will be discussed in each case. Then, an expression for the matrix element of the time evolution operator between coherent states will be developed, leading to an extension of path integrals known as *functional integration*. It provides a convenient framework for the study of many-particle systems described by second-quantized operators.

C.1 Coherent States

Let a_α and $a_\alpha^\dagger$ be many-body creation and annihilation operators, respectively. As discussed in Appendix A, the effect of a_α acting on any many-body state is to annihilate one particle in the state α from this many-body state, while $a_\alpha^\dagger$ creates one particle in the state α:

$$\begin{aligned} a_\alpha|n_1, n_2, \ldots n_\alpha, \ldots\rangle &= \sqrt{n_\alpha}\,|n_1, n_2, \ldots n_\alpha - 1, \ldots\rangle; \\ a_\alpha^\dagger|n_1, n_2, \ldots n_\alpha, \ldots\rangle &= \sqrt{n_\alpha + 1}\,|n_1, n_2, \ldots n_\alpha + 1, \ldots\rangle. \end{aligned} \tag{C.1}$$

In the case of bosons, these operators can be shown to satisfy commutation relations [27],

$$\begin{cases} [a_\alpha, a_\beta^\dagger] = a_\alpha a_\beta^\dagger - a_\beta^\dagger a_\alpha = \delta_{\alpha\beta}, \\ [a_\alpha, a_\beta] = [a_\alpha^\dagger, a_\beta^\dagger] = 0, \end{cases} \tag{C.2}$$

while they satisfy anti-commutation relations in the case of fermions,

$$\begin{cases} \{a_\alpha, a_\beta^\dagger\} = a_\alpha a_\beta^\dagger + a_\beta^\dagger a_\alpha = \delta_{\alpha\beta}, \\ \{a_\alpha, a_\beta\} = \{a_\alpha^\dagger, a_\beta^\dagger\} = 0. \end{cases} \tag{C.3}$$

A coherent state $|\Phi\rangle$ is defined as an eigenstate of the annihilation operator a_α with eigenvalue ϕ_α, that is,

$$a_\alpha|\Phi\rangle = \phi_\alpha|\Phi\rangle. \tag{C.4}$$

It is easy to see that the commutation or anti-commutation relations satisfied by a_α and $a_\alpha^\dagger$ imply corresponding relations for the eigenvalues ϕ_α:

$$\begin{cases} [\phi_\alpha, \phi_\beta] = 0 \text{ for bosons;} \\ \\ \{\phi_\alpha, \phi_\beta\} = 0 \text{ for fermions.} \end{cases} \tag{C.5}$$

Therefore, since the eigenvalues satisfy commutation relations in the case of bosons, they can be represented by ordinary (complex) numbers. However, since they anti-commute in the case of fermions, they must be represented by *Grassman numbers*, which are anti-commuting variables. These two cases will be considered separately.

C.2 Boson Coherent States

In order to obtain a more convenient expression for the boson coherent state $|\Phi\rangle$, consider its expansion in terms of many-body states $|n_1, n_2, \ldots, n_i \ldots\rangle$,

$$|\Phi\rangle = \sum_{n_1, n_2 \ldots} C_{n_1,\ldots,n_i,\ldots} |n_1, n_2, \ldots, n_i, \ldots\rangle, \tag{C.6}$$

where $C_{n_1,\ldots,n_i,\ldots}$ are complex coefficients. If one applies a_i to both sides and compares corresponding coefficients, one obtains:

$$C_{n_1,\ldots,n_i,\ldots} = \frac{\phi_i}{\sqrt{n_i}} C_{n_1,\ldots,n_i-1,\ldots}. \tag{C.7}$$

Therefore, if a_1 is applied n_1 times, a_2 is applied n_2 times, and so on, and the coefficient of the vacuum state is arbitrarily set equal to one ($C_{0,\ldots,0,\ldots} = 1$), one obtains:

$$C_{n_1,\ldots,n_i,\ldots} = \frac{\phi_1^{n_1}\, \phi_2^{n_2} \ldots \phi_i^{n_i} \ldots}{\sqrt{n_1!}\, \sqrt{n_2!} \ldots \sqrt{n_i!} \ldots}. \tag{C.8}$$

Substituting this in Eq.(C.6), and using the fact that

$$|n_1, n_2, \ldots, n_i, \ldots\rangle = \frac{(a_1^\dagger)^{n_1}}{\sqrt{n_1!}} \frac{(a_2^\dagger)^{n_2}}{\sqrt{n_2!}} \ldots \frac{(a_i^\dagger)^{n_i}}{\sqrt{n_i!}} \ldots |0\rangle, \tag{C.9}$$

one obtains:

$$|\Phi\rangle = \sum_{n_1,n_2,\ldots} \frac{(\phi_1 a_1^\dagger)^{n_1}}{n_1!} \ldots \frac{(\phi_i a_i^\dagger)^{n_i}}{n_i!} \ldots |0\rangle = \left[\sum_{n_1=0}^{\infty} \frac{(\phi_1 a_1^\dagger)^{n_1}}{n_1!}\right] \ldots \left[\sum_{n_i=0}^{\infty} \frac{(\phi_i a_i^\dagger)^{n_i}}{n_i!}\right] \ldots |0\rangle =$$

$$= e^{\phi_1 a_1^\dagger} \ldots e^{\phi_i a_i^\dagger} \ldots |0\rangle = e^{\sum_\alpha \phi_\alpha a_\alpha^\dagger} |0\rangle. \tag{C.10}$$

Let $|\Phi'\rangle$ be another bosonic coherent state which is the eigenstate of a_α with eigenvalue ϕ'_α. Using Eq.(C.6) with the coefficients $C_{n_1,\ldots,n_i\ldots}$ given by Eq.(C.8), the superposition of two coherent states $|\Phi\rangle$ and $|\Phi'\rangle$ will be written as:

$$\langle\Phi|\Phi'\rangle = \sum_{n_1,n_2,\ldots} \sum_{n'_1,n'_2,\ldots} \frac{(\phi_1^*)^{n_1}}{\sqrt{n_1!}} \ldots \frac{(\phi_i^*)^{n_i}}{\sqrt{n_i!}} \ldots \frac{(\phi'_1)^{n'_1}}{\sqrt{n'_1!}} \ldots \frac{(\phi'_i)^{n'_i}}{\sqrt{n'_i!}} \ldots \langle n_1, n_2, \ldots | n'_1, n'_2, \ldots \rangle. \tag{C.11}$$

With the help of the orthonormality relation for two many-body state vectors,

$$\langle n_1, n_2, \ldots, n_i, \ldots | n'_1, n'_2, \ldots, n'_i, \ldots \rangle = \delta_{n_1,n'_1}\, \delta_{n_2,n'_2} \ldots \delta_{n_i,n'_i} \ldots, \tag{C.12}$$

this becomes:

$$\langle\Phi|\Phi'\rangle = \sum_{n_1,n_2\ldots} \frac{(\phi_1^*\phi'_1)^{n_1}}{n_1!} \ldots \frac{(\phi_i^*\phi'_i)^{n_i}}{n_i!} \cdots = \left[\sum_{n_1=0}^{\infty} \frac{(\phi_1^*\phi'_1)^{n_1}}{n_1!}\right] \ldots \left[\sum_{n_i=0}^{\infty} \frac{(\phi_i^*\phi'_i)^{n_i}}{n_i!}\right] \cdots =$$

$$= e^{\phi_1^*\phi'_1} \ldots e^{\phi_i^*\phi'_i} \cdots = e^{\sum_\alpha \phi_\alpha^*\phi'_\alpha}. \tag{C.13}$$

The coherent states form a complete set of eigenvectors in Fock space, with respect to which any vector of this space can be expanded. In fact, the identity operator can be expressed in terms of bosonic coherent states by means of the following closure relation,

$$\mathbf{1} = \int \left[\prod_\alpha \frac{d\phi_\alpha^*\, d\phi_\alpha}{2i\pi}\right] e^{-\sum_\alpha \phi_\alpha^*\phi_\alpha}\, |\Phi\rangle\langle\Phi|. \tag{C.14}$$

In order to show that the right-hand side of this equation (which will be called $\mathcal{O}$) is in fact the identity operator, one can use the expansion of the coherent state $|\Phi\rangle$ given by

Eq.(C.6), with the coefficients $C_{n_1,\ldots,n_i,\ldots}$ given by Eq.(C.8), to write

$$\mathcal{O} = \int \left[\prod_i \frac{d\phi_i^*\, d\phi_i}{2i\pi}\right] e^{-\sum_i \phi_i^*\phi_i} \left[\sum_{n_1,n_2,\ldots} \frac{\phi_1^{n_1}\ldots\phi_i^{n_i}\ldots}{\sqrt{n_1!}\ldots\sqrt{n_i!}\ldots} |n_1, n_2\ldots\rangle\right] \times$$

$$\times \left[\sum_{m_1,m_2,\ldots} \frac{(\phi_1^*)^{m_1}\ldots(\phi_i^*)^{m_i}\ldots}{\sqrt{m_1!}\ldots\sqrt{m_i!}\ldots} \langle m_1, m_2\ldots|\right]. \quad \text{(C.15)}$$

Writing ϕ_i in polar form ($\phi_i = \rho_i e^{i\theta_i}$), changing variables from (ϕ_i, ϕ_i^*) to (ρ_i, θ_i), and recalling that the Jacobian of this variable transformation is $2i\rho_i$, one obtains:

$$\mathcal{O} = \int \left[\prod_i \frac{1}{\pi}\rho_i\, d\rho_i\, d\theta_i\right] e^{-\sum_i \rho_i^2} \sum_{\substack{n_1,n_2,\ldots \\ m_1,m_2,\ldots}} \frac{\left[\prod_i (\rho_i e^{i\theta_i})^{n_i}\right]\left[\prod_i (\rho_i e^{-i\theta_i})^{m_i}\right]}{\left[\prod_i \sqrt{n_i!}\right]\left[\prod_i \sqrt{m_i!}\right]} |n_1, n_2, \ldots\rangle\langle m_1, m_2, \ldots| =$$

$$= \sum_{\substack{n_1,n_2,\ldots \\ m1,m2,\ldots}} \prod_i \left[\frac{1}{\pi}\frac{1}{\sqrt{n_i!}\sqrt{m_i!}} \int_0^\infty \rho_i\, d\rho_i\, e^{-\rho_i^2}\, \rho_i^{n_i+m_i} \int_0^{2\pi} d\theta_i\, e^{i(n_i-m_i)\theta_i}\right] |n_1, n_2, \ldots\rangle\langle m_1, m_2, \ldots|. \quad \text{(C.16)}$$

Using that $\int_0^{2\pi} d\theta_i\, e^{i(n_i-m_i)\theta_i} = 2\pi\delta_{n_i,m_i}$, this expression becomes:

$$\mathcal{O} = \sum_{n_1,n_2,\ldots} \prod_i \left[\frac{1}{n_i!} \int_0^\infty 2\rho_i\, d\rho_i\, e^{-\rho_i^2}\, \rho_i^{2n_i}\right] |n_1, n_2, \ldots\rangle\langle n_1, n_2, \ldots|. \quad \text{(C.17)}$$

Changing variables again to $\xi_i = \rho_i^2$, it gives:

$$\mathcal{O} = \sum_{n_1,n_2,\ldots} \prod_i \left[\frac{1}{n_i!} \int_0^\infty d\xi_i\, e^{-\xi_i}\, \xi_i^{n_i}\right] |n_1, n_2, \ldots\rangle\langle n_1, n_2, \ldots|. \quad \text{(C.18)}$$

Finally, using the definition of the Gamma function,

$$\int_0^\infty dx\, e^{-x}\, x^n = \Gamma(n+1) = n!, \quad \text{(C.19)}$$

and invoking the completeness of the set of many-body state vectors in Fock space, one obtains:

$$\mathcal{O} = \sum_{n_1,n_2,\ldots} |n_1, n_2, \ldots\rangle\langle n_1, n_2, \ldots| = \mathbf{1}, \quad \text{(C.20)}$$

which concludes the proof of Eq.(C.14).

This closure relation in terms of bosonic coherent states provides a convenient way of expressing the trace of second-quantized operators, which will be useful in the calculation of the partition function of many-particle systems. If $\{|n\rangle\}$ is a complete set of eigenvectors

of an operator $\mathbf{A}$, then:

$$\begin{aligned}\mathrm{tr}\,\mathbf{A} = \sum_n \langle n|\mathbf{A}|n\rangle = \int \left[\prod_\alpha \frac{d\phi^*_\alpha\, d\phi_\alpha}{2i\pi}\right] e^{-\sum_\alpha \phi^*_\alpha \phi_\alpha} \sum_n \langle n|\Phi\rangle\langle\Phi|\mathbf{A}|n\rangle = \\ = \int \left[\prod_\alpha \frac{d\phi^*_\alpha\, d\phi_\alpha}{2i\pi}\right] e^{-\sum_\alpha \phi^*_\alpha \phi_\alpha} \langle\Phi|\mathbf{A}\left(\sum_n |n\rangle\langle n|\right)|\Phi\rangle = \\ = \int \left[\prod_\alpha \frac{d\phi^*_\alpha\, d\phi_\alpha}{2i\pi}\right] e^{-\sum_\alpha \phi^*_\alpha \phi_\alpha} \langle\Phi|\mathbf{A}|\Phi\rangle. \qquad \text{(C.21)}\end{aligned}$$

Finally, a useful property of coherent states is the simple form assumed by matrix elements of normal-ordered operators when represented in a basis of coherent states. An operator is said to be in normal form when the creation operators always appear to the left of the annihilation operators. Denoting by $:\mathbf{A}(a^\dagger_\alpha, a_\alpha):$ an operator reordered in normal form, the action of a_α to the right and $a^\dagger_\alpha$ to the left on coherent states immediately yields

$$\langle\Phi|\,:\mathbf{A}(a^\dagger_\alpha, a_\alpha):\,|\Phi'\rangle = \mathbf{A}(\phi^*_\alpha, \phi'_\alpha)\,\langle\Phi|\Phi'\rangle = \mathbf{A}(\phi^*_\alpha, \phi'_\alpha)\, e^{\sum_\alpha \phi^*_\alpha \phi'_\alpha}, \qquad \text{(C.22)}$$

where Eq.(C.13) for the overlap of two coherent states was used. We now turn our attention to the analysis of coherent states in the case of fermion operators.

C.3 Fermion Coherent States

As mentioned earlier, the anti-commutation relations satisfied by the fermionic many-body creation and annihilation operators imply corresponding relations for their eigenvalues. In fact, if $|\Xi\rangle$ is a fermion coherent state with eigenvalue ξ_α,

$$a_\alpha|\Xi\rangle = \xi_\alpha|\Xi\rangle, \qquad \text{(C.23)}$$

then the numbers $\{\xi_\alpha\}$, $\alpha = 1, \ldots, n$, will satisfy

$$\xi_\alpha\xi_\beta + \xi_\beta\xi_\alpha = 0, \qquad \text{(C.24)}$$

which implies, in particular, that $\xi^2_\alpha = 0$. The algebra of anti-commuting numbers is called *Grassmann algebra* and, for the present purposes, can be viewed simply as a clever mathematical construct that takes care of all minus signs arrising from anti-symmetry properties.

Contrary to what was done in the case of bosons, the most important properties of fermionic coherent states will be listed here without proof. The reader is referred to Ref. [27] for details on their derivation. The overlap of two fermion coherent states $|\Xi\rangle$ and $|\Xi'\rangle$, which are both eigenstates of a_α with eigenvalues ξ_α and ξ'_α, respectively, can be easily shown to be given by

$$\langle \Xi | \Xi' \rangle = e^{\sum_\alpha \xi^*_\alpha \xi'_\alpha}, \tag{C.25}$$

while the closure relation expressed in terms of fermionic coherent states can be written as

$$\int \left[\prod_\alpha d\xi^*_\alpha \, d\xi_\alpha \right] e^{-\sum_\alpha \xi^*_\alpha \xi_\alpha} \, |\Xi\rangle\langle\Xi| = \mathbf{1}, \tag{C.26}$$

where $\mathbf{1}$ denotes the identity operator in the fermion Fock space. Notice that the integration measure in this expression does not contain the $2\pi i$ factor that was found in the bosonic case (see Eq.(C.14)).

The trace of an operator $\mathbf{A}$ whose eigenstates form a complete set of vectors $\{|n\rangle\}$ in Fock space can be written in terms of fermionic coherent states as

$$\mathrm{tr}\, \mathbf{A} = \int \left[\prod_\alpha d\xi^*_\alpha \, d\xi_\alpha \right] e^{-\sum_\alpha \xi^*_\alpha \xi_\alpha} \, \langle -\Xi | \mathbf{A} | \Xi \rangle, \tag{C.27}$$

and the matrix element of a normal-ordered operator $:\mathbf{A}(a^\dagger_\alpha, a_\alpha):$ between two fermionic coherent states can be shown to reduce to exactly the same form as in the bosonic case, that is,

$$\langle \Xi | :\mathbf{A}(a^\dagger_\alpha, a_\alpha): | \Xi' \rangle = \mathbf{A}(\xi^*_\alpha, \xi'_\alpha) \, \langle \Xi | \Xi' \rangle = \mathbf{A}(\xi^*_\alpha, \xi'_\alpha) \, e^{\sum_\alpha \xi^*_\alpha \xi'_\alpha}. \tag{C.28}$$

Finally, it should be pointed out that, in contrast to the boson case, the expectation value of the number operator in a fermion coherent state,

$$\frac{\langle \Xi | N | \Xi \rangle}{\langle \Xi | \Xi \rangle} = \sum_\alpha \xi^*_\alpha \xi_\alpha, \tag{C.29}$$

is not a real number. Therefore, it is meaningless to talk about the average number of particles in a fermionic state, which cannot be used to describe physically observable systems. Nevertheless, fermionic coherent states are very useful in physics, and are employed in multiple techniques in quantum field theory.

C.4 Functional Integration

When the Hamiltonian of a many-particle system is written in second quantization form, a much more convenient expression for the propagator can be obtained using coherent states, instead of the position and momentum eigenstates used for the Feynman path integral. This leads to the so-called functional integral over coherent states. In this section, an expression for the matrix element of the time-evolution operator in a basis of coherent states will be obtained, enabling one to develop a functional integral formulation of the grand-canonical partition function of many-particle systems.

Let $\{|\Phi_k\rangle\}$ be a set of coherent states in Fock space, where $|\Phi_k\rangle$ is an eigenstate of a_α with eigenvalue $\phi_{\alpha,k}$,

$$a_\alpha \, |\Phi_k\rangle = \phi_{\alpha,k} \, |\Phi_k\rangle. \tag{C.30}$$

The objective is to develop a functional integral expression for the propagator from an initial state $|\Phi_i\rangle$ at time t_i to a final state $|\Phi_f\rangle$ at time t_f:

$$G(\phi^*_{\alpha,f}, t_f; \phi_{\alpha,i}, t_i) = \langle \Phi_f | e^{-\frac{i}{\hbar}\mathcal{H}(t_f - t_i)} | \Phi_i \rangle. \tag{C.31}$$

As in the case of the Feynman path integral, the time interval $(t_f - t_i)$ can be broken into N subintervals of equal size $\epsilon = (t_f - t_i)/N$, and a closure relation in terms of $|\Phi_k\rangle$, namely,

$$\mathbf{1} = \int \left[\prod_\alpha \frac{d\phi^*_{\alpha,k} \, d\phi_{\alpha,k}}{\mathcal{N}} \right] \, e^{-\sum_\alpha \phi^*_{\alpha,k} \phi_{\alpha,k}} \, |\Phi_k\rangle\langle\Phi_k|, \tag{C.32}$$

with $\mathcal{N} = 2\pi i$ for bosons and $\mathcal{N} = 1$ for fermions, is inserted at the k^{th} time step, with $k = 1, \ldots, N-1$. Using the notation

$$\begin{cases} \phi_{\alpha,N} \equiv \phi_{\alpha,f}; \\ \phi_{\alpha,0} \equiv \phi_{\alpha,i}, \end{cases} \tag{C.33}$$

one obtains:

$$G(\phi^*_{\alpha,f},t_f;\phi_{\alpha,i},t_i)=\langle\Phi_f|\left(e^{-\frac{i}{\hbar}\epsilon\mathcal{H}(a^\dagger_\alpha,a_\alpha)}\right)^N|\Phi_i\rangle=$$

$$=\langle\Phi_N|e^{-\frac{i}{\hbar}\epsilon\mathcal{H}}\left[\int\left(\prod_\alpha\frac{d\phi^*_{\alpha,N-1}\,d\phi_{\alpha,N-1}}{\mathcal{N}}\right)e^{-\sum_\alpha\phi^*_{\alpha,N-1}\phi_{\alpha,N-1}}|\Phi_{N-1}\rangle\langle\Phi_{N-1}|\right]e^{-\frac{i}{\hbar}\epsilon\mathcal{H}}\ldots$$

$$\ldots e^{-\frac{i}{\hbar}\epsilon\mathcal{H}}\left[\int\left(\prod_\alpha\frac{d\phi^*_{\alpha,1}\,d\phi_{\alpha,1}}{\mathcal{N}}\right)e^{-\sum_\alpha\phi^*_{\alpha,1}\phi_{\alpha,1}}|\Phi_1\rangle\langle\Phi_1|\right]e^{-\frac{i}{\hbar}\epsilon\mathcal{H}}|\Phi_0\rangle=$$

$$=\left[\int\prod_{k=1}^{N-1}\prod_\alpha\frac{d\phi^*_{\alpha,k}\,d\phi_{\alpha,k}}{\mathcal{N}}\right]e^{-\sum_{k=1}^{N-1}\sum_\alpha\phi^*_{\alpha,k}\phi_{\alpha,k}}\prod_{k=1}^{N}\langle\Phi_k|e^{-\frac{i}{\hbar}\epsilon\mathcal{H}(a^\dagger_\alpha,a_\alpha)}|\Phi_{k-1}\rangle. \tag{C.34}$$

In order to evaluate the matrix elements that appear in this expression, one can assume that $\mathcal{H}(a^\dagger_\alpha,a_\alpha)$ is written in normal form, that is, with the creation operators always preceding the annihilation operators. As in the path integral case, the error introduced by this approximation is of order ϵ^2 and, therefore, will be negligible in the limit of $N\to\infty$. Using Eq.(C.22) for the matrix element of normal ordered operators in a basis of coherent states, one obtains:

$$\langle\Phi_k|e^{-\frac{i}{\hbar}\epsilon\mathcal{H}(a^\dagger_\alpha,a_\alpha)}|\Phi_{k-1}\rangle=\lim_{N\to\infty}\langle\Phi_k|:e^{-\frac{i}{\hbar}\epsilon\mathcal{H}(a^\dagger_\alpha,a_\alpha)}:|\Phi_{k-1}\rangle=$$

$$=\lim_{N\to\infty}\langle\Phi_k|\Phi_{k-1}\rangle\,e^{-\frac{i}{\hbar}\epsilon\mathcal{H}(\phi^*_{\alpha,k},\phi_{\alpha,k-1})}=\lim_{N\to\infty}e^{\sum_\alpha\phi^*_{\alpha,k}\phi_{\alpha,k-1}-\frac{i}{\hbar}\epsilon\mathcal{H}(\phi^*_{\alpha,k},\phi_{\alpha,k-1})}, \tag{C.35}$$

where the notation $:\mathbf{A}:$ indicates that the operator $\mathbf{A}$ was reordered into normal form. Using this result back into Eq.(C.34):

$$G(\phi^*_{\alpha,f},t_f;\phi_{\alpha,i},t_i)=$$

$$=\lim_{N\to\infty}\left[\int\prod_{k=1}^{N-1}\prod_\alpha\frac{d\phi^*_{\alpha,k}\,d\phi_{\alpha,k}}{\mathcal{N}}\right]e^{-\sum_{k=1}^{N-1}\sum_\alpha\phi^*_{\alpha,k}\phi_{\alpha,k}}e^{\sum_{k=1}^{N}\left\{\sum_\alpha\phi^*_{\alpha,k}\phi_{\alpha,k-1}-\frac{i}{\hbar}\epsilon\mathcal{H}\right\}}=$$

$$=\lim_{N\to\infty}\left[\int\prod_{k=1}^{N-1}\prod_\alpha\frac{d\phi^*_{\alpha,k}\,d\phi_{\alpha,k}}{\mathcal{N}}\right]\exp\left\{\sum_\alpha\phi^*_{\alpha,N}\phi_{\alpha,N-1}-\frac{i}{\hbar}\epsilon\mathcal{H}(\phi^*_{\alpha,N},\phi_{\alpha,N-1})+\right.$$

$$\left.+\sum_{k=1}^{N-1}\left[-\sum_\alpha\phi^*_{\alpha,k}(\phi_{\alpha,k}-\phi_{\alpha,k-1})-\frac{i}{\hbar}\epsilon\mathcal{H}(\phi^*_{\alpha,k},\phi_{\alpha,k-1})\right]\right\} \tag{C.36}$$

It is now convenient to introduce the trajectory notation, analogous to the one used in the

case of path integrals, bearing in mind that it does not imply continuity or differentiability:

$$\begin{cases} \phi_{\alpha,k} \to \phi_\alpha(t) \quad ; \\ \dfrac{\phi_{\alpha,k} - \phi_{\alpha,k-1}}{\epsilon} \to \dfrac{\partial}{\partial t}\phi_\alpha(t). \end{cases} \tag{C.37}$$

Defining the integration measure as

$$\int \mathcal{D}[\phi^*_\alpha(t);\phi_\alpha(t)] \equiv \lim_{N\to\infty}\left[\int \prod_{k=1}^{N-1}\prod_\alpha \frac{d\phi^*_{\alpha,k}\, d\phi_{\alpha,k}}{\mathcal{N}}\right], \tag{C.38}$$

Eq.(C.36) becames:

$$G(\phi^*_{\alpha,f},t_f;\phi_{\alpha,i},t_i) = \int \mathcal{D}[\phi^*_\alpha(t);\phi_\alpha(t)] \exp\left\{ \sum_\alpha \phi^*_\alpha(t_f)\phi_\alpha(t_f) + \right.$$
$$\left. + \frac{i}{\hbar}\int_{t_i}^{t_f} dt \left[i\hbar \sum_\alpha \phi^*_\alpha(t)\frac{\partial\phi_\alpha(t)}{\partial t} - \mathcal{H}(\phi^*_\alpha(t),\phi_\alpha(t))\right]\right\}. \tag{C.39}$$

Finally, writing the Lagrangian as

$$L[\phi^*_\alpha(t);\phi_\alpha(t)] \equiv i\hbar\sum_\alpha \phi^*_\alpha(t)\frac{\partial\phi_\alpha(t)}{\partial t} - \mathcal{H}(\phi^*_\alpha(t),\phi_\alpha(t)), \tag{C.40}$$

the functional integral expression for the quantum mechanical propagator becames:

$$\boxed{G(\phi^*_{\alpha,f},t_f;\phi_{\alpha,i},t_i) = \int \mathcal{D}[\phi^*_\alpha(t);\phi_\alpha(t)]\, e^{\sum_\alpha \phi^*_\alpha(t_f)\phi_\alpha(t_f) + \frac{i}{\hbar}\int_{t_i}^{t_f} dt\, L[\phi^*_\alpha(t);\phi_\alpha(t)]}}. \tag{C.41}$$

C.5 Grand-canonical Partition Function

As discussed in the case of the Feynman path integral, the partition function can be written as the trace of the time-evolution operator with the quantity $\tau = \beta\hbar$ playing the role of the time interval. However, in the case of a system described by a Hamiltonian written in second quantization form, this trace is more conveniently evaluated with respect to a base of coherent states.

In order to develop a functional integral expression for the grand-canonical partition function, consider a quantum mechanical system in equilibrium with a particle reservoir (with which it may exchange particles) as well as with a thermal reservoir. Recalling

Eq.(C.21) for the trace of an operator with respect to coherent states, one can write

$$\mathcal{Z} = \mathrm{tr}\left(e^{-\beta(\mathcal{H}-\mu\mathbf{N})}\right) = \left[\int \prod_{\alpha} \frac{d\phi_{\alpha}^{*}\, d\phi_{\alpha}}{\mathcal{N}}\right] e^{-\sum_{\alpha}\phi_{\alpha}^{*}\phi_{\alpha}} \langle\Phi|e^{-\beta(\mathcal{H}-\mu\mathbf{N})}|\Phi\rangle, \tag{C.42}$$

where the number operator $\mathbf{N}$ is given by

$$\mathbf{N} = \sum_{\alpha} a_{\alpha}^{\dagger}\, a_{\alpha}. \tag{C.43}$$

One can now define the quantity $\tau = \beta\hbar$ (which has dimension of time), break the "time" interval into N subintervals of equal size $\epsilon = \tau/N$, and insert a closure relation in the form of Eq.(C.14) $N-1$ times between consecutive time-evolution operators. Also, one has to impose the condition that the initial and final states coincide, that is,

$$|\Phi\rangle \equiv |\Phi_0\rangle = |\Phi_N\rangle. \tag{C.44}$$

This way, Eq.(C.42) gives:

$$\mathcal{Z} = \left[\int \prod_{\alpha} \frac{d\phi_{\alpha,N}^{*}\, d\phi_{\alpha,N}}{\mathcal{N}}\right] e^{-\sum_{\alpha}\phi_{\alpha,N}^{*}\phi_{\alpha,N}} \langle\Phi_N| \left(e^{-\frac{1}{\hbar}\epsilon(\mathcal{H}-\mu\mathbf{N})}\right)^{N} |\Phi_0\rangle =$$

$$= \left[\int \prod_{k=1}^{N}\prod_{\alpha} \frac{d\phi_{\alpha,k}^{*}\, d\phi_{\alpha,k}}{\mathcal{N}}\right] e^{-\sum_{k=1}^{N}\sum_{\alpha}\phi_{\alpha,k}^{*}\phi_{\alpha,k}} \prod_{k=1}^{N} \langle\Phi_k|e^{-\frac{1}{\hbar}\epsilon(\mathcal{H}-\mu\mathbf{N})}|\Phi_{k-1}\rangle. \tag{C.45}$$

Notice that, in this case, there are N integrations over coherent state variables $\phi_{\alpha,k}$, due to the extra integration over $\phi_{\alpha,N} = \phi_{\alpha,0}$ introduced by the trace operation.

In order to calculate the matrix elements, one can assume again that the Hamiltonian is in normal form, since the error introduced by this approximation becomes negligible in the limit of $N \to \infty$. Using Eq.(C.22) for the matrix element of normal ordered operators in a basis of coherent states, and recalling the expression for the number operator given by Eq.(C.43), one obtains:

$$\langle\Phi_k|e^{-\frac{1}{\hbar}\epsilon(\mathcal{H}(a_{\alpha}^{\dagger},a_{\alpha})-\mu\mathbf{N}(a_{\alpha}^{\dagger},a_{\alpha}))}|\Phi_{k-1}\rangle = \lim_{N\to\infty} \langle\Phi_k| : e^{-\frac{1}{\hbar}\epsilon(\mathcal{H}(a_{\alpha}^{\dagger},a_{\alpha})-\mu\mathbf{N}(a_{\alpha}^{\dagger},a_{\alpha}))} : |\Phi_{k-1}\rangle =$$

$$= \lim_{N\to\infty} \langle\Phi_k|\Phi_{k-1}\rangle\, e^{-\frac{1}{\hbar}\epsilon(\mathcal{H}(\phi_{\alpha,k}^{*},\phi_{\alpha,k-1})-\mu\sum_{\alpha}\phi_{\alpha,k}^{*}\phi_{\alpha,k-1})} =$$

$$= \lim_{N\to\infty} e^{\sum_{\alpha}\phi_{\alpha,k}^{*}\phi_{\alpha,k-1} - \frac{1}{\hbar}\epsilon(\mathcal{H}(\phi_{\alpha,k}^{*},\phi_{\alpha,k-1})-\mu\sum_{\alpha}\phi_{\alpha,k}^{*}\phi_{\alpha,k-1})}. \tag{C.46}$$

Using this back into Eq.(C.45):

$$\mathcal{Z} = \lim_{N\to\infty}\left[\int\prod_{k=1}^{N}\prod_{\alpha}\frac{d\phi^*_{\alpha,k}\,d\phi_{\alpha,k}}{\mathcal{N}}\right]\exp\left\{-\frac{1}{\hbar}\sum_{k=1}^{N}\epsilon\left[\sum_{\alpha}\left(\hbar\phi^*_{\alpha,k}\frac{\phi_{\alpha,k}-\phi_{\alpha,k-1}}{\epsilon}+\right.\right.\right.$$
$$\left.\left.\left.-\mu\phi^*_{\alpha,k}\phi_{\alpha,k-1}\right)+\mathcal{H}(\phi^*_{\alpha,k},\phi_{\alpha,k-1})\right]\right\}. \quad \text{(C.47)}$$

Making use of the trajectory notation introduced in Eq.(C.37), and defining the integration measure according to

$$\oint_{\phi_\alpha(0)=\zeta\phi_\alpha(\beta\hbar)}\mathcal{D}[\phi^*_\alpha(\tau);\phi_\alpha(\tau)] \equiv \lim_{N\to\infty}\left[\int\prod_{k=1}^{N}\prod_{\alpha}\frac{d\phi^*_{\alpha,k}\,\phi_{\alpha,k}}{\mathcal{N}}\right], \quad \text{(C.48)}$$

the partition function becomes:

$$\mathcal{Z} = \oint_{\phi_\alpha(0)=\zeta\phi_\alpha(\beta\hbar)}\mathcal{D}[\phi^*_\alpha(\tau);\phi_\alpha(\tau)]\exp\left\{-\frac{1}{\hbar}\int_0^{\beta\hbar}d\tau\left[\sum_{\alpha}\phi^*_\alpha(\tau)\left(\hbar\frac{\partial}{\partial\tau}-\mu\right)\phi_\alpha(\tau)+\right.\right.$$
$$\left.\left.+\mathcal{H}(\phi^*_\alpha(\tau),\phi_\alpha(\tau))\right]\right\}, \quad \text{(C.49)}$$

where the notation $\phi_\alpha(0) = \zeta\phi_\alpha(\beta\hbar)$ indicates that the integration is over complex variables satisfying periodic boundary conditions in the case of bosons ($\zeta = +1$) and over Grassman variables satisfying anti-periodic boundary conditions in the case of fermions ($\zeta = -1$). Finally, writing the Euclidian action as

$$\boxed{\mathcal{S}_e[\phi^*_\alpha(\tau),\phi_\alpha(\tau)] \equiv \int_0^{\beta\hbar}d\tau\left[\sum_{\alpha}\phi^*_\alpha(\tau)(\hbar\,\partial_\tau-\mu)\phi_\alpha(\tau)+\mathcal{H}(\phi^*_\alpha(\tau),\phi_\alpha(\tau))\right]}, \quad \text{(C.50)}$$

the functional integral expression for the grand-canonical partition function becomes:

$$\boxed{\mathcal{Z} = \oint_{\phi_\alpha(0)=\zeta\phi_\alpha(\beta\hbar)}\mathcal{D}[\phi^*_\alpha(\tau);\phi_\alpha(\tau)]\,e^{-\frac{1}{\hbar}\mathcal{S}_e[\phi^*_\alpha(\tau),\phi_\alpha(\tau)]}}. \quad \text{(C.51)}$$

C.6 Gaussian Functional Integrals

Several functional integrals of practical relevance involve exponential functions that are polynomials in either complex or Grassmann variables. In the cases where these polynomials can be reduced to quadratic forms, such integrals become generalizations of the more familiar Gaussian integrals. Among other applications, they are important to implement the

so-called Hubbard-Stratonovich transformation, which is a valuable tool in field-theoretical calculations. It is convenient for future reference to list some of these integrals here (for a detailed derivation, see Ref. [27]).

Let $\phi(x)$ and $\chi(x)$ be complex-valued functions of the complex variable x, and let $\mathbf{A}$ be a positive definite matrix. The following boson Gaussian integral can be shown to hold:

$$\int \frac{\mathcal{D}[\phi,\phi^*]}{2\pi i}\, e^{\int dx[-\phi^*(x)\mathbf{A}\phi(x)+\chi^*(x)\phi(x)+\chi(x)\phi^*(x)]} = \frac{1}{\det \mathbf{A}}\, e^{\int dx\, \chi^*(x)\mathbf{A}^{-1}\chi(x)}. \tag{C.52}$$

An analogous identity can be derived for Grassmann variables. Let $\psi(\xi)$ and $\eta(\xi)$ be two fermionic fields that depend on the Grassmann variable ξ, and let $\mathbf{H}$ be an arbitrary matrix. It can be shown that the following fermion Gaussian integral holds:

$$\int \mathcal{D}[\psi,\psi^\dagger]\, e^{\int d\xi\left[-\psi^\dagger(\xi)\mathbf{H}\psi(\xi)+\eta^\dagger(\xi)\psi(\xi)+\eta(\xi)\psi^\dagger(\xi)\right]} = [\det \mathbf{H}]\; e^{\int d\xi\, \eta^\dagger(\xi)\mathbf{H}^{-1}\eta(\xi)}. \tag{C.53}$$

Notice that the determinant of the matrix appears on the right-hand side of the identity in the fermionic case, while the inverse of the determinant appears in the bosonic case.

APPENDIX D

MATSUBARA SUMS

Many calculations in finite temperature quantum field theory require the computation of sums of the following general form,

$$S_B(\tau) = \sum_{\nu_m} M(i\nu_m)\, e^{i\nu_m \tau}, \tag{D.1}$$

where the variable $\nu_m = 2m\pi/\beta$ (with $\beta = 1/k_B T$) is called a *bosonic Matsubara frequency*, for reasons that will soon become clear, and m is an integer that runs from $-\infty$ to $+\infty$. The function $M(i\nu_m)$ is assumed to have an arbitrary number of off-imaginary-axis poles on the complex plane. For calculations involving fermion variables, one finds analogous sums over *fermionic Matsubara frequencies* $\omega_n = (2n+1)\pi/\beta$, where n is also an integer that runs from $-\infty$ to $+\infty$. In order to evaluate such sums, one can make use of complex variables calculus by means of Cauchy's residue theorem [38].

The first step, however, is to realize that the Boson function $n_B(\nu)$, which is defined as

$$n_B(\nu) = \frac{1}{e^{\beta\nu} - 1}, \tag{D.2}$$

has infinite simple poles along the imaginary axis at the positions $\nu = i\nu_m$. In fact, it is easy to see that the denominator of Eq.(D.2) vanishes at these points. Furthermore, the residue of $n_B(\nu)$ at all its poles is equal to $1/\beta$. To show this, one must recall that the residue of a function $f(x)$ at a simple pole x_0 is given by $\lim_{x\to x_0}[f(x)(x - x_0)]$. Therefore:

$$\mathrm{Res}\left[n_B(\nu)\right]_{i\nu_m} = \lim_{\nu \to i\nu_m}\left[\frac{\nu - i\nu_m}{e^{\beta\nu} - 1}\right] = \lim_{\nu \to i\nu_m}\left[\frac{1}{\beta e^{\beta\nu}}\right] = \frac{1}{\beta}\frac{1}{e^{i\beta\nu_m}} = \frac{1}{\beta}. \tag{D.3}$$

Analogously, the Fermi function $n_F(\omega)$, which is given by

$$n_F(\omega) = \frac{1}{e^{\beta\omega} + 1}, \tag{D.4}$$

has an infinite number of simple poles at the positions $\omega = i\omega_n$ along the imaginary axis.

In this case, however, the residue of $n_F(\omega)$ at its poles is equal to $-1/\beta$. In fact,

$$\mathrm{Res}\left[n_F(\omega)\right]_{i\omega_n} = \lim_{\omega\to i\omega_n}\left[\frac{\omega - i\omega_n}{e^{\beta\omega}+1}\right] = \lim_{\omega\to i\omega_n}\left[\frac{1}{\beta e^{\beta\omega}}\right] = \frac{1}{\beta}\frac{1}{e^{i\beta\omega_n}} = -\frac{1}{\beta}. \tag{D.5}$$

One can now explore this fact to rewrite the Matsubara sums in the bosonic and fermionic cases as

$$S_B(\tau) = \sum_{\nu_m} M(i\nu_m)e^{i\nu_m\tau} = \beta\sum_{m=-\infty}^{\infty}\mathrm{Res}\left[M(\nu)e^{\nu\tau}n_B(\nu)\right]_{\nu=i\nu_m} \quad \text{(Boson)}; \tag{D.6}$$

$$S_F(\tau) = \sum_{\omega_n} M(i\omega_n)e^{i\omega_n\tau} = -\beta\sum_{n=-\infty}^{\infty}\mathrm{Res}\left[M(\omega)e^{\omega\tau}n_F(\omega)\right]_{\omega=i\omega_n} \quad \text{(Fermion)}. \tag{D.7}$$

The Cauchy theorem can now be invoked in order to express the sum over residues as an integral along a contour in the complex plane that encloses all the residues:

$$S_B(\tau) = \beta\oint_C \frac{dz}{2\pi i}M(z)e^{z\tau}n_B(z) \quad \text{(Boson)}; \tag{D.8}$$

$$S_F(\tau) = -\beta\oint_C \frac{dz}{2\pi i}M(z)e^{z\tau}n_F(z) \quad \text{(Fermion)}, \tag{D.9}$$

where the contour C runs from $\epsilon - i\infty$ up to $\epsilon + i\infty$, and then back from $-\epsilon + i\infty$ down to $-\epsilon - i\infty$, where ϵ is an infinitesimally small distance. That is, the contour runs parallel to the imaginary axis, headed up just to the right of the axis and down just to the left of the axis, as shown in Fig. D.1-a, thus enclosing all the poles of the functions $n_B(z)$ or $n_F(z)$. The crucial step now is the following: if the function $M(z)$ has only poles but no branch cuts in the right and left half planes, the contour C can be continuously deformed to include all of the complex plane but the poles of $M(z)$, as shwon in Fig. D.1-b. The resulting contour will then consist of the long arc $\tilde{C}$, whose radius can be taken to be infinitely large, and the small loops Γ_j that encircle the poles of $M(z)$ in a clockwise sense. However, using Jordan's Lemma, one can show that the integral along the arc $\tilde{C}$ vanishes in the limit of an infinite radius, and one is left with the integrals around the poles of $M(z)$ only:

$$S_B(\tau) = -\beta\sum_j\oint_{\Gamma_j}\frac{dz}{2\pi i}M(z)e^{z\tau}n_B(z) \quad \text{(Boson)}; \tag{D.10}$$

$$S_F(\tau) = \beta\sum_j\oint_{\Gamma_j}\frac{dz}{2\pi i}M(z)e^{z\tau}n_F(z) \quad \text{(Fermion)}. \tag{D.11}$$

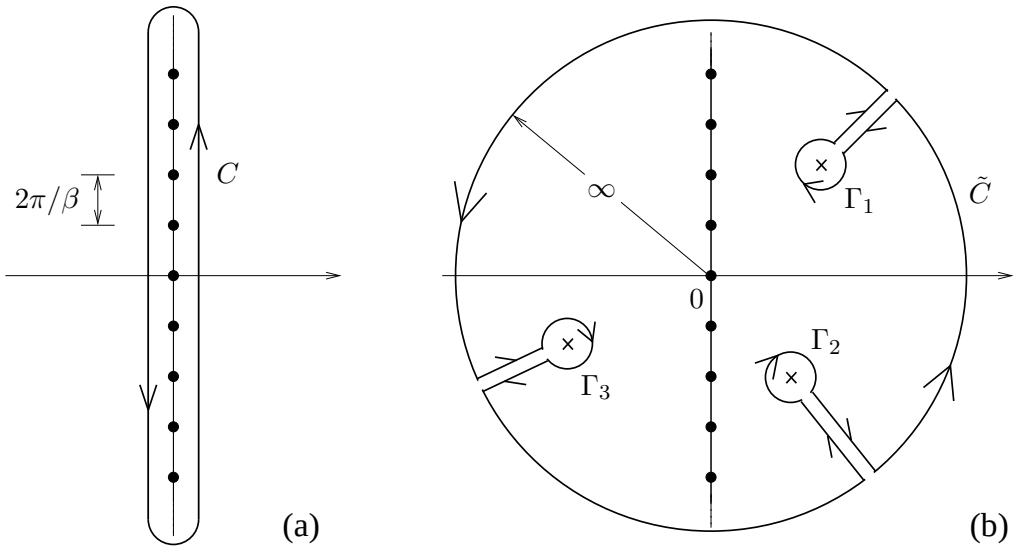

Figure D.1: (a) Integration contour C enclosing all the poles of $n_B(\nu)$; (b) The same contour after a continuous deformation, enclosing all the poles $\tilde{\nu}_j$ of the function $M(z)$ in the left and right half planes. (A similar sketch holds in the fermionic case, except that the poles of $n_F(\omega)$ would be vertically displaced by π/β).

Notice that the signs in these expressions were inverted with respect to Eqs.(D.8) and (D.9) to reflect the clockwise direction of the contours Γ_j. Finally, Cauchy's theorem can be used again, this time in the reverse direction, to rewrite the integral around each one of the poles of $M(z)$ as the residue of the integrand at that pole. Denoting these poles by $\tilde{\nu}_j$ in the bosonic case and $\tilde{\omega}_j$ in the fermionic case, one obtains:

$$S_B(\tau) = -\beta \sum_j \mathrm{Res}\left[M(z)e^{z\tau}n_B(z)\right]_{z=\tilde{\nu}_j} \quad \text{(Boson)}; \tag{D.12}$$

$$S_F(\tau) = \beta \sum_j \mathrm{Res}\left[M(z)e^{z\tau}n_F(z)\right]_{z=\tilde{\omega}_j} \quad \text{(Fermion)}, \tag{D.13}$$

which are finite sums over the poles of $M(z)$. Therefore, this "trick" has allowed us to trade off the infinite sum over poles along the imaginary axis for a presumably simpler, finite sum over poles in the right and left half planes.

As an example, let us consider a fermionic Matsubara sum that appears quite frequently in field theoretical calculations (the bosonic counterpart can be obtained in the exact same way),

$$S_F(\tau) = \sum_{\omega_n} \frac{e^{i\omega_n\tau}}{i\omega_n + E}. \tag{D.14}$$

In this case, the function $M(\omega) = 1/(\omega + E)$ has only one simple pole located at $\tilde{\omega} = -E$, and a direct application of Eq.(D.13) gives

$$S_F(\tau) = \beta \,\mathrm{Res}\left[M(z)e^{z\tau}n_F(z)\right]_{z=-E} = \beta \,\mathrm{Res}\left[\frac{e^{z\tau}}{z+E}\frac{1}{e^{\beta z}+1}\right]_{z=-E} =$$

$$= \beta \lim_{z\to -E}\left[\frac{e^{z\tau}}{z+E}\frac{1}{e^{\beta z}+1}(z+E)\right] = \beta\frac{e^{-E\tau}}{e^{-\beta E}+1} = \frac{\beta e^{-E\tau}}{2}\left[1+\tanh\left(\frac{\beta E}{2}\right)\right]. \qquad \text{(D.15)}$$

In particular, taking the limit of $\tau \to 0$, and recalling that the hyperbolic tangent is an odd function, one finally obtains:

$$\boxed{\sum_{\omega_n}\frac{1}{i\omega_n \pm E} = \frac{\beta}{2}\left[1 \pm \tanh\left(\frac{\beta E}{2}\right)\right]}. \qquad \text{(D.16)}$$

REFERENCES

[1] H. K. Onnes, Commun. Phys. Lab. **12**, 120 (1911).

[2] J. Bardeen, L. N. Cooper, and J. R. Schrieffer, Phys. Rev. **108**, 1175 (1957).

[3] L. N. Cooper, Phys. Rev. **104**, 1189 (1956).

[4] J. G. Bednorz and K. A. Müller, Zeitschrift für Physik B **64**, 189 (1986).

[5] A. J. Leggett, J. Phys. Colloq. (Paris) **41**, 7 (1980).

[6] M. Randeria, J. Duan, and L. Shieh, Phys. Rev. B **41**, 327 (1990).

[7] D. M. Eagles, Physical Review **186**, 456 (1969).

[8] J. K. Hulm, C. K. Jones, R. C. Miller, and T. Y. Tien, in *Proceedings of the Tenth International Conference on Low-Temperature Physics, Moscow, 1966*, edited by M. P. Malkov, Vol. IIA, pp. 86-114 (1967).

[9] A. J. Leggett, in *Modern Trends in the Theory of Condensed Matter*, edited by A. Pekalsky and R. Przystawa (Springer-Verlag, Berlin, 1980).

[10] P. Nozières and S. Schmitt-Rink, J. Low Temp. Phys. **59**, 195 (1985).

[11] C. A. R. Sá de Melo, M. Randeria, and J. R. Engelbrecht, Phys. Rev. Lett. **71**, 3202 (1993).

[12] N. Andrenacci, A. Perali, P. Pieri, and G. C. Strinati, Phys. Rev. B **60**, 12410 (1999).

[13] J. P. Wallington and J. F. Annett, Phys. Rev. B **61**, 1433 (2000).

[14] R. D. Duncan and C. A. R. Sá de Melo, Phys. Rev. B **62**, 9675 (2000).

[15] V. M. Loktev and V. M. Turkowski, Low Temp. Phys. **30**, 179 (2004).

[16] S. Stintzing and W. Zwerger, Phys. Rev. B **56**, 9004 (1997).

[17] L. Belkhir and M. Randeria, Phys. Rev. B **49**, 6829 (1994).

[18] M. Randeria, N. Trivedi, A. Moreo, and R. T. Scalettar, Phys. Rev. Lett. **69**, 2001 (1992).

[19] M. Capone, C. Castellani, and M. Grilli, Phys. Rev. Lett. **88**, 126403 (2002).

[20] R. Haussmann, Phys. Rev. B **49**, 12975 (1994).

[21] C. C. Tsuei and J. R. Kirtley, Rev. Mod. Phys. **72**, 969 (2000).

[22] N. C. Yeh *et al*, Phys. Rev. Lett. **87**, 087003 (2001).

[23] J. A. Skinta, M. Kim, T. R. Lemberger, T. Greibe, and M. Naito, Phys. Rev. Lett. **88**, 207005 (2002).

[24] For details, visit http://www.lucent.com/news_events/researchreview.html (2002).

[25] C. H. Ahn, J. M. Triscone, and J. Mannhart, Nature **424**, 1015 (2003).

[26] M. Randeria, J. Duan, and L. Shieh, Phys. Rev. Lett. **62**, 981 (1989).

[27] J. W. Negele and H. Orland, *Quantum Many-Particle Systems* (Advanced Book Classics, Perseus Books Group, 1998), Chap. 2.

[28] V. N. Popov, *Functional Integrals and Collective Excitations* (Cambridge Monographs on Mathematical Physics, Cambridge University Press, 1987).

[29] A. L. Fetter and J. D. Walecka, *Quantum Theory of Many-Particle Systems* (Dover Publications, 2003).

[30] J. R. Schrieffer, *Theory of Superconductivity* (Advanced Book Classics, Perseus Books Group), Chap. 2.

[31] J. R. Engelbrecht, M. Randeria, and C. A. R. Sá de Melo, Phys. Rev. B **55**, 15153 (1997).

[32] I. M. Lifshitz, Zh. Eksp. Teor. Fiz. **38**, 1569 (1960).

[33] A. A. Abrikosov, *Fundamentals of the Theory of Metals* (North-Holland, 1988), pp. 111-114.

[34] R. P. Feynman, *Statistical Mechanics* (W. A. Benjamin, Inc., Reading, MA, 1972), Chap. 10.

[35] C. J. Gorter and H. G. B. Casimir, Phys. Z. **35**, 963 (1934); Z. Tech. Phys. **15**, 539 (1934).

[36] V. P. Mineev and K. V. Samokhin, *Introduction to Unconventional Superconductivity* (Gordon and Breach Science Publishers, 1999), Chap. 22.

[37] S. Ilani, A. Yacoby, D. Mahalu, and H. Shtrikman, Phys. Rev. Lett. **84**, 3133 (2000).

[38] G.B. Arfken and H.J. Weber, *Mathematical Methods for Physicists* (Academic Press, Fourth Edition, 1995), Chap. 7.

[39] S. S. Botelho and C. A. R. Sá de Melo, Phys. Rev. B **71**, 134507 (2005).

[40] R. K. Pathria, *Statistical Mechanics*, 2nd Edition (Butterworth-Heinemann, 1996).

[41] N. D. Mermin and H. Wagner, Phys. Rev. Lett. **17**, 1133 (1966).

[42] P. C. Hohenberg, Phys. Rev. **158**, 383 (1967).

[43] V. L. Berezinskii, Sov. Phys. JETP **32**, 493 (1971).

[44] J. M. Kosterlitz and D. Thouless, J. Phys. C **5**, L124 (1972).

[45] P. Minnhagen, Rev. Mod. Phys. **59**, 1001 (1987).

[46] J. M. Kosterlitz and D. Thouless, J. Phys. C **6**, 1181 (1973).

[47] V. P. Gusynin, V. M. Loktev, and S. G. Sharapov, J. Exp. Theor. Physics (JETP) **88**, 685 (1999).

[48] V. M. Loktev and V. Turkowski, cond-mat/0404335 (2004).

[49] V. Loktev, R. Quick, and S. Sharapov, Phys. Rep. **349**, 1 (2000).

[50] A. Einstein, Sitzungsber. Kgl. Preuss. Akad. Wiss. **1924**, 261 (1924); *ibid.* **1925**, 3 (1925).

[51] S. N. Bose, Z. Phys. **26**, 178 (1924).

[52] M. Anderson, J. Ensher, M. Matthews, C. Wieman, and E. Cornell, Science **269**, 198 (1995).

[53] K. B. Davis, M. O. Mewes, M. R. Andrews, N. J. van Druten, D. S. Durfee, D. M. Kurn, and W. Ketterle, Phys. Rev. Lett. **75**, 3696 (1995).

[54] C. Bradley, C. Sackett, J. Tollett, and R. Hulet, Phys. Rev. Lett. **75**, 1687 (1995).

[55] For two very comprehensive review articles, including detailed descriptions of the experiments, see E. A. Cornell *et al*, cond-mat/9903109 (1999) and W. Ketterle *et al*, cond-mat/9904034 (1999).

[56] W. C. Stwalley, Phys. Rev. Lett. **37**, 1628 (1976).

[57] E. Tiesinga, B. J. Verhaar, and H. T. C. Stoof, Phys. Rev. A **47**, 4114 (1993).

[58] C. A. Regal, C. Ticknor, J. L. Bohn, and D. S. Jin, Nature **424**, 47 (2003).

[59] C. H. Schunck, M. W. Zwierlein, C. A. Stan, S. M. F. Raupach, W. Ketterle, A. Simoni, E. Tiesinga, C. J. Williams, and P. S. Julienne, Phys. Rev. A **71**, 045601 (2005).

[60] T. Bourdel, J. Cubizolles, L. Khaykovich, K. M. F. Magalhães, S. J. J. M. F. Kokkelmans, G. V. Shlyapnikov, and C. Salomon, cond-mat/0303079 (2003).

[61] C. A. Regal and D. S. Jin, Phys. Rev. Lett. **90**, 230404 (2003).

[62] M. W. Zwierlein, C. A. Stan, C. H. Schunck, S. M. F. Raupach, S. Gupta, Z. Hadzibabic, and W. Ketterle, Phys. Rev. Lett. **91**, 250401 (2003).

[63] T. Bourdel, L. Khaykovich, J. Cubizolles, J. Zhang, F. Chevy, M. Teichmann, L. Tarruell, S. J. J. M. F. Kokkelmans, and C. Salomon, Phys. Rev. Lett. **93**, 050401 (2004).

[64] K. E. Strecker, G. B. Partridge, and R. G. Hullet, Phys. Rev. Lett. **91**, 080406 (2003).

[65] M. Bartenstein, A. Altmeyer, S. Riedl, S. Jochim, C. Chin, J.H. Denschlag, and R. Grimm, Phys. Rev. Lett. **92**, 120401 (2004).

[66] J. Kinast, S.L. Hemmer, M.E. Gehm, A. Turlapov, and J.E. Thomas, Phys. Rev. Lett. **92**, 150402 (2004).

[67] M. Greiner, C. A. Regal, and D. S. Jin, Nature **426**, 537 (2003).

[68] C. A. Regal, M. Greiner, and D. S. Jin, Phys. Rev. Lett. **92**, 040403 (2004).

[69] M.W. Zwierlein, C.A. Stan, C.H. Schunck, S.M.F. Raupach, A.J. Kerman, and W. Ketterle, Phys. Rev. Lett. **92**, 120403 (2004).

[70] M. W. Zwierlein, J. R. Abo-Shaeer, A. Schirotzek, C. H. Schunck, and W. Ketterle, Nature **435**, 1047 (2005).

[71] B. de Marco and D. S. Jin, Science **285**, 1703 (1999).

[72] A. G. Truscott, K. E. Strecker, W. I. McAlexander, G. B. Partridge, and R. G. Hulet, Science **291**, 2570 (2001).

[73] M. Holland, S. J. J. M. F. Kokkelmans, M. L. Chiofalo, and R. Walser, Phys. Rev. Lett. **87**, 120406 (2001).

[74] Y. Ohashi and A. Griffin, Phys. Rev. Lett. **89**, 130402 (2002).

[75] A. Perali, P. Pieri, and G. C. Strinati, Phys. Rev. Lett. **93**, 100404 (2004).

[76] S. Y. Chang, V. R. Pandharipande, J. Carlson, and K. E. Schmidt, Phys. Rev. A **70**, 043602 (2004).

[77] C. A. Regal, C. Ticknor, J. L. Bohn, and D. S. Jin, Phys. Rev. Lett. **90**, 053201 (2003).

[78] J. Zhang, E. C. M. van Kempen, T. Bourdel, L. Khaykovich, J. Cubizolles, F. Chevy, M. Teichmann, L. Tarruel, S. J. J. M. F. Kokkelmans, and C. Salomon, Phys. Rev. A **70**, 030702(R) (2004).

[79] O. Morsch, M. Cristiani, J. H. Müller, D. Ciampini, and E. Arimondo, Phys. Rev. A **66**, 021601(R) (2002).

[80] M. Greiner, O. Mandel, T. Esslinger, T. W. Hänsch, and I. Bloch, Nature **415**, 39 (2002).

[81] J. F. Annett, Adv. in Phys. **39**, 83 (1990).

[82] L. D. Landau and E. M. Lifshitz, *Statistical Physics*, 3$^{\text{rd}}$ edition, Part 1 (Butterworth-Heinemann, 1980), Chap. 2.

[83] R. P. Feynman, *Statistical Mechanics* (W. A. Benjamin, Inc., Reading, MA, 1972), Chap. 6.